

An Improved Transmitted Near-Field Intensity Profile Method for Deriving the
Refractive Index Profile of a Waveguide

by

Chao-hsiung Paul Su

B.A.Sc., The University of British Columbia, 1997

A THESIS SUBMITTED IN PARTIAL FULFILMENT OF
THE REQUIREMENTS FOR THE DEGREE OF

MASTER OF APPLIED SCIENCE

in

THE FACULTY OF GRADUATE STUDIES

Department of Electrical Engineering

We accept this thesis as conforming
to the required standard

THE UNIVERSITY OF BRITISH COLUMBIA

January 2003

© Chao-hsiung Paul Su, 2003

In presenting this thesis in partial fulfilment of the requirements for an advanced degree at the University of British Columbia, I agree that the Library shall make it freely available for reference and study. I further agree that permission for extensive copying of this thesis for scholarly purposes may be granted by the head of my department or by his or her representatives. It is understood that copying or publication of this thesis for financial gain shall not be allowed without my written permission.

Department of Electrical Engineering

The University of British Columbia
Vancouver, Canada

Date Jan. 30, 2003

Abstract

Refractive index profile determines many physical properties of an optical waveguide. The Transmitted Near-Field Intensity Profile Method (TNFIPM) is a simple and convenient way to measure the refractive index distribution of a waveguide. Despite its simplicity, this technique also presents a lot of challenges and limitations one must overcome to obtain a usable result. In this thesis, we have introduced an improved TNFIPM that focuses on providing more useful results. To begin with, the calculation of the refractive index profile is based on the intensity profile. Therefore, it is important to have an accurate measurement of the intensity profile. However, one of the challenges faced is that the intensity profile itself is most often distorted by diffraction. In this thesis, we have introduced a diffraction-reduced algorithm which, with the gaussian beam equation and an iterative algorithm, produces a precise representation of the intensity profile at the end facet of the waveguide. Besides the diffraction effects, the equipment and spatial noise, if not treated properly, present another error source for standard TNFIPM . We have chosen to use a Savitzky-Golay filter to eliminate the noise in the intensity profile, which provides a good trade-off between noise reduction and the need to preserve the shape of the profile. Although traditionally, waveguides with high frequency components in their index profiles cannot provide accurate results, we have introduced a redundancy test and a morphing algorithm, which searches for the best possible index profile to describe the waveguide under study. In this thesis, the proposed improved method is analyzed and demonstrated for a Ti:LiNbO_3 waveguide.

Table of Contents

Abstract	ii
Table of Contents	iii
List of Figures	v
List of Tables.....	vii
Acknowledgments	viii
Chapter 1: Introduction	1
Chapter 2: Theory.....	6
2.1 INTRODUCTION	6
2.2 TRANSMITTED NEAR-FIELD INTENSITY PROFILE METHOD	7
2.3 DIFFRACTION	10
2.4 ABERRATIONS	17
2.5 GAUSSIAN BEAM EQUATIONS	18
2.6 SAVITZKY-GOLAY SMOOTHING FILTER	21
2.7 MORPHING ALGORITHM	25
2.8 CONCLUSION.....	28
Chapter 3: Algorithm	30
3.1 INTRODUCTION	30
3.2 DIFFRACTION-REDUCTION ALGORITHM	32
3.3 CURVE COMPARISON CRITERIA AND GENERATION OF PREDICTED PROFILE	38
3.4 DERIVING THE REFRACTIVE INDEX PROFILE.....	41
3.4.1 Inverse Wave Equation and Redundancy Test Algorithm	46
3.4.2 Simple Morphing Algorithm	49
3.6 CONCLUSION.....	54
Chapter 4 Simulation.....	55
4.1 INTRODUCTION	55
4.2 SIMULATION SETUP DESCRIPTION	56
4.3 SIMULATION RESULT OF A STANDARD TNFIPM	57
4.4 SIMULATION OF DIFFRACTION-REDUCTION ALGORITHM.....	62
4.5 SIMULATION FOR DERIVING THE FIRST GUESS OF THE INDEX PROFILE.....	65
4.6 SIMULATION FOR MORPHING ALGORITHM.....	69
4.7 CONCLUSION.....	72
Chapter 5 Experimental Results.....	73
5.1 INTRODUCTION	73
5.2 EXPERIMENTAL SETUP DESCRIPTION.....	74
5.3 BEAM MAGNIFICATION CALCULATION	79

5.4 DIFFRACTION REDUCED ALGORITHM	83
5.5 REFRACTIVE INDEX PROFILE MEASUREMENT.....	89
5.5.1 Results of Applying the Inverse Wave Equation	89
5.5.2 Redundancy Test Algorithm.....	94
5.5.3 Morphing Algorithm	97
5.6 CONCLUSION.....	104
Chapter 6: Conclusion and Suggestions for Future Work.....	105
Appendix A: Savitzky-Golay Filter	108
Appendix B: Beam Propagation Method(BPM)	111
Appendix C: Calibration of Lens Model.....	113
References	117

List of Figures

Figure 1-1: A typical configuration for refractive index profile measurement using TNFIPM	3
Figure 2-1: Diffraction effects analysis.....	12
Figure 2-2: Two planes	13
Figure 2-3: Fourier Transform System.....	15
Figure 2-4: Gaussian beam passing through a lens	20
Figure 2-5: Filter performance comparison for Moving Window Averaging Filter (with equal-weighting coefficients) and the Savitzky-Golay Filter.....	24
Figure 2-6: some of the possible refractive index functions for single mode waveguide.	27
Figure 3-1: Flow Chart of the Proposed TNFIPM	31
Figure 3-2: Coordinates definition for the waveguide under study	33
Figure 3-3: Diffraction-Reduction Algorithm.....	34
Figure 3-4-a: Intensity profile along the x direction of a Ti:LiNbO ₃ diffused waveguide	36
Figure 3-4-b: Intensity profile along the y direction of a Ti:LiNbO ₃ diffused waveguide	36
Figure 3-5: Comparison of the original and noisy intensity profiles	41
Figure 3-6: Comparison of index profiles derived from the original intensity profile and the filtered noisy intensity profile.....	42
Figure 3-7: Filtered index profiles from figures 3-6 c) and d)	43
Figure 3-8: A flowchart for obtaining the index profile of the waveguide	45
Figure 3-9: Redundancy Test Algorithm	48
Figure 3-10: flowchart of the morphing algorithm	50
Figure 3-11: Comparison between Parabola and Gaussian functions.....	51
Figure 3-12: Magnified view of the curve morphing from parabola to gaussian	53
Figure 4-1: A typical configuration for refractive index profile measurement using TNFIPM	57
Figure 4-2: Intensity Profiles at the output of each diagram.....	58
Figure 4-3: Object-plane Intensity Profiles and Image-plane Intensity Profiles.....	59
Figure 4-4: Comparison of original and calculated intensity profiles.....	60
Figure 4-5: Derived index profiles.....	61
Figure 4-6: Functional Block Diagram of Iteration and Convergence Algorithm.....	63
Figure 4-7: Comparison between the original intensity profile and the derived intensity	64
Figure 4-8: Comparison of intensity profiles at the image-plane.....	65
Figure 4-9: Initial derived index profile and its intensity profile comparisons.....	67
Figure 4-10: Index profiles and the corresponding intensity profiles after applying redundancy test algorithm	68
Figure 4-11: Block Diagrams for Morphing Algorithm Simulation.....	69
Figure 4-12: The final index profile from the morphing algorithm and its corresponding intensity profile at the end facet of the waveguide.....	71
Figure 5-1: Transmitted Near-Field Intensity Profile System.....	74

Figure 5-2: Single mode optical fiber coupled with a DFB laser.....	75
Figure 5-3: Sample Stage	76
Figure 5-4: Cutting-Knife Edge Scanning System.....	77
Figure 5-5: Detector with rotating drum	77
Figure 5-6: Intensity profile along the depth of an optical waveguide	78
Figure 5-7: Comparison of TE and TM mode profiles along x direction	82
Figure 5-8: Comparison of TE and TM mode profiles along y direction	83
Figure 5-9: List of profiles with the sharply decaying portion replaced with exponentially decaying functions.....	85
Figure 5-10: List of filtered profiles in figure 5-9.....	85
Figure 5-11: Comparison of intensity profiles at the end facet of the waveguide	87
Figure 5-12: Comparison of intensity profiles at the image-plane.....	88
Figure 5-13: Derived index profiles using diffraction reduced intensity profile	90
Figure 5-14: Constructed index profile along the x and y directions.....	91
Figure 5-15: Derived index profiles using a standard TNFIPM	93
Figure 5-16: Intensity profiles at the end facet of the waveguide with the derived index profiles	94
Figure 5-17: The index profiles and their simulated intensity profiles in applying the redundancy test for the second time	96
Figure 5-18: The index profiles and their simulated intensity profiles in applying the redundancy test for third time.....	96
Figure 5-19: Functions generated during the morphing process for x direction.....	98
Figure 5-20: Functions generated during the morphing process for y direction.....	98
Figure 5-21: Final index profiles found in the morphing process with their corresponding intensity profile.....	100
Figure 5-22: Index profile comparison.....	102
Figure 5-23: Intensity profile comparison.....	103
Figure C-1: CodeV TM paraxial setup of a lens system	114
Figure C-2: Intensity profile at the image-plane simulated with the diffraction-based Beam Propagation Tool	115
Figure C-3: Image profile comparison	116

List of Tables

Table 5-1: Tabulated measurements of the mode intensity profile	81
---	----

Acknowledgments

I would like to thank my supervisor, Dr. N. A. Jaeger for offering me an opportunity to work in the area of integrated optics. Besides his invaluable support and guidance during this research, his time and patience during the preparation of this thesis is greatly appreciated.

In addition, I like to thank Professor Pieter Swart for assisting me with the Savitzky-Golay filter. My thanks also extend to Dr. Alina Kulpa and Mr. Jeff Bull for their help in the fabrication of the optical waveguide used in my experiments.

Finally, I am grateful to my parents and my wife for their support and encouragement throughout this work.

Chapter 1: Introduction

Optical waveguides are the main building blocks of a large variety of photonic devices, from optical fibers to optical switches. A crucial property of optical waveguides is the distribution of the refractive index in the guiding region. Many physical properties of a waveguide such as bandwidth, spot size, mode-condition etc., are related to the refractive index distribution. The refractive index distribution determines the shape of the guided light field. Also, when designing an optical waveguiding based device, it is important to be able to measure the refractive index profile accurately as a part of the device characterization process.

The purpose of this thesis is to implement an accurate refractive index profile measuring system. Once the refractive index profile of an optical waveguide is obtained, it can be used to improve the design of the waveguide. It can also be used to determine the fabrication parameters of the manufacturing process. For example, if one is designing a modulator, you would like the spot size to be in certain size, which would require the refractive index profile information.

Several techniques have been developed to determine the refractive index profile of an optical waveguide. However, because the size of optical waveguides tends to be very

small, which causes measurement inaccuracy, most of the techniques have limitations and drawbacks. Some of the most adopted methods are:

- 1) Compositional measurement: an indirect method to determine the index profile is to first obtain the dopant concentration using secondary ion mass spectrometry [1]. Then from the dopant concentration, as a function of waveguide depth, one can determine the refractive index distribution. This method requires that the index profile change and the dopant concentration relation are known in advance, which may not be readily available in many cases.
- 2) Effective Index Method: The refractive index profile of a waveguide can be determined from its effective indices using the Inverse WKB Method [2][3][4]. The effective indices are calculated by measuring the incidence angles at which the guided modes are excited. The drawbacks are that this method cannot be used for single mode waveguides [5] and the Inverse WKB Method cannot provide an accurate result if the index profile has a discontinuity [6].
- 3) Transmitted Near-Field Intensity Profile Method (TNFIPM): The index profile is calculated from its mode field intensity by an inversion of the scalar wave equations [6] – [15]. It requires that the waveguides are weakly guiding and only their fundamental mode is excited. Since in the optical waveguide devices these types of waveguides are the most commonly found, we will concentrate on this method:

TNFIPM is one of the preferred methods for measuring an optical waveguide refractive index profile because of its simplicity, non-destructive nature, and low-cost. In addition, it can be used for slab or channel waveguides and for single mode or multi-mode

waveguides as long as only the fundamental mode is excited [7]. We have chosen the TNFIPM as the preferred index profile measuring system and we have implemented several important improvements. To begin with, figure 1-1 shows a typical configuration of a TNFIPM system. A laser or LED source is used to launch light into one end of a waveguide using a single mode fiber. After the light travels through the waveguide, it exits at the other end. Because of the small dimension of typical optical waveguide, the divergence angle of the waveguide output can be large, therefore, a lens is used to focus the output light onto a photo-detector. A polarizer separates the intensity profile coming out from the waveguide into TE (Transverse Electric) or TM (Transverse Magnetic) components. The detector can be a video camera or a cutting-knife-edge photo detector. The output of the detector is connected to a data processing unit where sampling and signal processing are performed.

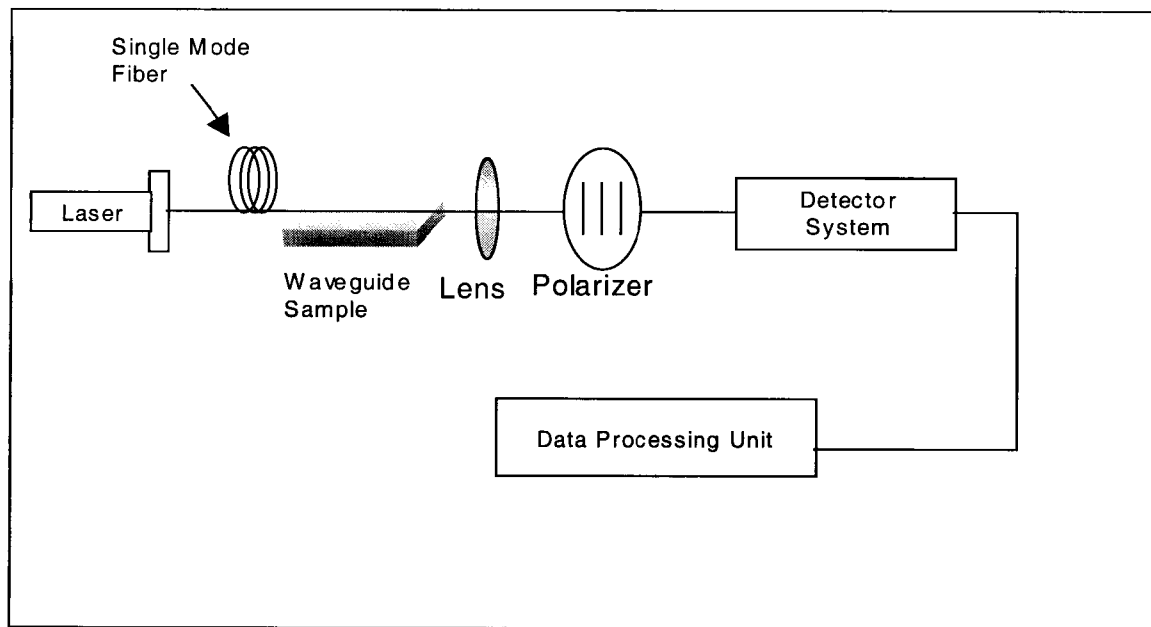


Figure 1-1: A typical configuration for refractive index profile measurement using TNFIPM

The TNFIPM possesses some difficulties and limitations to its implementation. One of the limiting factors is the noise in the measured intensity profile. Noise in the profile can be introduced from many sources, such as vibration and quantization noise in A/D conversion. The inversion of the scalar wave equation contains a second derivative of the intensity profile, which will dramatically amplify any noise and can render the results unusable. Therefore, this method requires a good noise filter and a very high signal-to-noise ratio in the measurements. Another source of the problems that can lead to inaccurate results is the errors in the acquired data due to misalignment and defocusing. Sometimes, errors can be prevented or minimized by accurate preparation of the experimental setup. However, one error cannot be removed from a typical TNFIPM setup, diffraction, which is the effects from light passing through an aperture such as the focusing lens [16][17]. The common approach is to claim the minimum resolution of the intensity profile is due to the resolving power of the lens using Abbe's criterion for coherent light [6][8][9], which can be a very rough estimate of the profile and can easily lead to inaccuracy in the final results.

One of the improvements introduced in this thesis is to design a diffraction-reduction algorithm that reduces the diffraction effects on the intensity profile before applying the inverse wave equation. The diffraction-reduction algorithm is based on an iterative method and a light propagation model. It generates an output intensity profile for a particular waveguide's refractive index distribution that produces an image-plane intensity profile that matches to the experimentally measured one. Compared to the

lensmaker's formula used in a standard TNFIPM, this approach produces significantly better results.

Due to the high spatial noise in some types of waveguides, for example, an ion diffused waveguide, the second derivative in the inverse wave equation introduces high frequency noise in the derived index profile, even if the profile is noise and diffraction free. Therefore, after obtaining the index profile, a typical TNFIPM would apply a fitting function to the index profile to smooth out any residual noise [6][14]. However, this approach does not really improve the accuracy of the final index profile. It only makes the profile look similar to what it might "typically" be. A second improvement introduced in this thesis is to use a morphing algorithm to modify the shape of the derived index profile until a better match to the output intensity profile is found.

This thesis consists of six chapters: Introduction, Theory, Algorithm, Simulation, Experimental Results ,and Conclusion and Suggestion for Future Work. In the next chapter, Theory, I present the theories for the TNFIPM and the proposed improvements. After introducing these theories, in the Algorithm chapter I describe in details the proposed algorithm. Then I analyze the simulation results of the proposed TNFIPM compared with a typical result in the Simulation chapter. Following that, the experimental results are presented. Finally, I summarize my research results and offer some suggestions for future work in the last chapter.

Chapter 2: Theory

2.1 Introduction

The Transmitted Near-Field Intensity Profile Method (TNFIPM) has been utilized to obtain the transverse refractive index profile of a longitudinally invariant waveguide in many published papers [6]-[15]. While this method requires an accurate intensity profile at the end facet of a waveguide, due to the configuration of a TNFIPM system one usually starts with an intensity profile of a waveguide's output in the image-plane. Then, in order to calculate the intensity profile at the end facet of the waveguide, a common method is to apply the geometrical optics-based lensmaker's equation to the intensity profile in the image-plane. However, since the focused intensity profile contains the aberrations and diffraction from the optical system, the lensmaker's equation cannot eliminate the effect of these defects from the profile and can result in the final index profile being inaccurate. Therefore, one of the motivations for this thesis is to improve the TNFIPM by reducing the effects of diffraction and aberrations on the intensity profile. By carefully designing our optical system and reducing the diffraction effects, we were able to improve our accuracy on our profile and thus, obtain a more accurate index profile.

This chapter introduces the basic operating principle of the Transmitted Near-Field Intensity Profile Method in section 2.2. Following the TNFIPM discussion, a theoretical analysis of the diffraction effects and the proposed solution are presented in section 2.3. Besides the diffraction problem, aberrations can also severely affect our profile and are taken into account and discussed in section 2.4. In section 2.5, the Gaussian beam equations, which are used to calculate the magnification of our lens, are introduced. Typically, there is always noise in the experimental data. However, due to a second derivative term in the inverse wave equation, the noise is highly amplified in this method. Therefore, in section 2.6, the discussion of the Savitzky-Golay smoothing filter that we have employed is provided. In order to improve the accuracy of the result of the TNFIPM, a morphing algorithm is required to find the best matching profile to describe the actual index profile, which is introduced in section 2.7. Finally, in section 2.8 a conclusion that summarizes the main features and the improvements of our proposed TNIFPM is provided.

2.2 Transmitted Near-Field Intensity Profile Method

Using the Transmitted Near-Field Intensity Profile Method (TNFIPM), the refractive index profile can be derived from the intensity profile at the end facet of a waveguide [6]-[15]. For a weakly guiding waveguide, in which the peak refractive index change is small, the optical field intensity of a mode can be described by the scalar wave equation[6][7][8]:

$$\nabla_T^2 \psi(x, y) + (k_o^2 n^2(x, y) - \beta^2) \psi(x, y) = 0 \quad (2.1)$$

where $\nabla_T^2 = \frac{\partial^2}{\partial x^2} + \frac{\partial^2}{\partial y^2}$ and $k_o = \frac{2\pi}{\lambda_o}$ is the free space wave number; $n(x, y)$ is the transverse refractive index distribution; and β is the propagation constant of a mode.

TNFIPM is based on the inverse of the wave equation. By doing the inversion, we can extract the refractive index distribution term, $n(x, y)$ from the equation. It is used for the fundamental mode since it is the mode of most interest in integrated optics and it is the mode that can be most easily extracted experimentally.

Scanning in 1D gives the same intensity profile if the field is separable, no matter what the refractive index profile in the other direction is. Since the electric field of a weakly guiding waveguide is separable [18][19], we can obtain the refractive index profile of a waveguide along the x and y directions separately, which makes the cutting-knife-edge technique a cheaper and more effective choice for the detector than using a CCD based video camera. It also means that we can simplify our two-dimensional problem into two simpler one-dimensional ones. Here, we can replace the 2D scalar wave equation (2.1) with equation (2.2), which represents the 1-D scalar wave equation along either the x or y direction, p .

$$\frac{\partial^2}{\partial p^2} \psi(p) + (k_o^2 n^2(p) - \beta^2) \psi(p) = 0 \quad (2.2)$$

If we substitute $n_{eff} k_o$ for β , we can obtain

$$n^2(p) = -\frac{\nabla_T^2 \psi(p)}{\psi(p) k_o^2} + n_{eff}^2 \quad (2.3)$$

where n_{eff} is the effective refractive index of the 1-D waveguide. Letting the refractive index profile $n(p)=n_o+\Delta n(p)$, where n_o is the substrate refractive index and $\Delta n(p)$ is the change of the refractive index along the p direction, we can approximate $n^2(p)$ with $n_o^2 + 2n_o\Delta n(p)$, since $\Delta n(p)$ is small. Substituting $n_o^2 + 2n_o\Delta n(p)$ for $n^2(p)$ in equation (2.3), we obtain

$$n_o^2 + 2n_o\Delta n(p) = -\frac{\nabla_T^2 \psi(p)}{\psi(p)k_o^2} + n_{eff}^2 \quad (2.4)$$

Putting $\Delta n(p)$ on one side and dividing all the terms by $2n_o$, we get the change of refractive index profile along an arbitrary direction p of the waveguide

$$\Delta n(p) = -\frac{\frac{\partial^2}{\partial x^2} \psi(p)}{\psi(p)k_o^2 2n_o} + \frac{n_{eff}^2}{2n_o} - \frac{n_o}{2} \quad (2.5)$$

Adding both sides of equation (2.5) with the substrate index n_o , the refractive index profile $n(p)$ can be expressed as

$$n(p) = -\frac{\frac{\partial^2}{\partial p^2} \psi(p)}{\psi(p)k_o^2 2n_o} + \frac{n_{eff}^2}{2n_o} + \frac{n_o}{2} \quad (2.6)$$

In equation (2.6), the refractive index profile $n(p)$ is a function of $\psi(p)$, n_{eff} and n_o . Since n_o is the substrate index and n_{eff} is the effective index of a waveguide, n_{eff} and n_o are both constants and $\frac{n_{eff}^2}{2n_o} + \frac{n_o}{2}$, in equation (2.6) can be replaced with a constant, μ , giving

$$n(p) = -\frac{\frac{\partial^2}{\partial p^2} \psi(p)}{\psi(p)k_o^2 2n_o} + \mu \quad (2.7)$$

Although we cannot calculate n_{eff} directly to determine μ , we do know that $n(p)$ far from the waveguide core, say p_0 , is equal to the substrate index, n_o . Therefore, by setting

$-\frac{\partial^2}{\partial p^2} \psi(p_0)$ in equation (2.7) equal to $n_o - \mu$, we can determine μ . Equation 2.7 is

also derived, in slightly different forms, in [6][7][8].

2.3 Diffraction

Since the light exiting from the waveguide diverges, the intensity profile is obtained after it is focused and magnified by a lens system. However, once the beam propagates through a lens system, the profile becomes the focused image of the actual profile with distortions from diffraction and aberrations [16][17][20]. The diffraction will make our final image smoother, which is not desirable for obtaining the rapid change in a refractive index profile. It will also make the profile appear larger. Therefore, when one applies equation (2.7) to these profiles to obtain the index profile, the results become noisy and wider than they should be.

In most of the published papers, these effects are oversimplified. The common approach is to calculate the diffraction limit using Abbe's criterion for coherent light [6][7][8] and claim the resolution of the diffraction is the minimum resolution of the profile for analysis. However, depending on the lens, the diffraction limit can range from 1 μ m to

2 μ m, which is significant for a typical waveguide size of 10 to 20 μ m. In addition, Abbe's criterion determines the ability of a lens system to distinguish two point sources from an image and it cannot be used to claim their experimental profiles are diffraction free. Therefore, by simply applying Abbe's criterion and the lensmaker's formula, the mode profiles are still severely affected, especially at the discontinuities.

In order to demonstrate how diffraction renders the Abbe's criterion and lensmaker's formula unacceptable for obtaining the intensity profile of a waveguide in TNFIPM, a simulation using two software packages, BeamPROPTM, a tool to simulate beam travel through a longitudinally invariant waveguide with a particular transverse refractive index profile, and CodeVTM, a software package that simulates light propagating through an optical system, is presented.

A simulated intensity profile at the end facet of a waveguide can be obtained using BeamPROPTM. Figure 2-1 a) shows the normalized intensity profile for the fundamental TE mode at the end facet of a typical titanium diffused waveguide($\lambda=1.3\mu$ M). In order to see how diffraction affects the original intensity profile shown in figure 2-1 a), this intensity profile is then fed into an optical system in CodeVTM, to acquire the intensity profile in the image-plane that includes the effects of diffraction through a lens. Applying lensmaker's equation to the acquired focused intensity profile, the calculated intensity profile with the effects of diffraction is obtained and shown in figure 2-1 b). Comparing figure 2-1 a) and b) shows how diffraction not only distorts the shape of the intensity profile but also makes the intensity profile larger. The diffraction affected

profile in 2-1 b) is increased 17% along the x direction and 27% along the y direction compared to the original intensity profile in figure 2-1 a). Applying equation 2.7, the inverse wave equation, to the intensity profile in figure 2-1 b) will give a refractive index profile that is quite different from the original index profile. Therefore, without considering diffraction, the intensity profile in the image-plane cannot be used in the TNFIPM.

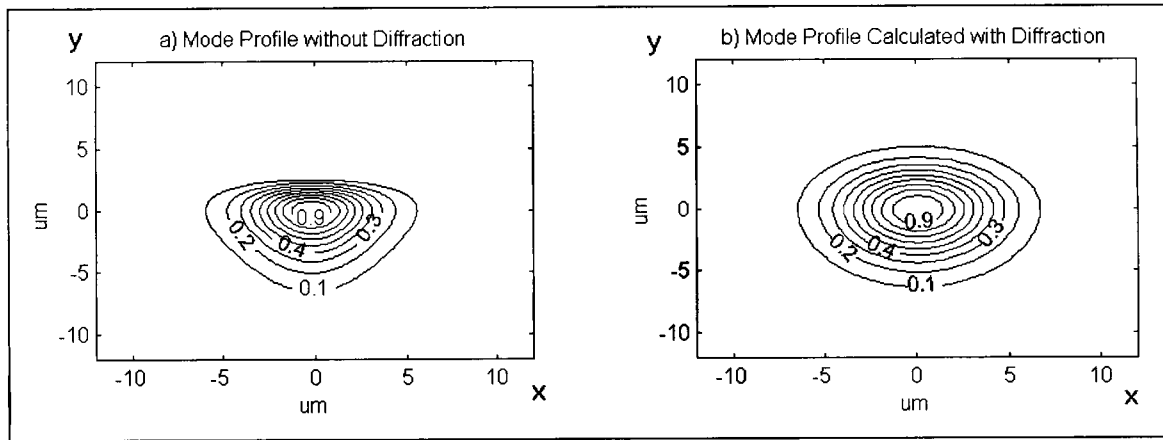


Figure 2-1: Diffraction effects analysis

Before discussing the method implemented in our proposed TNFIPM for removing the diffraction, a theoretical analysis of the diffraction effects is presented in the following, where the Fresnel Diffraction Integral is used [21].

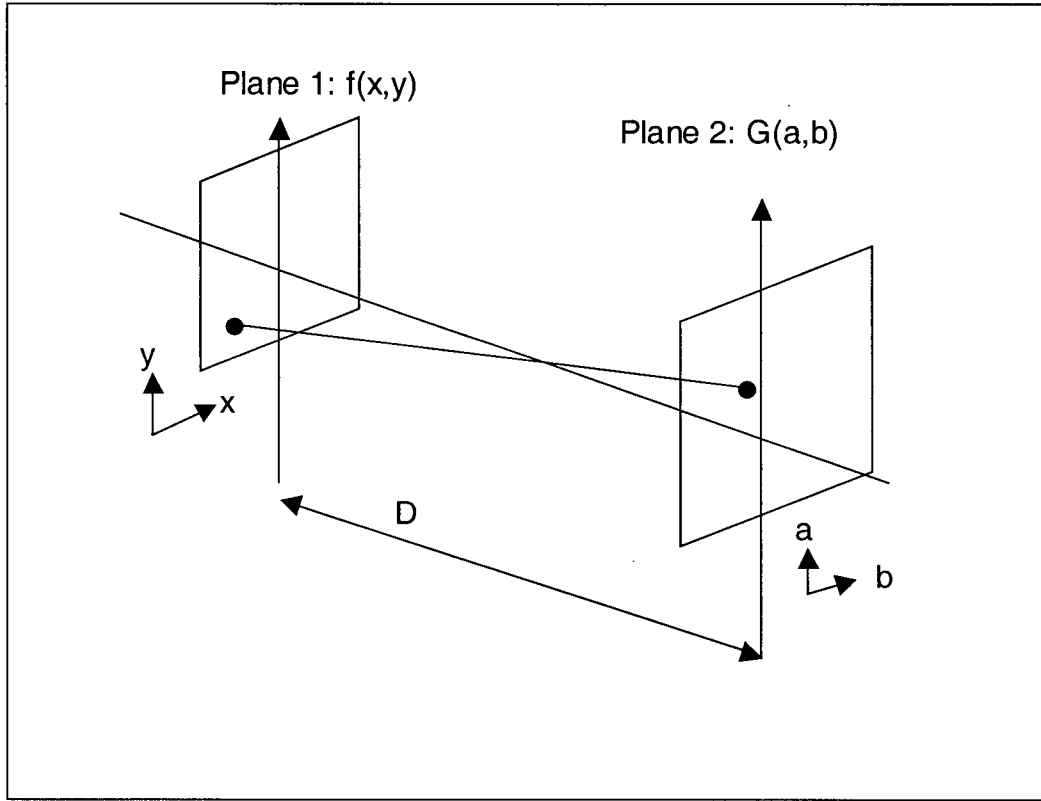


Figure 2-2: Two planes

First, the Fresnel Diffraction Integral describes the diffraction effects by relating the complex-valued distributions located at two planes separated by free space [22]. For Example, in figure 2-2, by using the Fresnel Diffraction Integral, a light distribution $G(a,b)$ in Plane 2 at a distance D can be obtained from the light distribution $f(x,y)$ at plane 1. The following equation is the Fresnel Diffraction Integral [21][22]:

$$G(a,b) = \frac{je^{-jkD}}{\lambda D} \iint f(x,y) e^{-j(\pi/\lambda D)\{(x-a)^2+(y-b)^2\}} dx dy \quad (2.8)$$

where $f(x,y)$ represents the light distribution in plane 1 and $G(a,b)$ is the light distribution of plane 2 at a distance D along the propagation path. The exponential term inside the double integral represents the phase change through the path. Since amplitude is

inversely proportional to the path distance, the amplitude can be approximated by $1/D$. λ is the scaling factor that accounts for the wavelength of the light. Because the phase accumulation is present along the path and does not affect the final result, the first exponential term, which is the phase accumulation, is ignored. Therefore, for a one-dimensional light distribution function, the Fresnel Diffraction Integral can be reduced to [17]

$$G(q) = \sqrt{\frac{j}{\lambda D}} \int f(p) e^{-j(\pi/\lambda D)(p-q)^2} dp \quad (2.9)$$

where p is our one-dimensional variable, i.e. either x or y in plane 1 and q is our one-dimensional variable, i.e. a or b in the plane2.

Now, we can apply equation 2.9 to describe light propagation after exiting the end facet of the waveguide in a TNFIPM system. First, we can represent the light distributions along the propagation path as shown in figure 2-3 where $k(q)$ is the focused intensity profile of $f(p)$, the intensity profile at the end facet of a waveguide, and $g(u)$ and $h(u)$ are the distribution functions of the beam before and after passing through a lens.

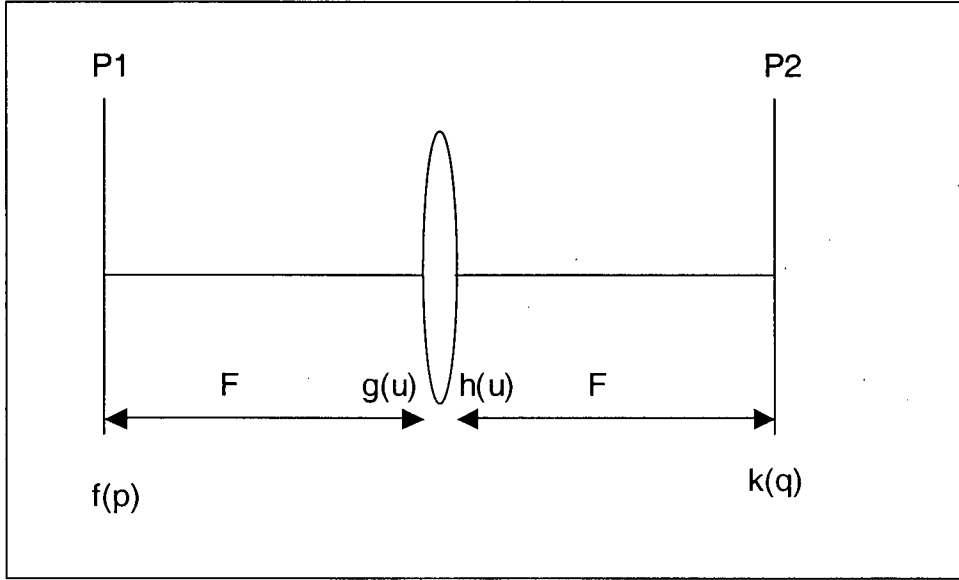


Figure 2-3: Fourier Transform System

Applying equation 2.9, the one-dimensional Fresnel Diffraction Integral, to $f(p)$ and $h(u)$, $g(u)$ and $k(q)$ can be expressed as

$$g(u) = \sqrt{\frac{j}{\lambda D}} \int f(p) e^{-j(\pi/\lambda D)(p-u)^2} dp \quad (2.10)$$

$$k(q) = \sqrt{\frac{j}{\lambda D}} \int h(u) e^{-j(\pi/\lambda D)(u-q)^2} du \quad (2.11)$$

In addition to the Fresnel Diffraction Integral, a lens transformation can be used to relate the light distribution $h(u)$ from $g(u)$ as described by [20]

$$h(u) = g(u) e^{\frac{ju^2}{\lambda F}} \quad (2.12)$$

where F is the focal length of the lens.

After collecting all the exponential terms in equations (2.10), (2.11) and (2.12) and through a change of variables, one can describe the focused intensity profile of a waveguide by a Fourier Transform,

$$k(q) = \sqrt{\frac{j}{\lambda F}} \int f(p) e^{\frac{j2\pi pq}{\lambda F}} dp \quad (2.13)$$

where $f(p)$ is the intensity profile at the end facet of a waveguide. Therefore, theoretically, $f(p)$ can be obtained by applying an inverse Fourier Transform of focused intensity profile, $k(q)$.

In order to apply the inverse Fourier Transform of $k(q)$, both amplitude and phase information of the focused intensity profile of the waveguide are required. However, for a TNFIPM system, the only information available is the amplitude, intensity, of the profile of $k(q)$. Thus, the essential information, the phase cannot be obtained. Therefore, it is impossible to analytically recover the original intensity profile of a waveguide, $f(p)$. This problem is referred to as “The phase problem” [23].

Although an analytical solution is not possible, there are many techniques for recovering the phase information: phase closure, phase averaging, shift and add, and iteration [23]. One method, which is implemented in our experiment, is the iterative method where an iterative search is performed to find an intensity profile that produces a focused intensity profile that matches the experimentally measured one. To start the iterative search, one can construct an initial guess of the intensity profile exiting the end facet of the waveguide with some a-priori knowledge of the waveguide. Then, the intensity profile of the waveguide in the image-plane can be calculated by applying the Fourier Transform to this initial guess of the original intensity profile. Comparing the calculated intensity profile in the image-plane with the profile obtained experimentally, one can produce an error function, which is used to adjust the next guess for the intensity profile at the end

facet of the waveguide. This process is repeated until a good match between the calculated and experimental focused intensity profiles is obtained.

2.4 Aberrations

In addition to the diffraction effects, the aberration of the images due to a lens system can also dramatically change the intensity profile in the image-plane, making it not suitable for obtaining the final index profile of a waveguide. Aberration effects can be analysed under paraxial and ray tracing theory [24]. They are mainly due to the geometry or the ray path differences of a lens. The following is a discussion of some of the major types of aberrations and the techniques implemented to address their affects on the measurements[25]:

1. **Spherical Aberration:** This defect is mainly due to the curvature of the lens. Light passing through different locations of a lens is refracted at different angles, which can produce multiple focal points along an axis of a lens. For example, wave passing through the centre of a lens is refracted slightly and can not brought in to the same focal point with wave passing through the peripheral of a lens, which is refracted at a much greater degree. However, with careful design of the curvature of a lens, this aberration can be eliminated. Aspheric lenses are specially designed to correct this problem, and were chosen for our experiment.

2. **Chromatic Aberration:** Chromatic Aberration is caused by the change of the refractive index of the lens for different light wavelength. The refractive index of every optical glass formula changes with wavelength. When light passes through a lens system, different wavelength components of a light are refracted different. Since TNFIPM only uses monochromatic light, this aberration is not a concern.
3. **Comatic aberration:** This aberration is mainly encountered in the off-axis systems and is most severe when the lens is out of alignment. It can make the image of a point become asymmetrical. This aberration can be minimized by careful alignment of the optical system. Here we used a visible laser to assist in the precise alignment of the lens.

2.5 Gaussian Beam Equations

Instead of the lensmaker's equation, the Gaussian Beam equations are used in our proposed TNFIPM to calculate the original mode size of the waveguide under study. The output of a waveguide coupled with a laser source is better described using Gaussian Beam equations since they incorporate the diffraction effects of a laser beam in an optical system right from beginning [26][27]. Thus, the magnification of an optical system calculated using Gaussian Beam equations is much more accurate than the one using the lensmaker's formula. In this section, brief descriptions of a Gaussian beam and the magnification equations employed in our algorithm are provided.

In reality, Gaussian beams either converge or they diverge from a region where the beam is the smallest. The amount of divergence or convergence is measured by the full angle beam divergence, θ . In geometrical optics, a Gaussian beam should focus to a point, but, because of the diffraction, the beam can only reach a minimum size, d_0 , the beam waist diameter. d_0 is the distance between two points on the opposite side of the maximum value where the power drops to $1/e^2$. The region where the beam stays less than $\sqrt{2}d_0$ is called the Rayleigh range. The beam waist diameter, d_0 , and the Rayleigh range, Z_r , are described as [27]

$$d_0 = \frac{4\lambda}{\pi\theta} \quad (2.14)$$

and

$$Z_r = \frac{d_0}{\theta} = \frac{4\lambda}{\pi\theta^2} \quad (2.15)$$

where θ is the beam divergence angle.

Although the Gaussian beam equation can describe the magnification of the intensity profile obtained from TNFIPM more accurately, some equations from geometrical optics are good approximations in order to choose the appropriate lens and waist location for an optical system. In fact, for Gaussian beams, there exists an equivalent equation to the thin lens equation [26]. Instead of size and distance to the central plane of the object and image, the Gaussian beam equation utilizes the beam waist diameter and the distance from the beam waist location to the focal point of a lens. Figure 2-4 shows a Gaussian beam passing through a lens.

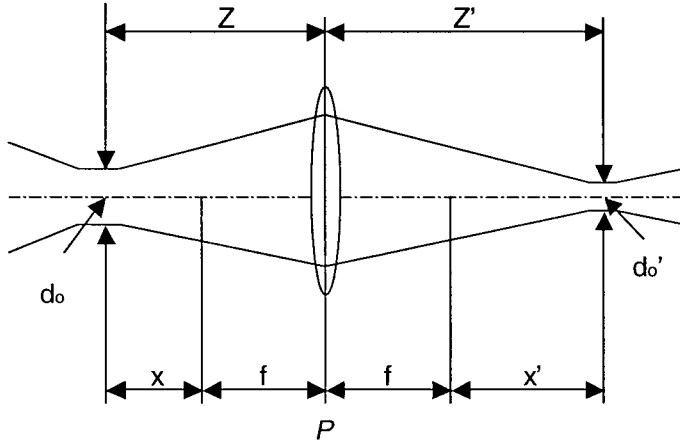


Figure 2-4: Gaussian beam passing through a lens

The equation used to calculate the magnification of a Gaussian beam is [26]

$$\frac{Z-f}{Z'-f} = \frac{d_0^2}{d_0'^2} = \frac{1}{M^2} \quad (2.16)$$

where f is the focus length of the lens, Z is the distance from the input waist to the central plane, P , of the lens, Z' is the distance from the central plane to the image plane, d_0 is the input beam waist, d_0' is the beam waist in the image plane, and M is the magnification.

In our proposed improved TNFIPM, equation 2.16 is employed to obtain the magnification associated with the acquired profiles in the image-plane. Z is the distance from the location of the end facet of the waveguide to the principal plane P of the lens. Z' is the distance from the principal plane P of the lens to the beam waist of the image, which is the location of the photo-detector. If we examine the variables in equation 2.16, the only unknown variable is d_0 , the mode size of the waveguide (here we substitute the mode size for the beam waist diameter). However, Z is very difficult to measure with high accuracy without knowing the location of the central plane of the lens. This problem

can be solved by placing the sample waveguide in two different locations and taking two sets of measurements. For the first set of measurements, equation 2.16 can be applied without any modification. However, for the second set of measurements, by substituting Z with $X+\Delta X$ in equation 2.16, it becomes

$$\frac{X + \Delta X - f}{Z' - f} = \frac{d_0^2}{d_0'^2} \quad (2.19)$$

where X equals Z of the first set of measurements and ΔX equals to the difference between the two waveguide locations, which can be measured precisely with a micropositioner. Then we have two equations with two unknowns, Z and d_0 , which can be calculated with much higher accuracy. In reality, these measurement values are very small and sensitive to any small noise in our experiment. Therefore, to avoid any errors in our measurements, more than 2 sets of data are required to obtain the correct d_0 , the original mode size.

2.6 Savitzky-Golay Smoothing Filter

The intensity profiles obtained from the data processing unit using TNFIPM usually contain significant high frequency noise, which is dramatically amplified due to the second derivative term in the inverse wave equation. This is the reason that before applying equation 2.7, the inverse wave equation, to the intensity profiles obtained experimentally, it is imperative to apply a filter to remove noise from measurements. Although there are many types of digital filters that can effectively eliminate high frequency components in the signal, unfortunately, they also, typically, affect the

intensity profile, especially if it contains a sharply falling edge such as occurs at a refractive index discontinuity or boundary. Therefore, in our proposed algorithm, the Savitzky-Golay filter is chosen for our numerical smoothing filter not only because of its computation efficiency in removing high-frequency noise but also because of its capacity to preserve sharp edges [28].

The Savitzky-Golay filter, also called the least-square smoothing filter, is a moving window average filter using polynomials in which the coefficients are chosen to minimize the least-square errors. Its operation is similar to the moving-window-averaging filter, a popular filter that can preserve the higher frequency components, however, moving-window-averaging filters have coefficients of equal weight for each point in the window which can reduce the sharpness of the peak of a profile for large size windows [29]. On the other hand, the Savitzky-Golay filter's coefficients change dynamically depending on the data values within a window. These coefficients can minimize the least-square errors for the data points within the window around a particular point. Everytime the window is shifted to the next data point, these coefficients are changed according to the data values and the chosen polynomial degree. This polynomial fitting around the data set is how a Savitzky-Golay filter can be designed to preserve the peaks in a profile.

Figure 2-5 shows a noisy signal, figure 2-5 (a), and two filtered signals, figures 2-5 (b) and (c). Figure 2-5 (b) is the signal filtered with a equal-weighting coefficients moving window averaging filter and figure 2-5 (c) is the signal filtered with the Savitzky-Golay filter. Both filters have the same window size of 25 points. If we compare figures 2-5 (b)

and (c), the peaks of the filtered signal in figure 2-5 (b) are reduced and smoothed out compared to the Savitzky-Golay filtered signal shown in figure 2-5 (c) . Even though the peaks of the signal are preserved in the Savitzky-Golay filtered signal, the noise level is seen to be slightly larger than in the signal filtered with the moving-window-averaging filter. However, for a moving-widow-averaging filter to achieve the same effectiveness in preseving the peaks as shown in figure 2-5 (d), the window size is much reduced and the noise is much worse than the signal filtered with the Savitzky-Golay filter. Therefore, the Savitzky-Golay filter provides a good trade-off for perserving the peaks of a profile and removing noise.

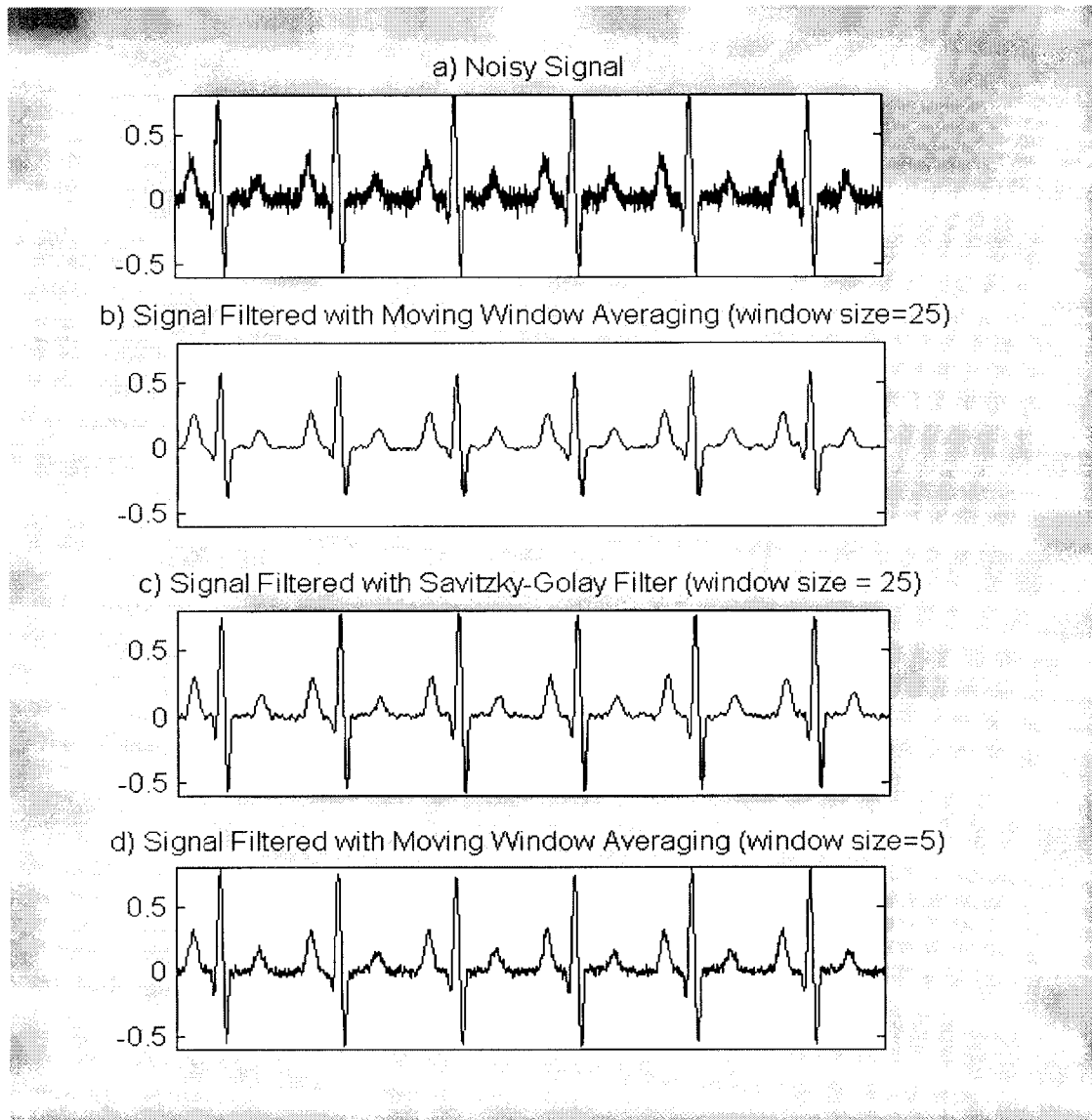


Figure 2-5: Filter performance comparison for Moving Window Averaging Filter (with equal-weighting coefficients) and the Savitzky-Golay Filter

The Savitzky-Golay filter algorithm is based on finding a least-squares best fit polynomial, of degree d , to a set of data with a window size of $2n+1$ [28][29]. For each point p in the samples, the window covers a set of data of size $2n+1$ with its center at p . The coefficients are chosen so that they provide the best least-square fit with a polynomial of degree d to this set of data. Then we replace the value p with the fitted value in the polynomial function at point p .

Although finding the least-square fit polynomial can be computationally intense, Savitzky and Golay showed that a set of integers could be derived as weighting coefficients to carry out the smoothing operation. These integers are called "convolution integers", which turn out to be exactly equivalent to fitting the data to a polynomial, and significantly reduce the computation time [30][31]. In appendix A, discussion of the derivation of these "convolution integers" taken from *"Introduction to Signal Processing"* by S. J. Orfanidis[28], is given.

2.7 Morphing Algorithm

Although the transverse refractive index profile of a longitudinally invariant waveguide can be calculated from TNFIPM, due to the amplification effect of the second derivative on the noise in the intensity profile, there can still be some differences between the actual index profile and the one obtained from TNFIPM. There are methods, like the effective index method and the inverse WKB method [2][3][4], for predicting the shape of the index profile, however, they either require accurate effective index or they are limited to certain uses [5]. A common method to solve this problem is to fit a typical index distribution function to the profile obtained from TNFIPM [6][7][10][14] but this will eliminate the possibility of finding index profiles with different types of distribution. For example, Gaussian functions are commonly assumed for a diffused waveguide [6][10]. However, due to the material defects and/or fabrication parameters, the index profile of the waveguide may not be perfectly Gaussian. This would impede any other potential

function that can better describe the actual index profile to be found. Here, we employ a simple morphing algorithm to find the best matching index profile function that can be used to describe the actual index profile.

First, one lists all of the functions that are typically used to describe the types of the waveguide under study. From the list, two of the functions are randomly selected and fitted to the predicted index profile obtained previously. Then the index profile is fitted to one function and gradually morphed it into another function to which the index profile has also been fitted. During the morphing process, the profile is divided into different sections. Then, each section is modified to generate a number of new index profiles. For every index profile produced during the morphing process, the corresponding optical intensity profile at the end-facet of the waveguide is calculated. This process is repeated for every possible combination of pair functions in the list. The index profile that produces the best matching mode profile to the actual mode profile is then taken to be the actual index profile. A more detailed description of the morphing procedures is described in the next chapter, Algorithm.

One of the disadvantages of this morphing algorithm is that it tends to generate a large amount of index profiles to be simulated. For example, figure 2-6 shows some of the functions that are typically used to describe a single mode waveguide. From this list, we can generate 21 possible pairs of functions to be morphed from one to another. If the curve of each index profile was divided into middle and outer sections and for each section, 5 different curves are used during the morphing process, there will be 25

different combinations of index profiles to be simulated for each pair. In addition, this procedure should be performed for the index profile in two transverse directions of the waveguide. Therefore, the number of different index profiles to be simulated for each pair of functions becomes 625, which makes the total number of index profiles to be simulated to be 13125. With the minimum computation time of 5 minutes for calculating the mode profile, it would take at least 45 days to find the best matching index profile. Therefore, an efficient mode solver is required or the number of functions used must be restricted to only a few types.

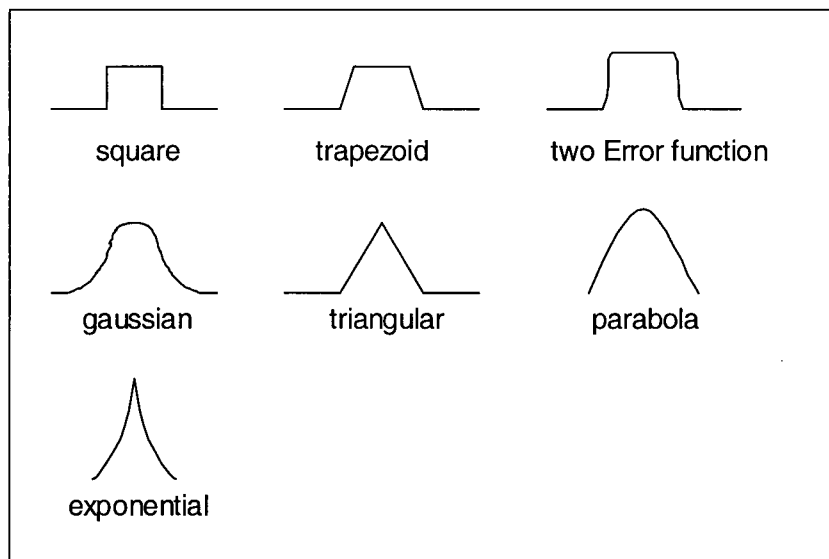


Figure 2-6: some of the possible refractive index functions for single mode waveguide

To find the index profile that produces the best matching intensity profile at the end facet of the waveguide, the Beam Propagation Method (BPM) is used to simulate beam travel through a longitudinally invariant waveguide with a particular transverse refractive index profile. BPM is the most widely used propagation technique for modeling integrated optics and fiber optic devices due to its simplicity and efficiency while still yielding very

accurate results. The main reason for choosing BPM for our application, besides its efficiency, is its limited input requirements. The simulated field at the end facet of a waveguide only depends on two main factors: the input field and the refractive index profile of the waveguide. Since the light source is a laser coupled with a single mode fiber, the input field can be approximated with a Gaussian function. The refractive index profiles obtained from our morphing algorithm are fed into the BPM to obtain the field intensity profiles at the end facet of the waveguide for each morphed index profile. Then, each of these intensity profiles output from the BPM is compared against the diffraction reduced intensity profile to determine whether the index profile fed into the BPM is the actual index profile of the waveguide. Accuracy of the BPM is proven to be crucial in our proposed TNFIPM algorithm in obtaining a valid result. However, even though the BPM is one of the efficient methods for mode modeling, due to the large amount of index functions produced from the morphing algorithm, we have to limit the number of morphing functions so we can obtain the result in a reasonable timeframe. A more detailed discussion of the BPM taken from the BPMpropTM manual is presented in Appendix B.

2.8 Conclusion

The main features and improvements of our proposed TNFIPM were presented in this chapter. To summarize, the diffraction effects on the focused intensity profile, a serious effect ignored in many published papers, was analyzed and considered in our proposed TNFIPM. We also took into account the aberration effects in the experimental setup,

which can dramatically distort the experimental intensity profile. In addition to the image distortions from diffraction and aberrations, Gaussian beam equations, instead of the lensmaker's equation, were used to accurately calculate the magnification of the lens system. Due to the second derivative term in the inverse wave equation in TNFIPM, any noise in our intensity profile will be amplified. Therefore, the Savitzky-Golay filter, an effective filter that provides a good trade-off between preserving the sharp edges and removing noise, was applied to eliminate the noise in the intensity profile in the image-plane. Finally, different from the common approach of fitting a known function to the index profile obtained from TNIFPM, a morphing algorithm that made use of the BPM was included to find the best function that can be used to describe the actual index profile.

Chapter 3: Algorithm

3.1 Introduction

The theory of the TNFIPM and the proposed improvements have been introduced in the previous chapter. In this chapter we describe the entire proposed TNFIPM incorporating those improvements. Figure 3-1 shows a flowchart of our proposed TNFIPM. The algorithm starts by acquiring the intensity profiles in the image plane. The noise in these profiles are removed by the Savitzky-Golay filter. Using the calculated lens magnification and the obtained system model, the diffraction-reduction algorithm eliminates the diffraction effects on the image-plane intensity profile and obtains the intensity profile at the end-facet of the waveguide. Applying the inverse wave equation to the profile, the initial estimate of the refractive index profile of the waveguide can be obtained. Furthermore, the morphing algorithm is applied to improve the accuracy of the final result.

The proposed improved TNFIPM can be subdivided into two main algorithms, the diffraction-reduction algorithm and the morphing algorithm, which are discussed in sections 3.2 and 3.5, respectively. The procedures to obtain the diffraction reduced intensity profile from the image-plane intensity profile are described in section 3.2. These

include calculating the magnification of the lens system, filtering the noisy signals, and converging to the diffraction reduced profile through the iterative method described in section 2.3. The iterative method modifies the predicted intensity profile at the end-facet of the waveguide based on the result of the comparison between the simulated intensity profiles and the experimental intensity profiles. Therefore, section 3.3 is added to discuss the criteria of the comparison, which are required for the feedback in the iterative

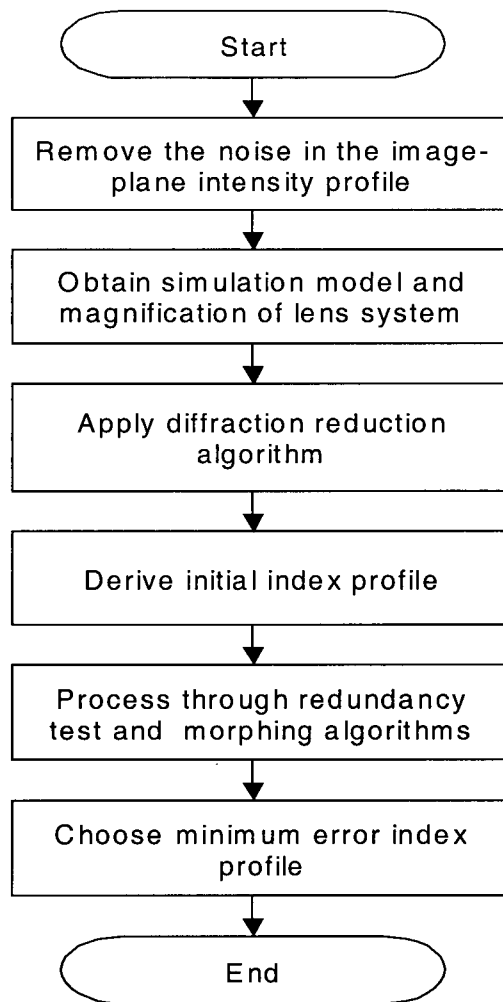


Figure 3-1: Flow Chart of the Proposed TNFIPM

method. After obtaining the diffraction reduced profile representing the intensity profile at the end-facet of the waveguide, the next step, which is described in section 3.4, is to

derive the initial guess of the index profile using the inverse wave equation. In section 3.5, an *ad hoc* morphing algorithm which uses BeamPROPTM to simulate the light traveling through a longitudinally invariant waveguide is presented. This morphing algorithm will produce a set of index profiles from which the refractive index profile with minimum errors is taken to be our final index profile.

3.2 Diffraction-Reduction Algorithm

In this section, the procedures for obtaining the diffraction reduced intensity profile at the end facet of the waveguide are presented. The image-plane intensity profile obtained experimentally cannot be applied directly to the inverse wave equation since the diffraction in the profile can render the result inaccurate as described in Section 2.3. The inverse wave equation can only derive an accurate index profile if the applied intensity profile is the intensity profile at the end-facet of the waveguide. Therefore, the diffraction-reduction algorithm discussed in this section is employed to obtain the intensity profile at the end-facet of the waveguide, which involves not just removing the diffraction effects in the image-plane intensity profile but also obtaining the magnification and a simulation model for the lens system.

Before describing our algorithm, let's define the coordinates of the intensity profiles along the transverse direction as the x and y directions as shown in figure 3-2. Using the cutting-knife edge technique, the focused intensity profiles in the image plane along the x and y directions (see figure 3-4-a and figure 3-4-b) are obtained by taking the derivative

of the accumulated intensity profile along the x and y directions. The goal of the diffraction-reduction algorithm is to find the intensity profile at the end-facet of the waveguide from the image-plane intensity profile. A flowchart detailing steps for the diffraction-reduction algorithm is shown in figure 3-3.

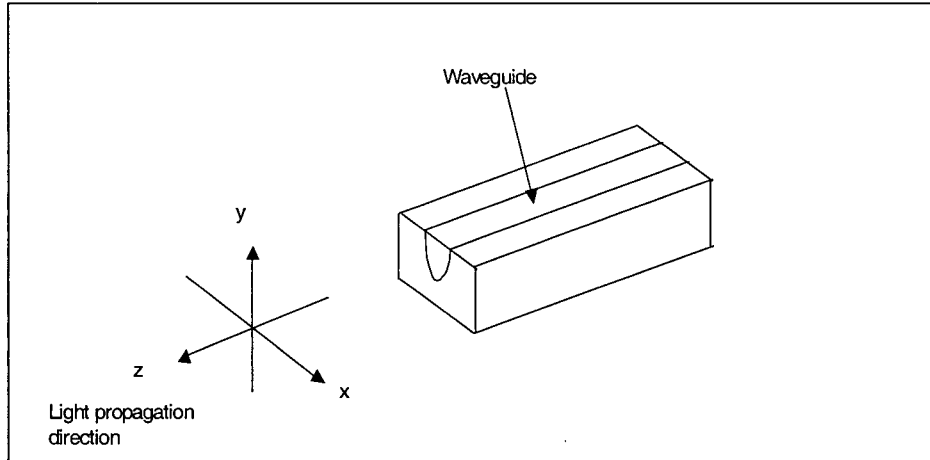


Figure 3-2: Coordinates definition for the waveguide under study

After obtaining the image-plane intensity profile, the first step of our diffraction-reduction algorithm is to remove noise in the profile by applying the Savitzky-Golay filter. Then, the iterative method as discussed in section 2.3 is used to recover the intensity profile from the diffraction affected image-plane intensity profile. One of the important required elements of the iterative method is the software simulation program which is used to simulate light propagating through a lens system and to obtain the simulated image-plane intensity profile for comparison. For our experiment, CodeVTM, a software package, is employed.

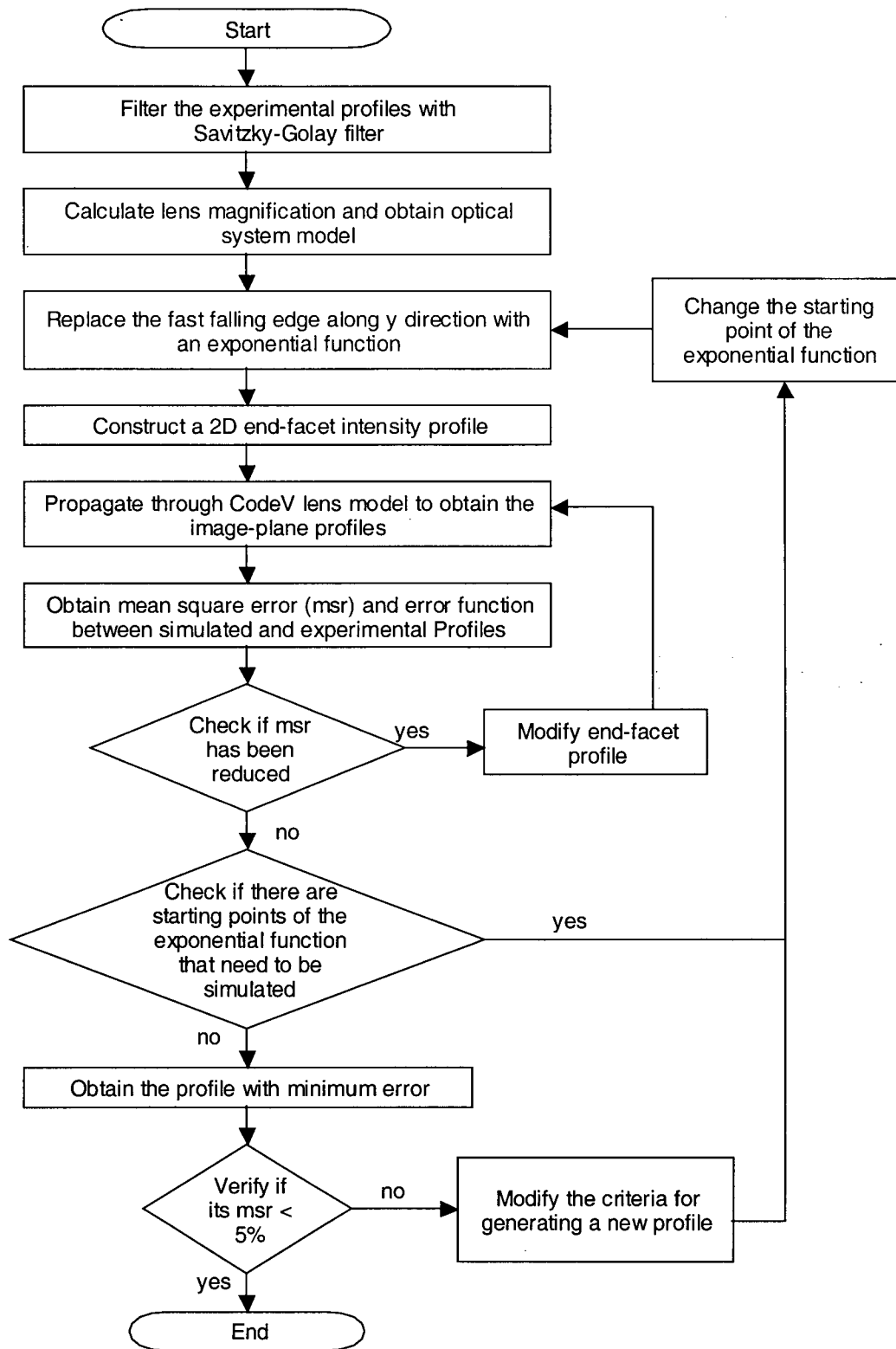


Figure 3-3: Diffraction-Reduction Algorithm

In order to construct an accurate simulation model in CodeVTM, we need the detailed lens data, the magnification of the image, and the locations of the lens, detector, and waveguide. First, the lens data is available through the lens vendor. Second, by using Gaussian Beam equations as discussed in section 2.5, the magnification of the image and the locations of the detector and the waveguide can be determined. After obtaining the magnification of the lens system, we implement the lens system model accurately in CodeVTM and we can also have a good estimate of the size of the intensity profile at the end-facet of the waveguide. The size information is important for obtaining the first guess of the diffraction reduced intensity profile, which is used as the input to our iterative method.

The first step of our iterative method is to obtain the first predicted intensity profile at the end-facet of the waveguide. Using the calculated lens magnification, the experimental image-plane intensity profiles along the x and y directions are scaled to the size of the end-facet intensity profiles. By simply scaling, the diffraction effects is not removed and these end-facet intensity profiles still have the shape of the image-plane intensity profiles with diffraction. Therefore, in order to reduce the number of iterations for finding the diffraction-reduced profiles, some modifications may be required before propagating these end-facet intensity profiles into our CodeVTM system. If one portion of a profile is severely affected, it is replaced with the appropriate curves using *a priori* knowledge of the waveguide under study. For example, in a titanium-diffused waveguide used in our experiment, the intensity profile should be a symmetric function (with a shape similar to

a Gaussian function) as shown in the figure 3-4-a. On the other hand, the intensity profile along the y direction should be an asymmetric function with a rapidly falling edge, due to the discontinuity at the boundary, and a gently falling edge as shown in figure 3-4-b. However, in figure 3-4-b, due to the diffraction effects as discussed in section 2.3, the rapidly falling edge of the image-plane intensity profile along the y direction is smoothed out and amplified significantly, i.e., it is not as rapidly falling as it should be.

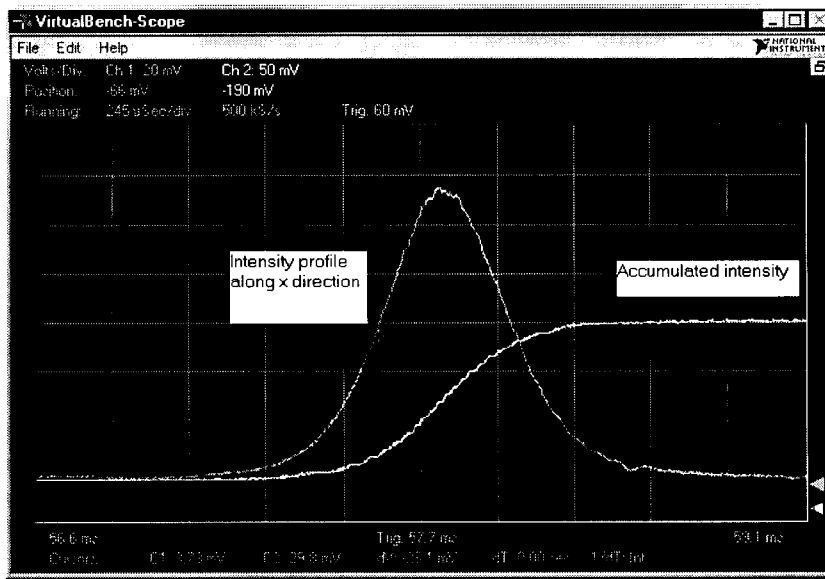


Figure 3-4-a: Intensity profile along the x direction of a Ti:LiNbO₃ diffused waveguide

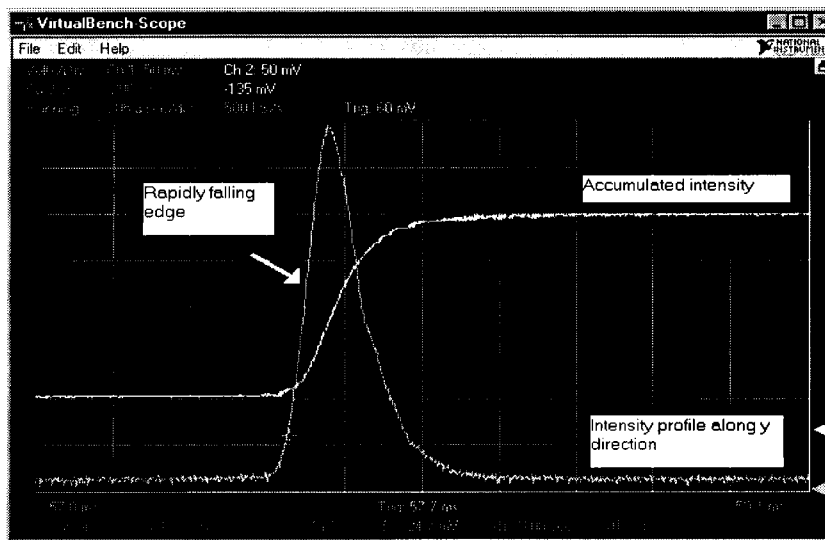


Figure 3-4-b: Intensity profile along the y direction of a Ti:LiNbO₃ diffused waveguide

Therefore, the rapidly falling edge of the intensity profile along the y direction is replaced with an exponentially decaying function f describing the evanescent field above the discontinuity [32], e.g., the interface of a titanium diffused lithium niobate waveguide and an optical buffer layer.

$$f(d) = E_0 \exp\left(-\frac{2\pi}{\lambda_0} \sqrt{(n_{eff}^2 - n_s^2)} d\right) \quad 3-2$$

where n_{eff} is the effective index of a waveguide, n_s is the superstrate refractive index, d is the distance to the interface, λ_0 is the free-space wavelength, and E_0 is the field at the starting location of f , i.e., at $d=0$. Due to the diffraction effects, the starting location of f can be anywhere above the maximum intensity point to the left portion of the figure 3-4-b. For the first guess of the end-facet intensity profile, the maximum intensity point is chosen to be the starting location of f . After replacing the rapidly falling edge of the intensity profile along the y direction with f , the new intensity profile along the y direction and the scaled intensity profile along the x direction are used as the first predicted intensity profiles at the end-facet of the waveguide.

After propagating the predicted end-facet intensity profiles in CodeVTM, the associated image-plane intensity profiles along the x and y directions are obtained. Then the iterative method needs to converge to the intensity profile that produces the minimum discrepancy between its image and the measured profiles. The method employed here is first to select a few positions (typically 8 to 12) above the maximum intensity point where the exponentially decaying function, f , can be placed. Then, for each of the exponential decaying functions, f , the predicted end-facet intensity profiles are modified until

modification cannot yield lower errors. The modifications are based on the error function between the simulated and the measured image-plane intensity profiles. Next, we adjust the end-facet profiles using the difference between the simulated image and the measured profile. However, after a few iterations, when changing the predicted near-field intensity profile using the error function cannot decrease the error, it has converged to the final image for this particular starting point of f . This procedure is repeated for every starting location of the exponential function. If the predicted end-facet intensity profile whose image has the minimum error has the mean square error less than 5%, it is taken to be our final diffraction reduced profile representing the end-facet intensity profile of the waveguide. If the error is not acceptable, the criteria for modifying the end-facet intensity profile is modified and the whole process is repeated until the final mean square error is less than 5%. The Savitzky-Golay filter is then applied to this final profile to eliminate any sharp changes due to our piecewise error adjustments during the modification process.

3.3 Curve Comparison Criteria and Generation of Predicted Profile

After propagating the predicted intensity profile through the optical system model in CodeVTM, the simulated image-plane intensity profile is compared with the image-plane intensity profile obtained experimentally. This section describes in detail the criteria we used to generate the error function and the new predicted profile.

Once the predicted intensity profile is propagated through the CodeVTM model, an image-plane two-dimensional intensity profile is constructed. It is then integrated to produce the accumulated intensity profiles along the x and y directions, which are used to compare with the accumulated experimental intensity profile, which is produced by the cutting knife edge technique. The comparison between two profiles is only performed in the region within the waists where the intensity is stronger. The reason is that the region with weaker intensity in the measured profile is more sensitive to noise, therefore, it has much less accuracy than the region chosen. In addition, the higher intensity portion of the profile contributes more to the diffraction effects on the image-plane image than the portion of the profile with weaker intensity.

Due to the limitation of the simulation software, the output resolution from the simulation cannot match exactly to the sampling resolution of our experiment. Although the measured profiles have much higher sampling frequency, not all of the output points of the simulated profile can be matched exactly to a point in the experimental profile. Therefore, a 2nd degree polynomial function is fitted to the measured profiles so that for each point in the simulated intensity profile an equivalent point can be calculated from the fitted polynomial function.

The difference between the simulated profiles and experimental profiles for every sample point within the waists is recorded to produce an error function. This error function can later be used to generate a new predicted end-facet intensity profile. In addition, to

determine the quality of the matching between the simulated and measured intensity profiles, the mean square error of the error function is calculated for each comparison.

To generate a new predicted intensity profile, the changes that need to be made to each sample point of the predicted intensity profile are obtained from the error function. After we have modified the portion of the predicted intensity profile within the waist, the left and right portions of the intensity profile outside of the waist locations are scaled to avoid a sharp edge at the junction. Then this new modified predicted intensity profile can be propagated to generate a new image-plane intensity profile. If the mean square error of the new simulated profile is lower, the process is repeated. However, if the mean square error of the present simulated profile is higher than the previous iteration, it means that the present modification overcorrected the diffraction effects and the previous predicted intensity profile is our best predicted profile. At the end of the diffraction-reduction algorithm, one needs to verify whether the final mean square error result from the profile comparison is satisfactory. If the matching is not satisfactory, the whole process is repeated with different methods of generating the new predicted profile. For example, the new predicted profile can be generated for either x or y directions in each repetition. Another example is to change the type of function employed to adjust for the difference in sampling resolutions during generation of the error function. This process is repeated until the final predicted profile can produce an image-plane intensity profile that matches the experimental intensity profile with less than 5% mean square error.

3.4 Deriving the Refractive Index Profile

By using the diffraction-reduction algorithm as described in sections 3.2 and 3.3, the predicted intensity profile at the end-facet of the waveguide can be obtained from the image-plane intensity profile. Even though the best effort has been employed to minimize the noise in the intensity profile, due to the nature of the second derivative in the inverse wave equation, the effect of any residual noise can still significantly distort the result.

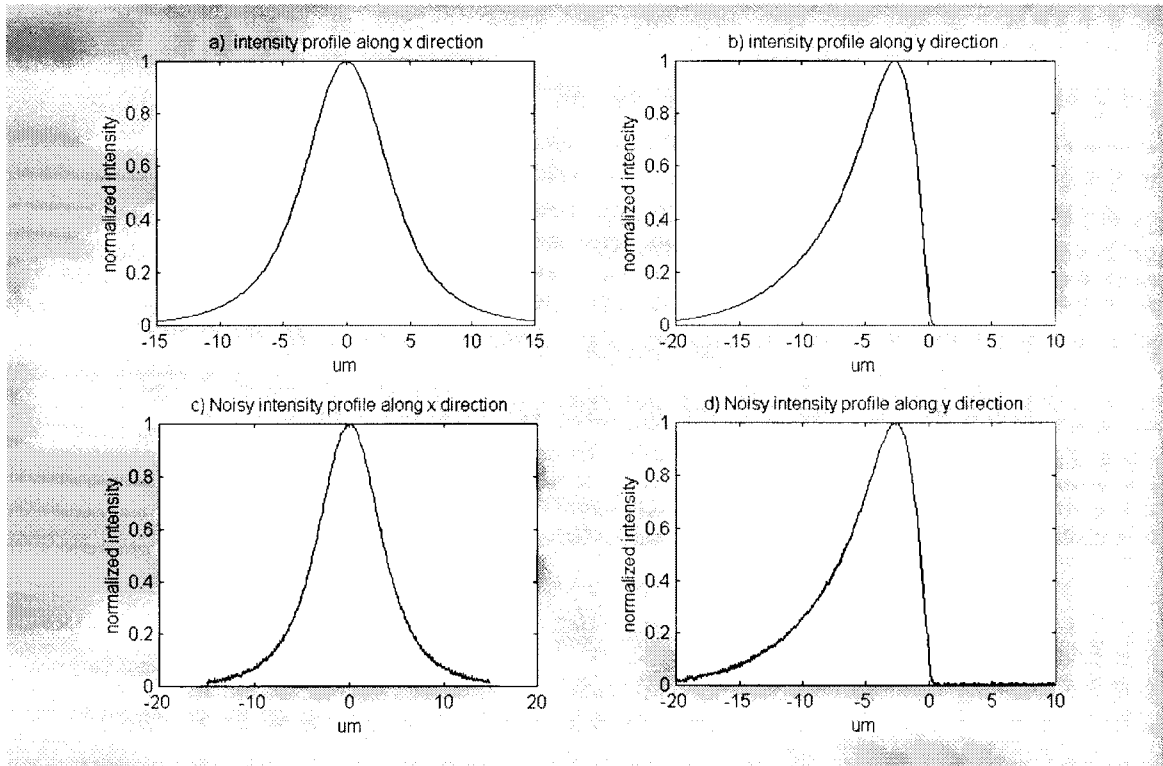


Figure 3-5: Comparison of the original and noisy intensity profiles

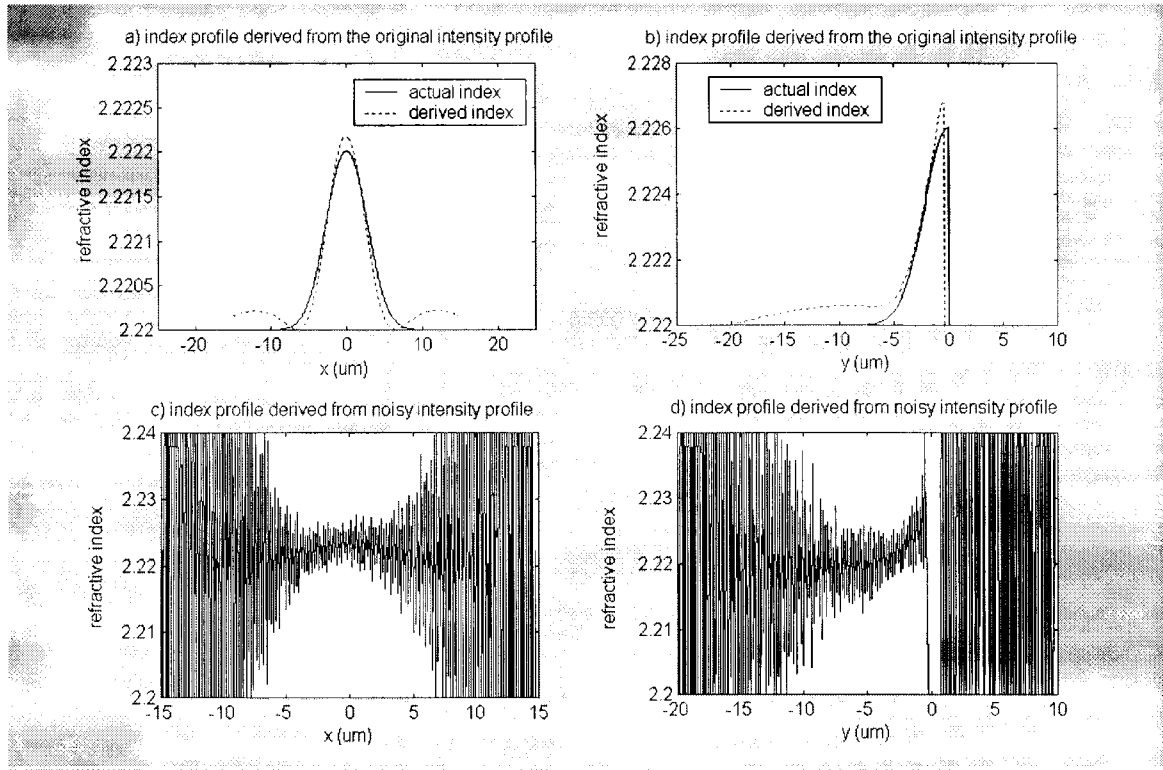


Figure 3-6: Comparison of index profiles derived from the original intensity profile and the filtered noisy intensity profile

Figures 3-5 and 3-6 are used to demonstrate the effect of the noise in the intensity profile to the derived index profiles from the inverse wave equation. Figures 3-5 a) and b) show the normalized intensity profile at the end-facet of a waveguide along the x direction and along the y direction, respectively. To introduce the noise in these profiles, random noise of less than 1% of the maximum intensity is added into these intensity profiles shown in figures 3-5 c) and d). Then a Savitzky-Golay filter is used to filter the random noise in these noisy intensity profiles. Next, in order to demonstrate the effect of any left over noise in the derived index profile, the inverse wave equation is applied to both the original intensity profiles and the Savitzky-Golay filtered profiles as shown in figures 3-6-a) and b) and 3-6-c) and d), respectively. Although the remaining noise is extremely

small in the filtered intensity profile after filtering, the derived index profiles, figures 3-6 c) and d), are still significantly distorted by the left over noise. Again, using a Savitzky-Golay filter the index profile of figures 3-6 c) and d) are filtered to reduce the noise in the derived profiles. Figures 3-7 a) and b) show the index profile of the filtered derived index profile. As can be seen, the profiles are still distorted by the noise, especially in regions far from the core area.

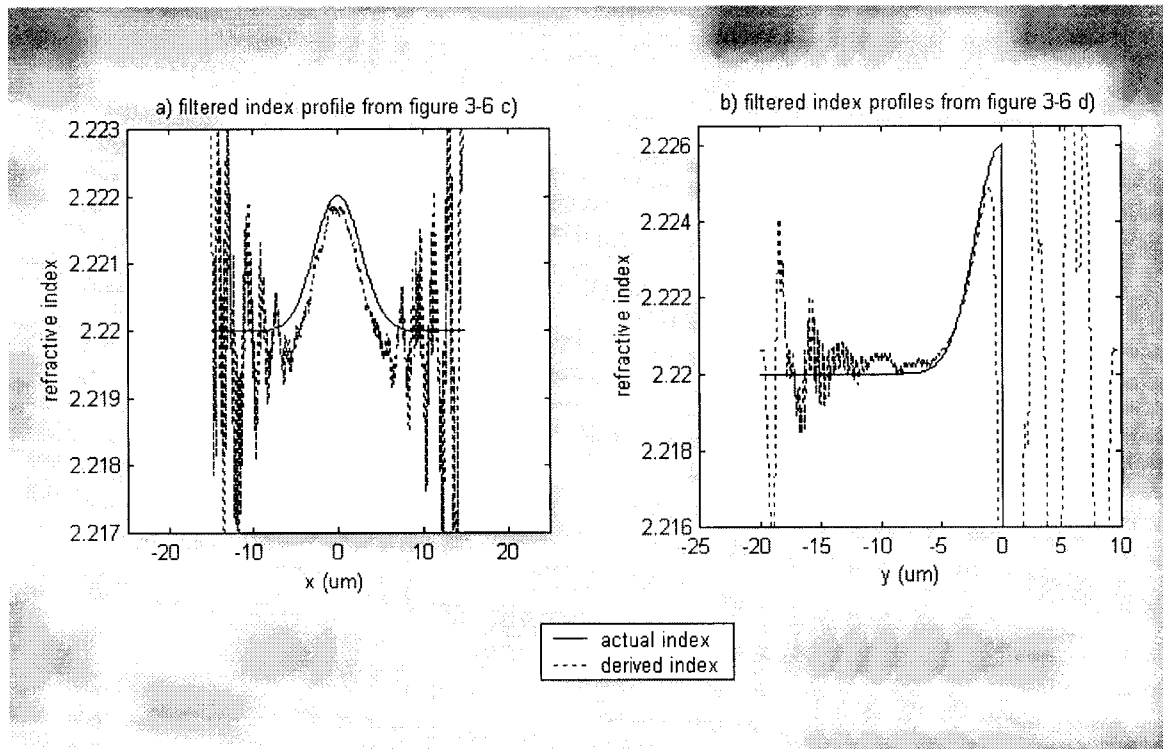


Figure 3-7: Filtered index profiles from figures 3-6 c) and d)

Although the index profile resulting from applying the inverse wave equation to the diffraction reduced intensity profile is not accurate due to the noise, it can be used as the first estimate of the size and magnitude of the index profile. In order to improve the accuracy of our final index profile, first, a redundancy algorithm is applied to obtain a

more accurate estimate of the magnitude and size of the index profile. This is accomplished by varying the magnitude and size of the derived index profiles and comparing the calculated end-facet intensity profiles from these index profiles with the diffraction reduced intensity profile. To obtain an index profile with more accurate shape, a morphing algorithm is required. Figure 3-8 summarizes the major steps required for obtaining the refractive index profile from the diffraction reduced intensity profile.

In section 3.4.1, the procedures for obtaining the first guess of the index profile, which is the combination of the inverse wave equation and the redundancy test algorithm, are provided. Following section 3.4.1, a simple morphing algorithm is discussed in detail in section 3.4.2 where the final index profile is obtained.

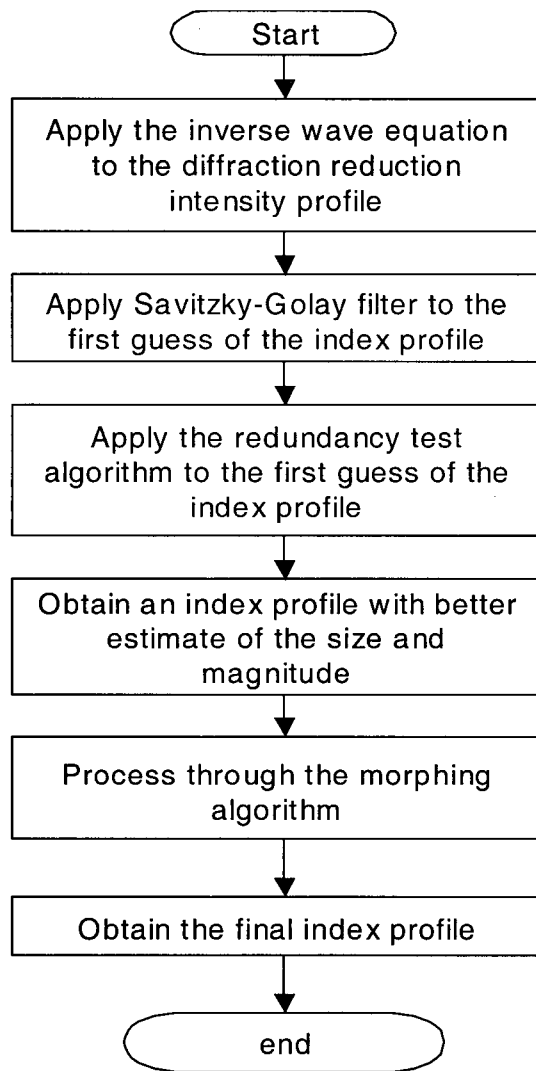


Figure 3-8: A flowchart for obtaining the index profile of the waveguide

3.4.1 Inverse Wave Equation and Redundancy Test Algorithm

The first step to obtain the index profile is to apply the inverse wave equation to the output of the diffraction reduced algorithm as discussed in section 2.2. However, due to the second derivative in the inverse wave equation, any noise or shape edge can significantly distort the resulting index profile. Although a Savitzky-Golay filter is applied to remove some of the noise in the resulting index profile from the inverse wave equation, the residual noise can still affect the accuracy of the index profile, which is shown in the previous section. As was discussed in section 2.2, the derived refractive index in the region far from the core waveguide is used to compare with the substrate refractive index of the waveguide and to adjust the magnitude of the derived index profile. Any noise in this section can be amplified and render the magnitude of the index profile inaccurate. In practice, the diffraction reduced intensity profile usually contains much greater residual noise than the inverse wave equation can allow for. Therefore, it is necessary to apply the redundancy test algorithm to the derived index profile to obtain a more accurate estimate of the magnitude and size of the index profile.

In the redundancy test algorithm, the index profile is chosen from a number of index profiles, whose optical profiles are produced and compared with the diffraction reduced intensity profile. Figure 3-9 shows a flowchart for the redundancy test algorithm. A number of index profiles are generated by varying the magnitude and the size of the index profile derived from the inverse wave equation. Initially, the range of the size and the magnitude of our search is set to be from 80% to 120% of the first guess of the index

profile. Then the intensity profiles at the end-facet of the waveguide can be obtained by modeling the propagation of a Gaussian distributed light source in the waveguide with the index profile. The Beam propagation method (BPM) is used to model the propagation of a Gaussian beam through this refractive index profile. BPM requires two inputs: refractive index profile and the input field distribution. The input field distribution depends on the selected light source. For example, in our experiment a laser source is used as the light source whose field has the characteristic of a Gaussian distribution. The refractive index profile is selected from the set of the index profiles generated from our redundancy test. For each index profile, the corresponding intensity profile at the end-facet of a waveguide can be simulated and compared with the diffraction reduced intensity profile. The profile with the least error is selected to be applied in the morphing algorithm. If the size or the magnitude of the index profile with the minimum error lies at the boundary of our search range, the range is modified and the process is repeated.

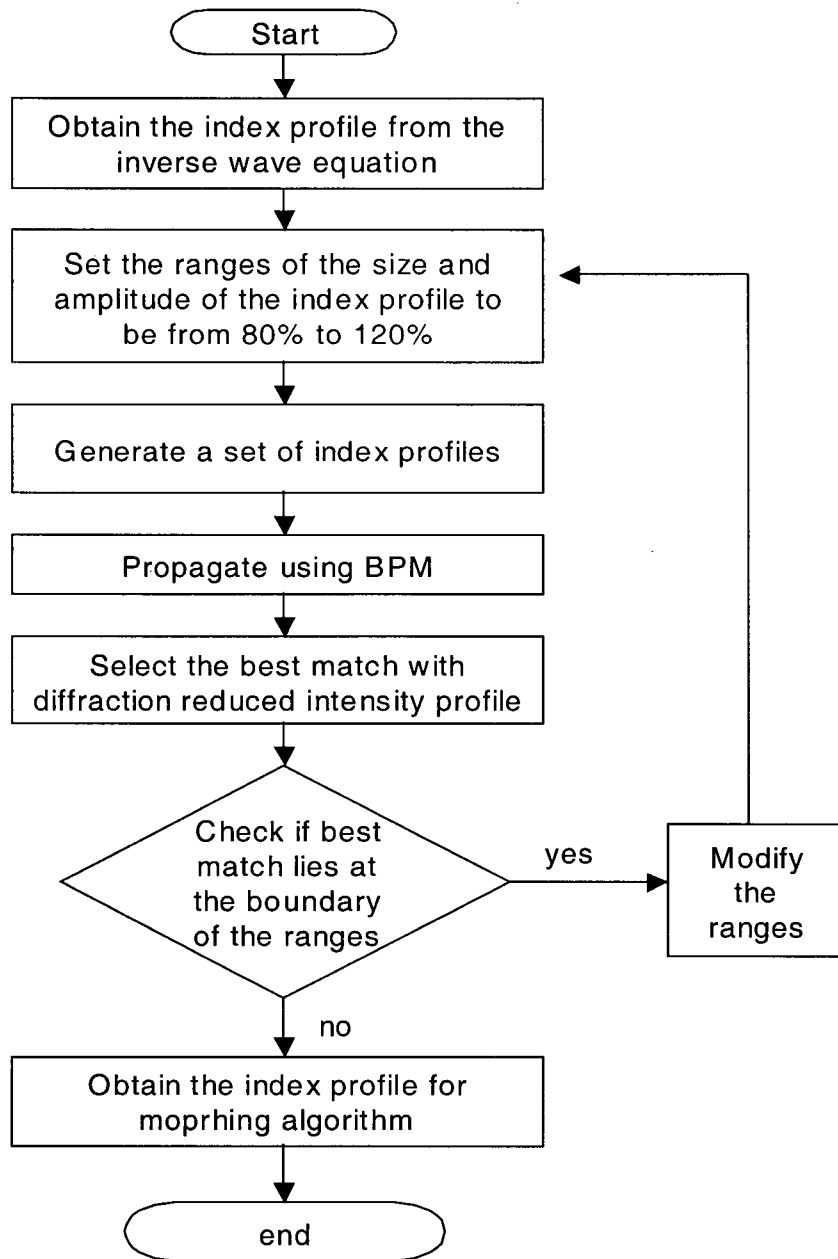


Figure 3-9: Redundancy Test Algorithm

3.4.2 Simple Morphing Algorithm

Although with a combination of filtering and redundancy test the predicted index profile from the inverse wave equation provides a good estimate of the actual index profile of the waveguide, there are still differences between the shapes of the predicted and the original index profiles. A common approach is to assume an index profile with a known distribution [6][7][10][14], which will eliminate the possibility of finding index profiles with different types of distribution. Therefore, the morphing algorithm, the final step of our TNFIPM, is included to help us obtain a more accurate shape of the index profile.

As discussed in the section 2.7, one of the disadvantages of this morphing algorithm is that the number of predicted index profiles to be simulated is generally large. For example, in section 2.7, it shows that for a single mode waveguide, BPM would require 45 days of computation time without even accounting the redundancy test time required for each index profile. This is the reason why a fast mode solver is required for this morphing algorithm or a better index profile selection criteria is required to simulate only the most probable index functions and make the computation time more efficient. Therefore, to improve the quality of index profiles that are simulated, we have adapted a simple morphing algorithm and used only the two functions that are typically associated with the type of waveguide under study.

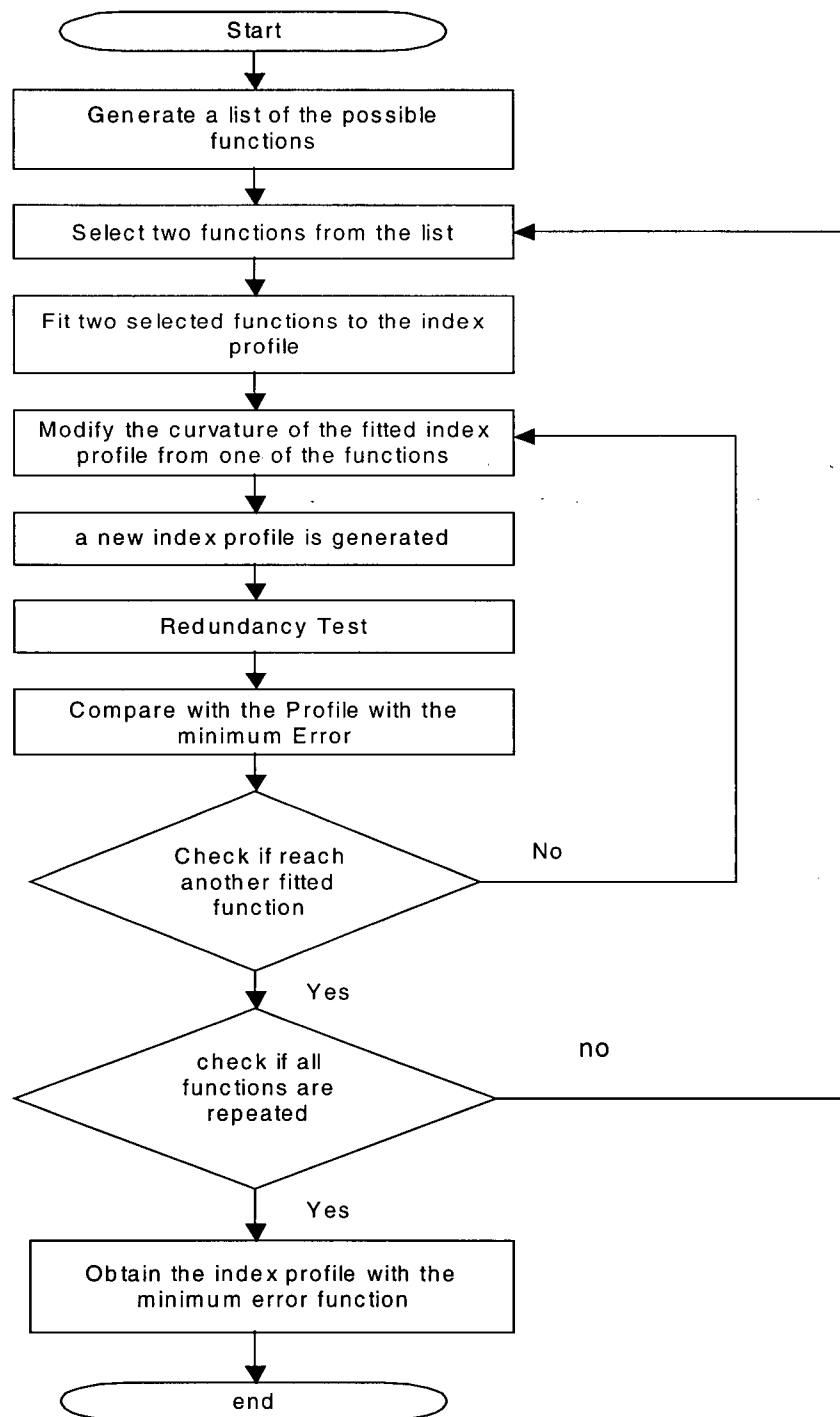


Figure 3-10: flowchart of the morphing algorithm

In our experiment where the waveguide under study is a Ti:LiNbO_3 indiffused waveguide, we have chosen the starting function to be the parabola, which is a simple function that can be fitted to other functions using a quadratic function. And for the final function, the Gaussian has been selected since it is the most often used function to describe this type of waveguides. Figure 3-10 shows a flowchart that summarizes the steps of the morphing algorithm. The details of how the parabola is morphed into the Gaussian is discussed in the following.

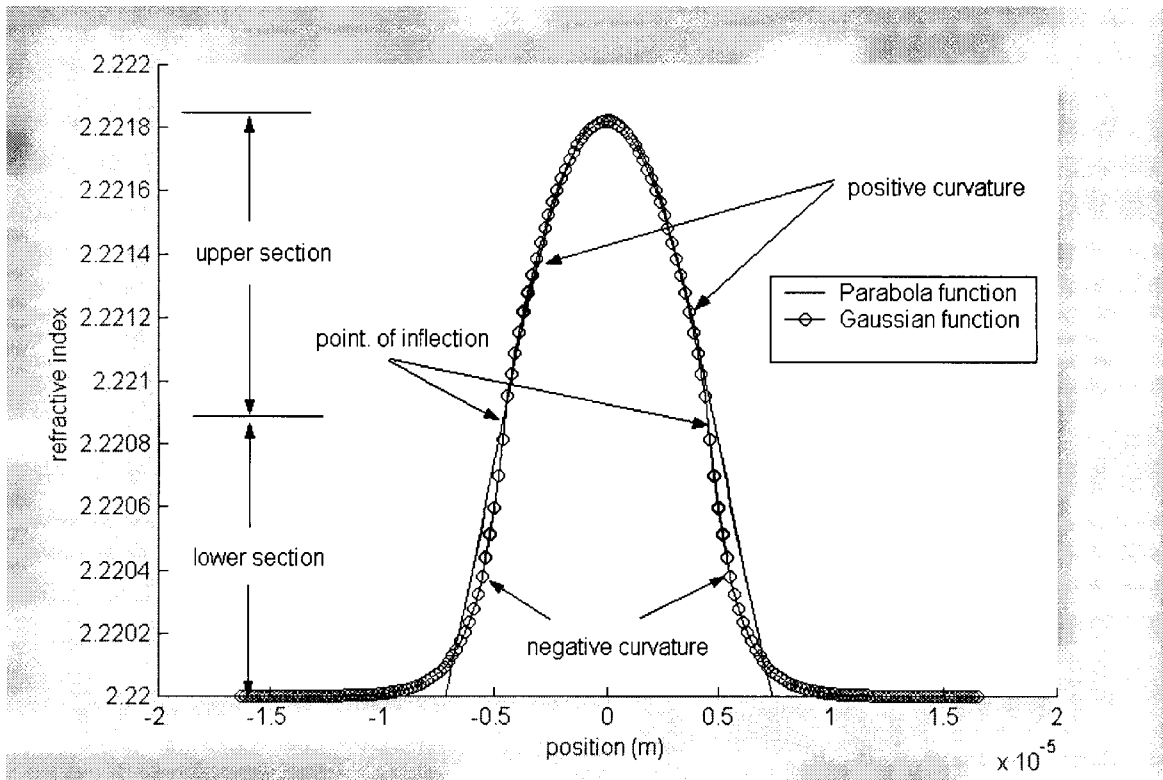


Figure 3-11: Comparison between Parabola and Gaussian functions

In order to demonstrate how the parabola is morphed to the Gaussian, first, the differences in their curvatures need to be analyzed. Figure 3-11 shows a parabola and Gaussian function. For a Gaussian function, the curvature is negative at the upper part of

the curve and positive at the lower part of the curve. On the other hand, the curvature for the parabola remains negative throughout the whole profile.

To change the index profile from a parabola to a Gaussian shape, a point of inflection is chosen to separate the curve of the parabola function into two main sections: middle and outer sections. In each section, the change of curvature depends on the data in the profile and by modifying these data values, the curvature of a portion of the profile can be changed. For example, if a polynomial function is fitted to the maximum, middle, and minimum points of one of the lower sections of the parabola, the curvature of the fitted section will be positive. To change the curvature of the profile in this section, the value of the middle point of the lower section is lowered to be between the original middle point value and the minimum value as shown in figure 3-12. Then after fitting a polynomial function to the maximum point, new middle point and the minimum point, the curvature of the fitted polynomial function can be made to change from positive to negative, which is similar to the lower section of a Gaussian function. Figure 3-12 shows a magnified view of the modified curvature for the lower part of the parabola. By changing the value of the middle point of the lower section, a parabola function can be gradually changed into the Gaussian types. For different type of function where the difference can exist in different sections, the same procedure can be applied to modify curves in different sections and this is how one function morphs to another function.

Although this simple morphing algorithm eliminates the possibility of finding the index profile with other types of functions, the probability of obtaining a more accurate result is

greater than simply fitting a known function to the result of the inverse wave equation because the actual index profile most likely has a shape that is between two of the most probable functions. In addition, with the redundancy test algorithm, the size and magnitude of each index profile from the morphing algorithm is modified so that the final index profile will have the best matching shape, magnitude, and size to the actual index profile.

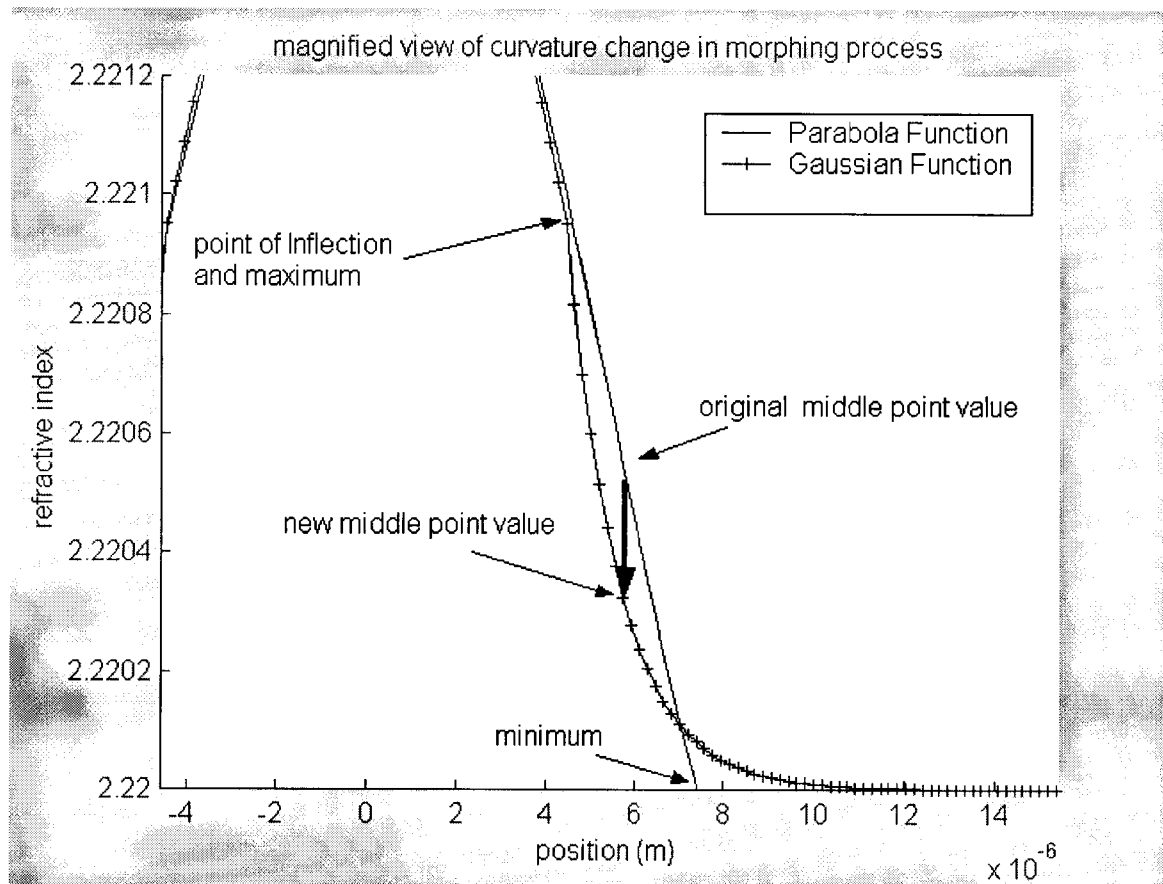


Figure 3-12: Magnified view of the curve morphing from parabola to gaussian

3.6 Conclusion

In this chapter, we have described the different algorithms required to obtain the refractive index profile from the image-plane intensity profile. The diffraction-reduction algorithm is employed not only to remove the diffraction effects on the image-plane intensity profile but also to obtain the intensity profile at the end facet of the waveguide, which is necessary for TNFIPM. The mean square error and the piecewise curve comparison are used to generate the feedback for the iterative method, which is the method chosen for solving the phase problem in the diffraction-reduction algorithm. To obtain a good estimate of the size and the magnitude of the index profile, a combination of the inverse wave equation and the redundancy test algorithm is used. Finally, an *ad hoc* morphing algorithm enables us to find a more accurate index profile among a number of index profiles that are generated from two of the most probable functions used to describe the type of waveguide under study. With these algorithms, the final index profiles found are free from diffraction effects and much more accurate than the index profiles obtained from a standard TNFIPM.

Chapter 4 Simulation

4.1 Introduction

This chapter presents the simulation results of our improved TNFIPM. The simulations are designed to determine the effectiveness and the limitations of our TNFIPM. Before describing the simulation results, this chapter starts with a description of the main components of the simulation configuration and their relationship to an actual TNFIPM system in section 4.2. After introducing the software tools used in the simulation, a simulation showing the results of a typical TNFIPM, which does not remove the diffraction effects nor apply the morphing algorithm, is presented in section 4.3. Then these results are compared with simulation results using the improved TNFIPM in the next few sections. There are three main parts in our algorithm: diffraction reduction, initial index profile derivation, and the morphing algorithm. The effectiveness of the proposed method in reducing the diffraction effects in the intensity profile at the end facet of a waveguide is discussed in section 4-4. In section 4-5, the first guess of the derived index profile from the diffraction reduced intensity profile is presented and compared with the index profile derived using a standard TNFIPM. Finally, the simulation result of the morphing algorithm, is presented in section 4.6, where the final index profile of our proposed, improved TNFIPM is obtained.

4.2 Simulation Setup Description

In order to verify the effectiveness of the proposed algorithm, a model that simulates a TNFIPM system is constructed. Before we discuss the simulation results, we describe the relationship between each of the software tools used in our model and the actual TNFIPM system:

a) BeamPROPTM: In a TNFIPM system, light propagates through the waveguide and exits at one end of the waveguide as shown in figure 4-1. In order to simulate this process, BeamPROPTM was employed. By providing a light source and a refractive index profile of a waveguide, BeamPROPTM can generate the intensity profile that represents the light distribution at the end facet of a waveguide. The first step of our simulation is to construct a refractive index profile of a waveguide and obtain its corresponding intensity profile at the end facet using BeamPROPTM. This intensity profile is similar to what we would see at the end of the waveguide as shown in figure 4-1, section a.

b) CodeVTM: The intensity profile at the end facet of the waveguide is then magnified and focused onto a detector by a lens system as shown in figure 4-1, section b. In order to simulate the diffraction effects by the lens system, CodeVTM is used to model the light propagating through the lens system. By feeding the intensity profile generated by BeamPROPTM to CodeVTM, it can generate an intensity profile at the image plane with the diffraction effects. For accurate modelling, CodeVTM requires an intensity profile, which is fed by the output of BeamPROPTM, and the detailed lens system data, which can

be obtained from a lens datasheet. A GelTech aspheric lens model is constructed in our simulation lens model. The same lens was also purchased for our experiment.

c) MatlabTM: In a typical TNFIPM system, after the image-plane intensity profile is obtained from the detector, a data processing unit is employed to digitally remove the noise and produce the refractive index profile of the waveguide under study as shown in figure 4-1, section c. In the simulation setup, after the image-plane intensity profile of the waveguide is obtained from CodeVTM, a set of MatlabTM programs was used to obtain the refractive index profile. These MatlabTM programs were implementations of the proposed improved TNFIPM.

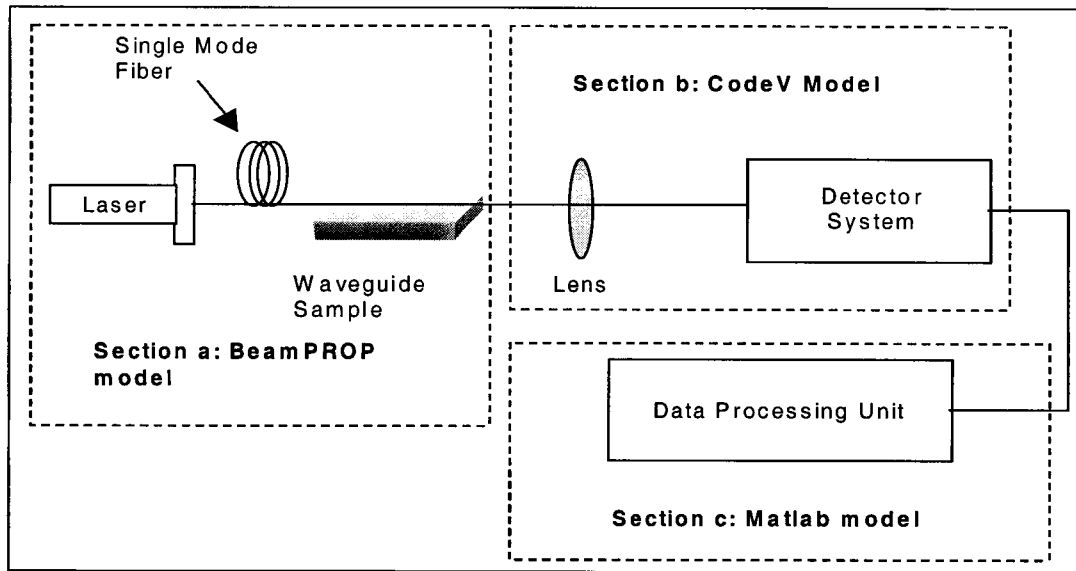


Figure 4-1: A typical configuration for refractive index profile measurement using TNFIPM

4.3 Simulation Result of a Standard TNFIPM

In a standard TNFIPM, the diffraction effects on the focused image-plane intensity

profiles are not considered and the derived index profile is fitted with a known "typical" index profile. The purpose of this section is to simulate the results of a standard TNFIPM and to analyze the accuracy of the obtained refractive index profile.

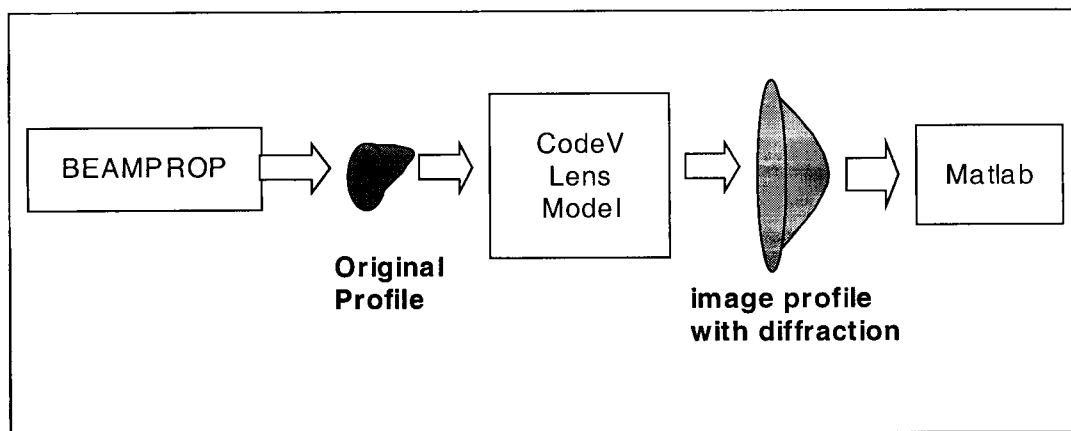


Figure 4-2: Intensity Profiles at the output of each diagram

A TNFIPM system starts with an intensity profile at the end-facet of a single-mode waveguide. A model of a titanium indiffused waveguide was constructed in BeamPROP™ as shown in figure 4.1 (a). Using BeamPROP™, the intensity profile at the end facet of the modelled waveguide is obtained. This intensity profile is then fed into a CodeV™ lens system to simulate the beam propagation and to introduce the diffraction effects from the lens into the image-plane intensity profile. The block diagram in figure 4-2 shows the relationship between each block and its output intensity profile. In this simulation, the intensity profile obtained from BeamPROP™ has a beam waist of 11.95μm along the x direction and 10μm along the y direction as shown in figure 4-3 (a) and (b), respectively.

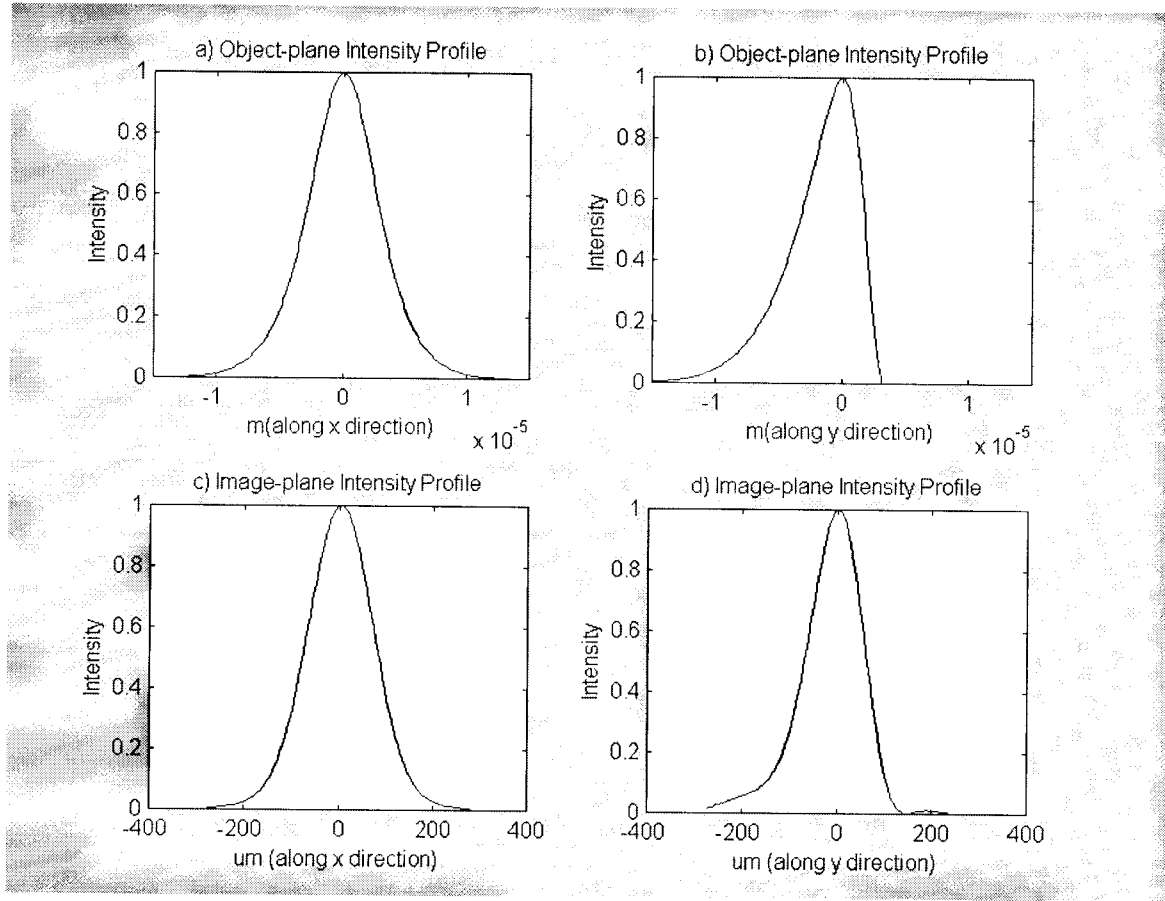


Figure 4-3: Object-plane Intensity Profiles and Image-plane Intensity Profiles

The lens model employed in this simulation has a focal length of 8mm. The distance from the object-plane to the principal plane of the lens and the distance from the image plane to the principal plane of the lens are 9.85 and 190.5mm, respectively. The focused intensity profile in the image plane has a waist of 273.5 μ m along the x direction and 250 μ m along the y direction as shown in figure 4-3(c) and (d), respectively.

In a typical TNFIPM, the lensmaker's formula is used to calculate the magnification of the lens, which yields a magnification of 19.5 in our simulation. This means that a typical TNFIPM, without considering diffraction, would tell us that the waveguide output

intensity profile had a 14 μm waist in the x direction and a 12.8 μm waist in the y direction. Figure 4-4 shows the comparison of the original intensity profiles and the calculated intensity profiles. That is an error of 16.5 % and 28% in the x and y directions, respectively. This means that the index profile obtained from the inverse wave equation is significantly wider than it should be. In practice, this error is usually much worse due to the difficulty in measuring the distance from the end facet of the waveguide to the principal plane of the lens with great accuracy. Any small misalignment in the experimental setup or equipment inaccuracy will result in much greater error than we are able to obtain in a simulation.

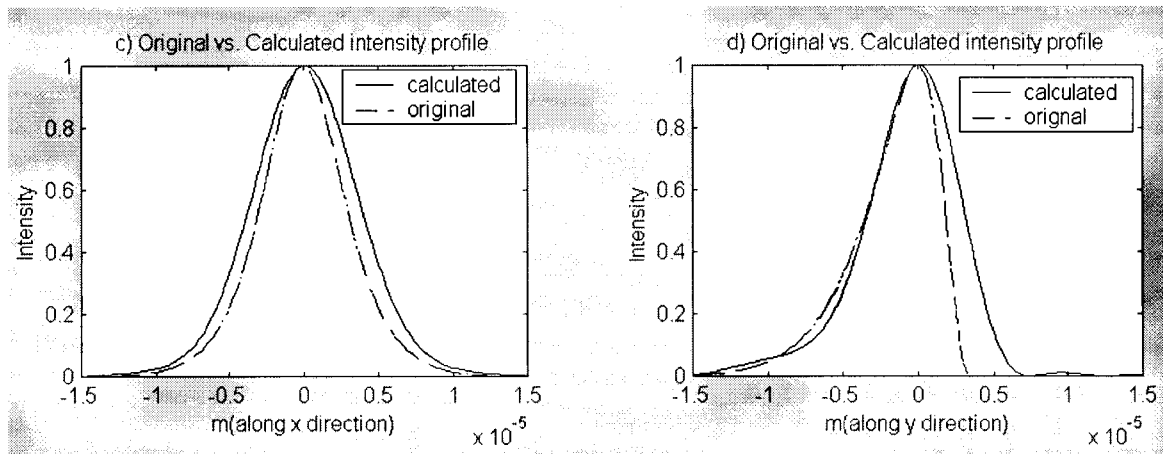


Figure 4-4: Comparison of original and calculated intensity profiles

To obtain the refractive index profile, the inverse wave equation is applied to the intensity profiles along x and y directions. The resulting refractive index profile is presented in figures 4-5(a) and (b), respectively. Due to the nature of the second derivative, any noise will be amplified. For example, at the region away from the core section of the waveguide, where the signal is the weakest, the derived index, as shown in

the figures 4-5 (a) and (b), oscillates significantly as compared to the original index profile. The derived index can be as much as three times higher than the original index in the core guiding area of the waveguide as shown in figure 4-5 (c) and (d). In a typical TNFIPM, a fitting mechanism is usually applied to smooth out the profile and to fit the derived index profile to a known shape. However, if the derived index profile is significantly greater than the actual sizes, even with fitting and filtering, the error in the derived index profile is still too high to be of much practical use. In addition, unlike the proposed TNFIPM where the diffraction effects have been greatly reduced, the size of the index profile is always much bigger than the actual index profile size due to diffraction.

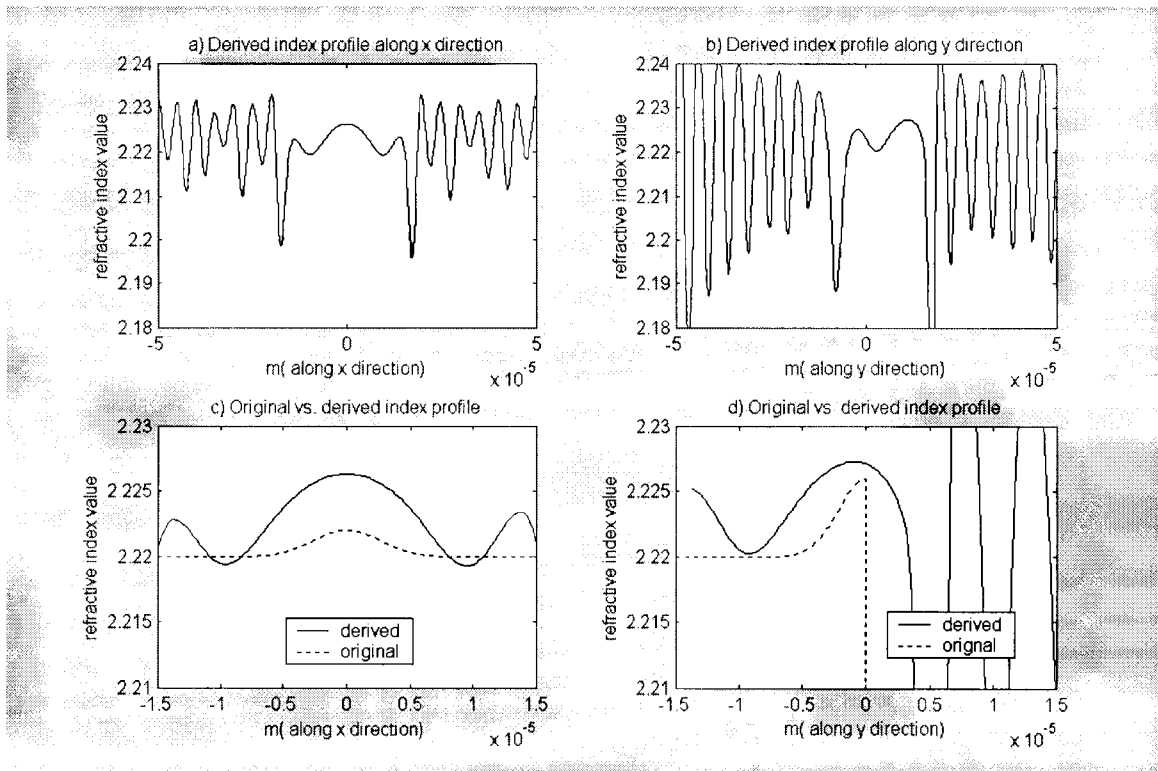


Figure 4-5: Derived index profiles

4.4 Simulation of Diffraction-Reduction Algorithm

The main purpose of this simulation is to determine the effectiveness and the accuracy of our proposed diffraction-reduction algorithm. Similar to a standard TNFIPM, we start with the same image-plane intensity profile with diffraction effects as shown in figure 4-3. Instead of applying the lensmarker's formula to this intensity profile, the diffraction-reduction algorithm employs two procedures, applying the Gaussian Beam equation and the iterative method, in searching for the intensity profile that can be represented as the intensity profile at the end facet of the waveguide, which yields the minimum error.

Before applying the iterative process to find the least error with diffraction accounted for, the first step is to employ the Gaussian Beam equations to obtain the beam waist, which yields a waist size of 13 μ m along the x direction and a waist size of 11.5 μ m along the y direction, which are still 5% and 15% larger than the original sizes. The error is smaller than using the lensmarker's formula, which has errors of 15% and 28% along the x and y directions, respectively.

After obtaining the sizes of the intensity profiles as in the previous section, which are still significantly affected by diffraction as shown in previous section, these intensity profiles need to be modified to remove the diffraction. Therefore, the second step of our diffraction-reduction algorithm is to apply the iterative method to search for the intensity profile at the end facet of the waveguide that will minimize the error. The iterative

algorithm starts with a predicted intensity profile and then obtains its image-plane intensity profile. This image-plane intensity profile is compared with the original image-plane intensity profile. Then the predicted intensity profile is modified with the error function obtain from the comparison. After several repetitions, this process converges to a final intensity profile that has the least error. Figure 4-6 shows the interaction between the required elements of the diffraction-reduction algorithm.

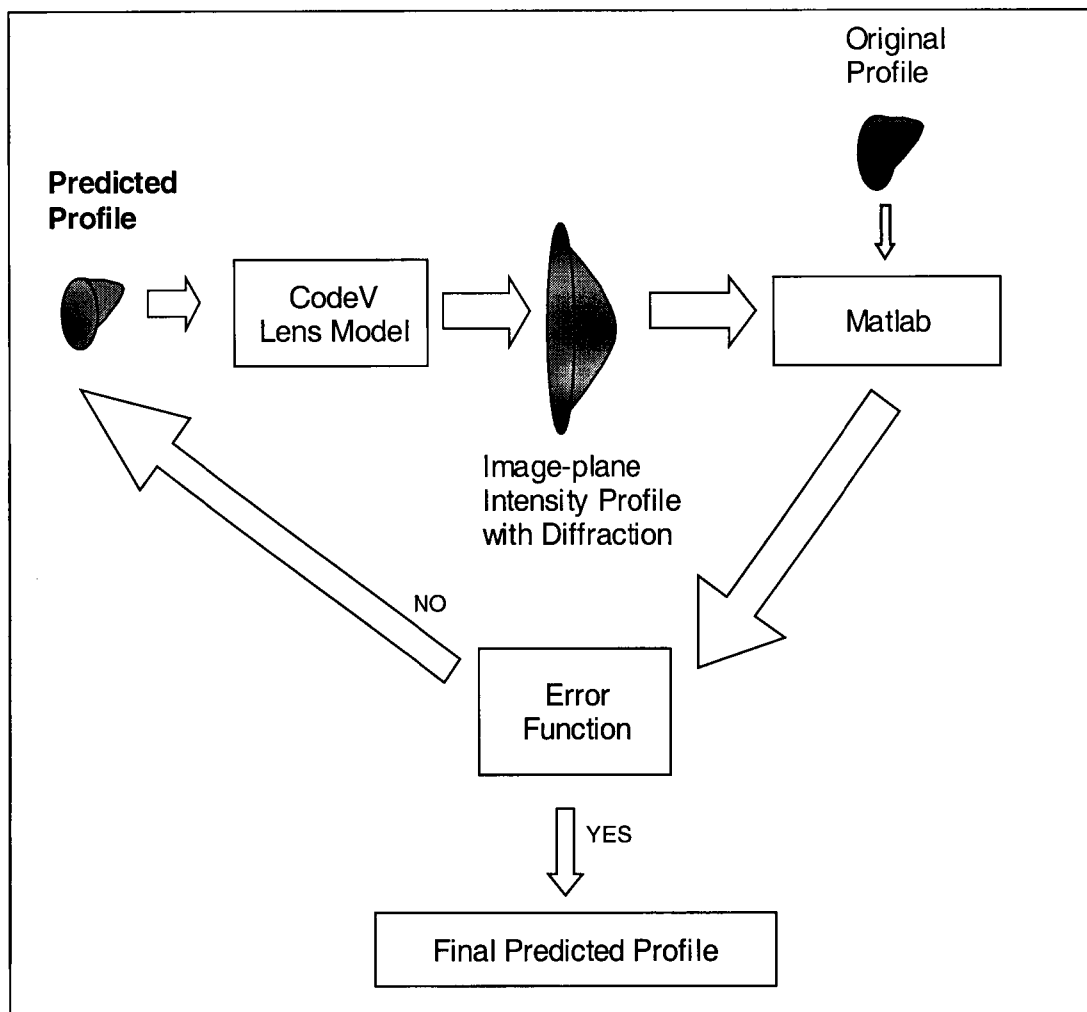


Figure 4-6: Functional Block Diagram of Iteration and Convergence Algorithm

Figures 4-7 (a) and (b) show the final diffraction reduced intensity profiles along the x

and y directions, which have been considerably improved as compared with the ones found using the lensmarker's formula. The new waist size along the x direction and y direction are 12 μm and 10.5 μm , respectively, which have less than 5% error. Besides waist size, the shape of the derived intensity profile is much closer to the original intensity profile. This improvement is particularly noticeable when one compares the intensity profile along the y direction. In figure 4-7(b), the derived intensity profile from the diffraction-reduction algorithm has a much sharper falling edge than that obtained from the standard TNFIPM, which is seen to be much broader in figure 4-4 (b).

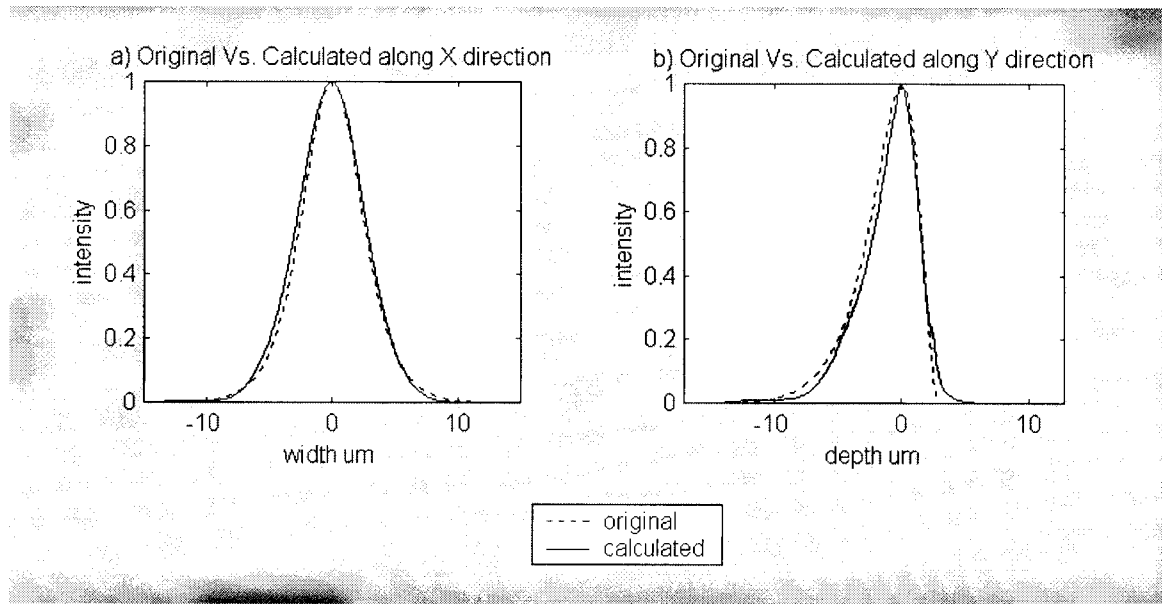


Figure 4-7: Comparison between the original intensity profile and the derived intensity

In order to determine the match between the diffraction reduced intensity profile and the original intensity profile, both of them are fed into CodeVTM to obtain their profiles at the image-plane. Figure 4-8 shows the match between the original and the diffraction reduced intensity profiles at the image-plane for both the x and y directions. The

diffraction reduced intensity profile at the image-plane almost lies on top of the original intensity profile at the image-plane. Therefore, the derived intensity profile from the diffraction-reduction algorithm has improved significantly, which is crucial for having an accurate derived index profile.

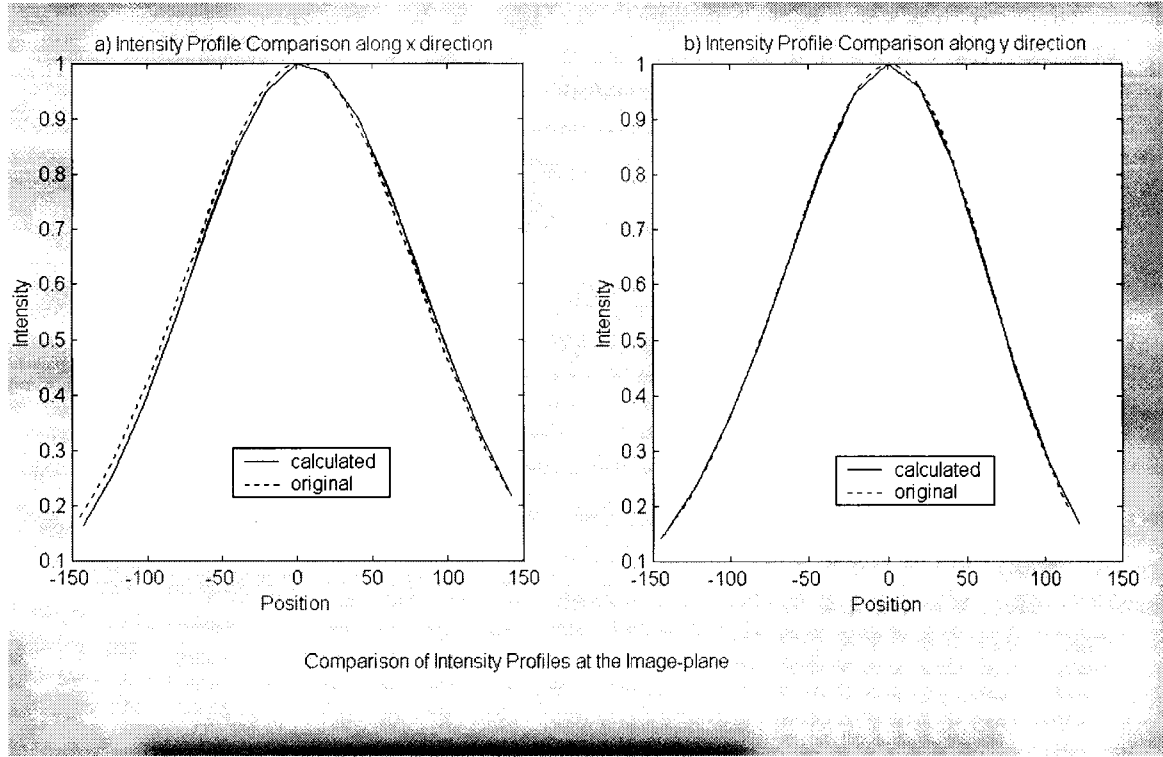


Figure 4-8: Comparison of intensity profiles at the image-plane

4.5 Simulation for Deriving the First Guess of the Index Profile

Once the diffraction reduced intensity profile at the end facet of the waveguide is obtained, an index profile can be derived by applying the inverse wave equation. Unlike a standard TNFIPM, where the final result is obtained by fitting a pre-defined function to

the derived index profile, this derived index profile will merely serve as the first guess of the index profile in our proposed TNFIPM. As discussed in the algorithm section, the redundancy test algorithm and a morphing algorithm are required to obtain a more accurate index profile. This section presents the simulation results of the first guess of the derived index profile and the results of the redundancy algorithm. In the next section, the results of the final index profile after employing the morphing algorithm will be discussed.

The first step of our simulation is to obtain the first guess of the index profiles from the diffraction reduced intensity profile. Figures 4-9 (a) and (b) show the derived index profile after applying the inverse wave equation and Savitzky-Golay filtering. The size of the derived index profile along the x direction has an error of about 15% and an error along the y direction of about 30%. Because of the diffraction-reduction algorithm, the size error of the index profile has been improved significantly, as compared with figure 4-5 where the size error is more than 100%. Before removing the diffraction effects, the error in the index profile is mainly due to the diffraction. However, the size mismatch now is mainly due to the small residual diffraction effects and the spatial noise induced from the second derivative in the inverse wave equation. The peak index has an error of 25% along x direction and 20% along y direction. This is definitely an improvement compared with the noisy profile using a standard TNFIPM. In order to verify with the original intensity profile at the end facet of the waveguide, the index profile is fed into BeamPROPTM to obtain its corresponding intensity profile. In this simulation, BeamPROPTM was used for modeling light travelling through the waveguide with the

derived index profiles. Figures 4-9 (c) and (d) show the simulated intensity profile from the derived index profile.

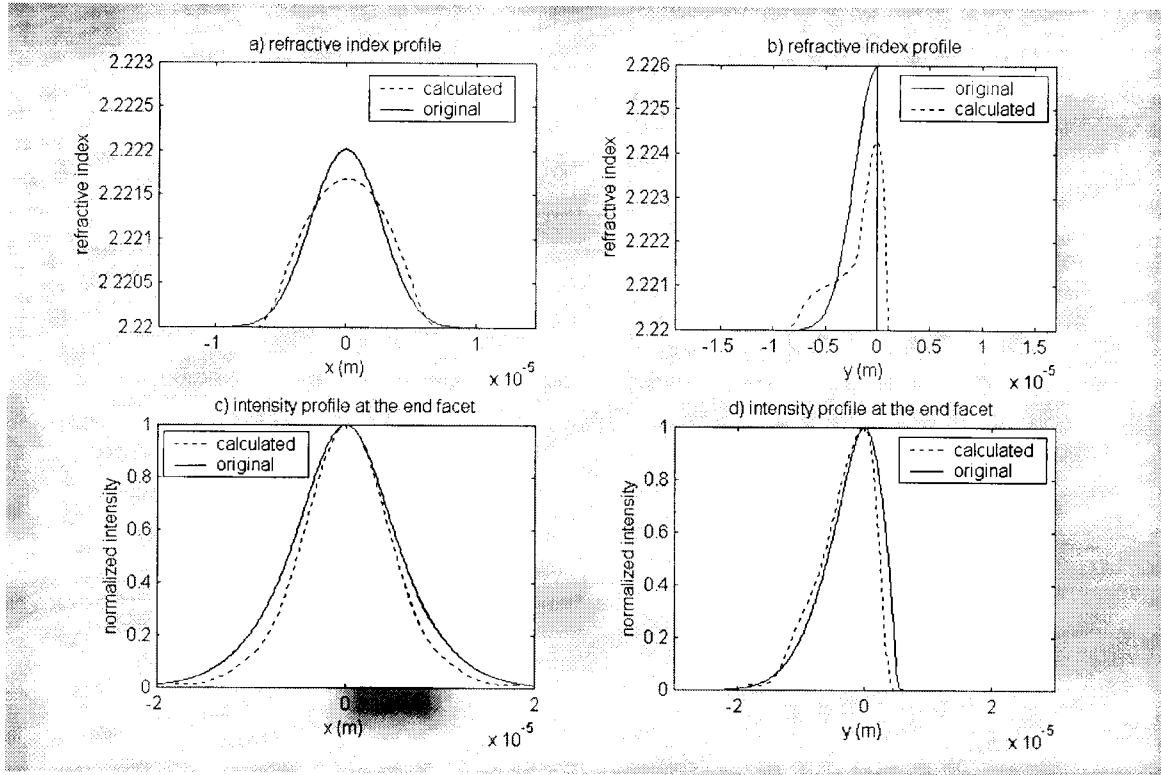


Figure 4-9: Initial derived index profile and its intensity profile comparisons

Although there is an improvement in the derived index profile, the error can be decreased further by applying the redundancy test algorithm as described in Chapter 3. The redundancy test algorithm varies the size and amplitude of the index profiles and compares the output intensity profile at the end facet of the waveguide against the diffraction reduced intensity profile. This extra step reduces the amplitude and waist search ranges in the morphing algorithm; therefore, it also serves as the preparation step for the morphing algorithm, which can be time consuming.

Figures 4-10(a) and (b) show the final index profiles produced by varying the size and the

amplitude of the index profiles. Although the improvement on the index profile along the x direction is marginal, the index profile along the y direction is much better. It has decreased the error in the amplitude from 30% to less than 10% in the core section of the waveguide. The improvement in the output intensity profile is even more noticeable when comparing figure 4-10(c) and (d) to figures 4-9 (c) and (d), where the intensity profile at the end facet of the waveguide along both the x and y directions match better the original intensity profiles. This means that the redundancy algorithm has further produced a better guess of the index profile, which will facilitate the search for the final index profile in the morphing algorithm.

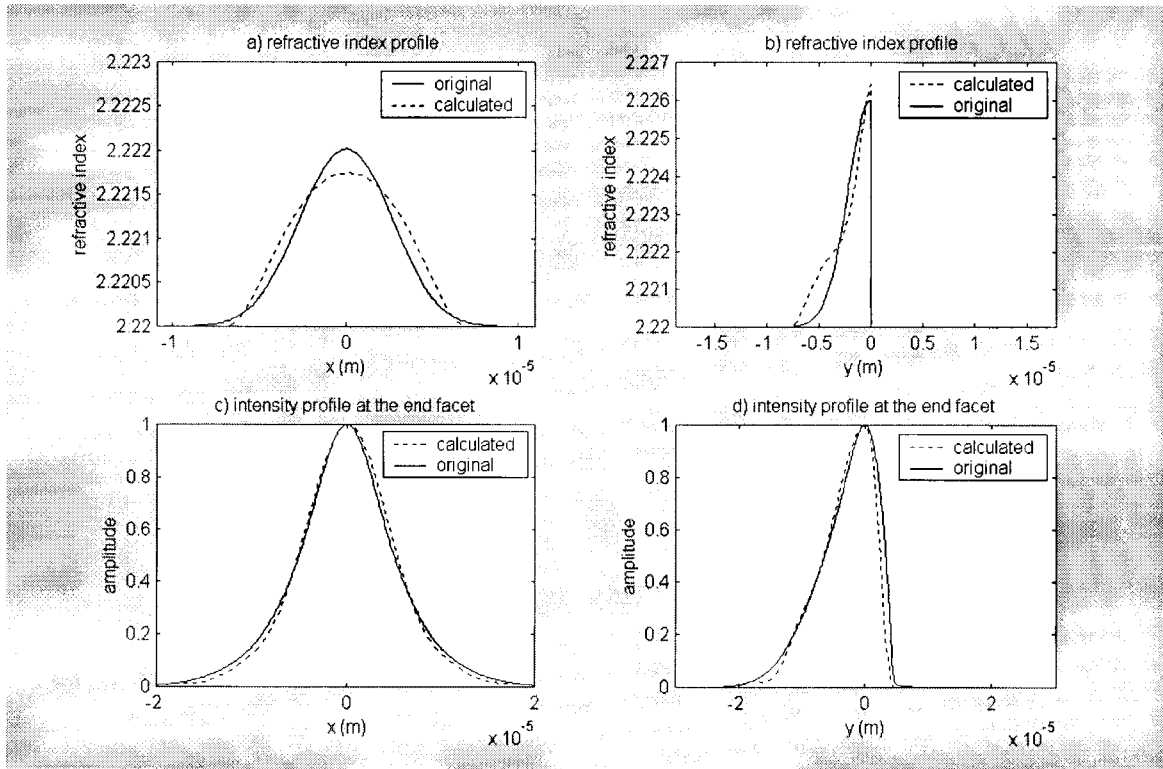


Figure 4-10: Index profiles and the corresponding intensity profiles after applying redundancy test algorithm

4.6 Simulation for Morphing Algorithm

This simulation is designed to study the effectiveness of the morphing algorithm and the accuracy of the proposed, improved TNFIPM. From the previous simulation, an initial index profile is derived, which, in this section, is processed with the morphing algorithm, where the shape of the index profile is varied from one function into another one as discussed in Chapter 3. During the morphing process, a list of index profiles is produced and fed into BeamPROP™ to obtain their intensity profiles at the waveguide's end-facet. The index profile that produces the intensity profile having the best match to the diffraction reduced intensity profile, is taken to be the index profile of our TNFIPM.

Figure 4-11 shows the connections between each function block.

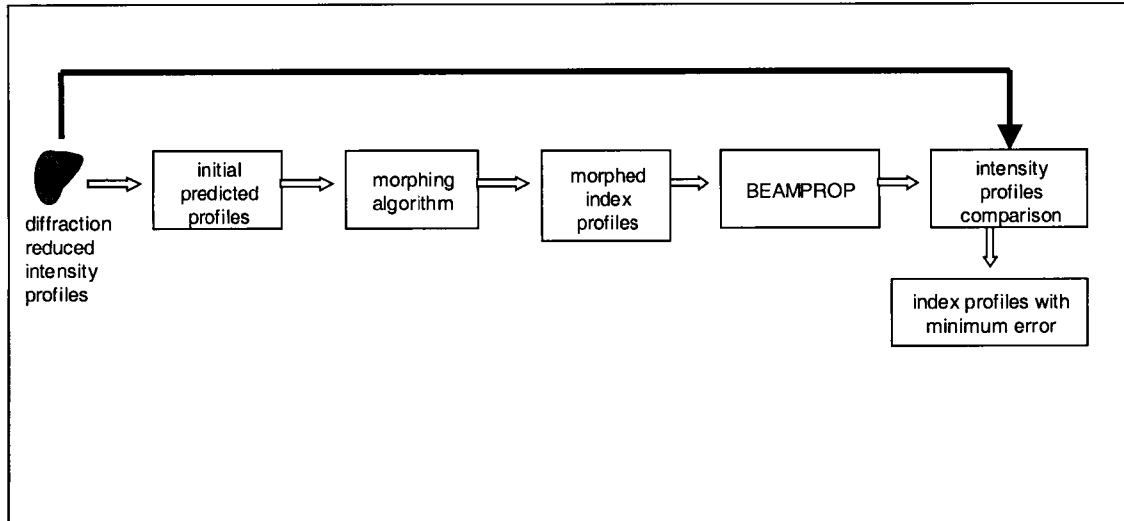


Figure 4-11: Block Diagrams for Morphing Algorithm Simulation

The type of the waveguide employed in our simulation is a titanium in-diffused type

waveguide. Parabola and Gaussian functions have been chosen to be the two functions used in the morphing algorithm. The Gaussian function is the function typically used to describe the refractive index function of an in-diffused type waveguide. The parabola function is a simple function that can be modified to another function. For every change of curvature in a function produced in the morphing process, a different index profile is generated. For each generated index profile, a redundancy test is also performed to ensure the best matching index found not only has the right shape but also the correct size and amplitude.

Figure 4-12 (a) and (b) show the resulting index profile after passing through the morphing algorithm. Although the shape of the index profile along the x direction does not change much, the shape of the index profile along the y direction is much closer to the original index profile. The amplitude of the index profile does not change significantly, which is expected because of the effect of applying the redundancy algorithm in the previous section. Figures 4-12(c) and (d) show the simulated intensity profile at the end facet of the waveguide for the final index profile. The intensity profile at the end facet of the waveguide along both the x and y directions produce the best matches as compared to the previous simulation results. This means that the shape or the curvature of the index profile plays an important role in producing the correct intensity profile. A good match in the intensity profile cannot be achieved by simply applying the inverse wave equation and the redundancy test. Therefore, the last step of our morphing algorithm is essential to yield a more accurate index profile.

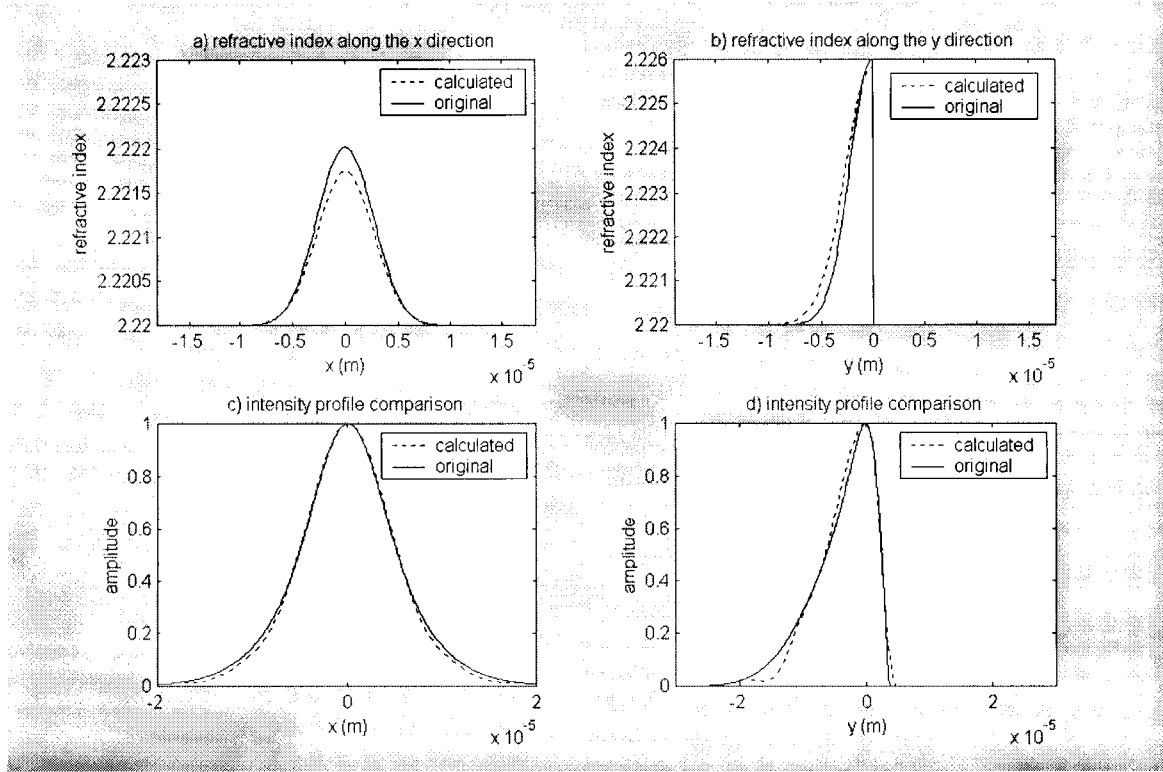


Figure 4-12: The final index profile from the morphing algorithm and its corresponding intensity profile at the end facet of the waveguide

Compared to a standard TNFIPM, where the index profile has an error of more than 100% in some cases, the proposed TNFIPM has significantly decreased the error to less than 10%. Due to the diffraction effects and the error in the second derivative of the inverse wave equation, the index profile from a standard TNFIPM is much noisier and wider than one obtained using our method. However, by using the diffraction-reduction algorithm to reduce the size and the morphing algorithm to fine-tune the shape and the amplitude of the derived index profile, the proposed TNFIPM has overcome these problems and produced much more useful results.

4.7 Conclusion

In this section, we have presented and discussed the simulation results of our proposed TNFIPM and a standard TNFIPM. Although a standard TNFIPM will provide a rough estimate of the size and the amplitude of a waveguide index profile, its value is limited due to its inaccuracy, which results from the diffraction effects and the high noise in the profile. To combat these problems, first a diffraction-reduction algorithm was employed to obtain an accurate estimate of the intensity profile at the end fact of the waveguide. This algorithm was shown to reduce the error to within 5% in both the intensity profile's shape and size. After the diffraction reduced intensity profile was obtained, the inverse wave equation and the redundancy test algorithm were applied and shown to improve the derived index profile. Finally, the morphing algorithm, which serves as a smart search to find the best match in the shape, size and amplitude of index profiles was employed. The simulation results showed that using the proposed TNFIPM yields a more accurate result.

Chapter 5 Experimental Results

5.1 Introduction

After presenting the theory and the algorithm of the proposed TNFIPM in chapters 2 and 3, the proposed algorithm was simulated and compared with a standard TNFIPM using CodeVTM, BeamPROPTM, and MatlabTM. In order to implement the proposed algorithm, a TNFIPM system was constructed to derive the index profile of a titanium in-diffused waveguide. The description of the implementation and the results are presented in this chapter.

An experiment using the proposed TNFIPM was constructed, which is described in section 5.2. In section 5.3, the calculation for the magnification of the lens system is presented. This magnification was used to obtain the size of the intensity profile of the waveguide at the end facet. Then the diffraction-reduction algorithm was applied and the resulting intensity profile is presented in section 5.4. After that, in section 5.5.1 the first prediction of the index profile of the waveguide is presented by applying the inverse wave equation. This index profile was then processed with the last two steps of our algorithm, redundancy test and morphing, these results are presented in section 5.5.2 and 5.5.3.

5.2 Experimental Setup Description

This section describes the implementation of a refractive index measurement system using TNFIPM, which consists of 5 building blocks: light source, sample, lens system, detector system, and data processing unit. Figure 5-1 shows an overview of the entire system.

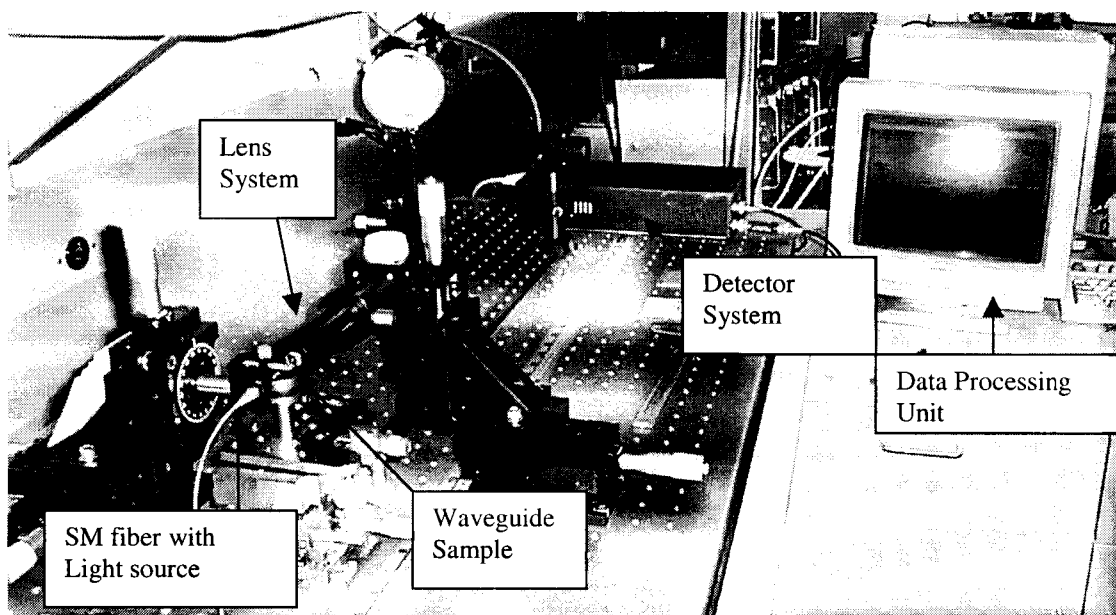


Figure 5-1: Transmitted Near-Field Intensity Profile System

A DFB laser of 1310nm wavelength was used to provide the light source. This laser, coupled with Corning SMF-28 single mode fiber, as shown in figure 5-2, was used to launch light into the waveguide under study. A single mode optical fiber was selected to provide a uniform source with near Gaussian distribution. It also facilitates coupling of light into a waveguide.

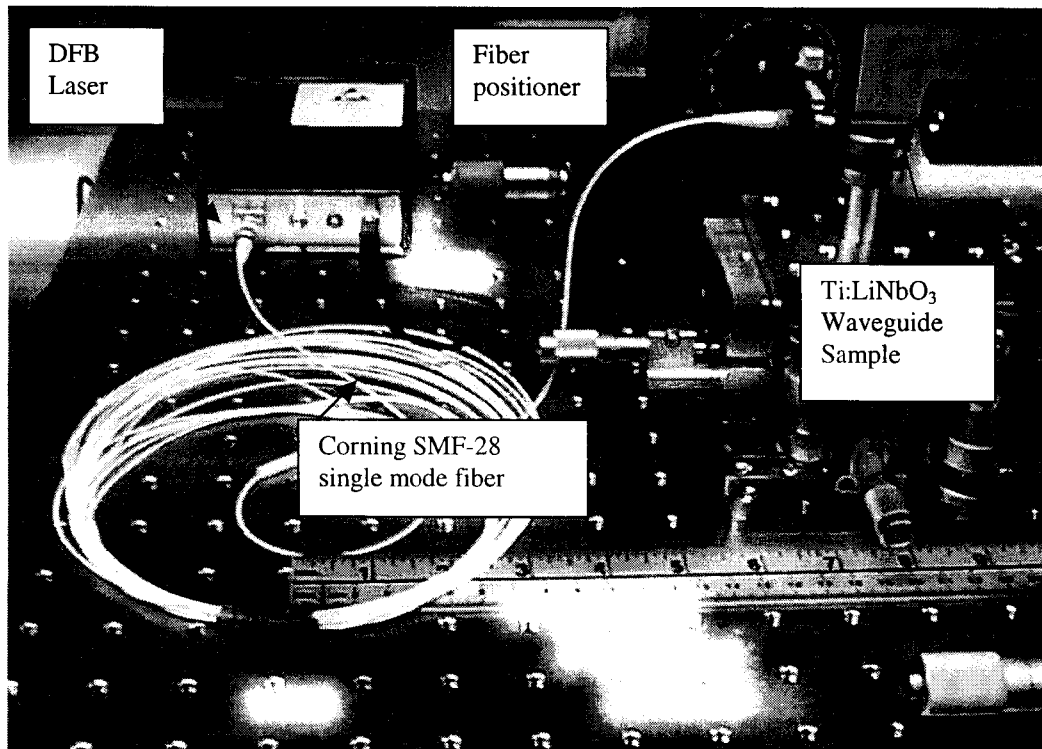


Figure 5-2: Single mode optical fiber coupled with a DFB laser

In order to provide maximum flexibility during the alignment process, the fiber was held with a kinematic mount, which in turn was held on a XYZ micropositioner from Edmunds Scientific. Using the micropositioner and a microscope, the fiber was carefully brought to the end of the waveguide. To ensure maximum coupling of light into waveguide, the distance between the fiber and the waveguide had to be minimized without making contact with the sample.

The waveguide sample under study was a Ti:LiNbO₃ indiffused single mode waveguide. It was fabricated by diffusing a 7 μ m wide and 800Å thick titanium strip into a slice of y-cut, z-propagate LiNbO₃ wafer. The titanium strip was successfully diffused into the LiNbO₃ crystal under 1050°C for 10 hours. The fabricated sample contains waveguides in

the z-propagation direction with no surface waveguide. The sample sat on a multi-axis translation stage with a tip/tilt stage mounted on top as shown in figure 5-3. This sample positioner allows flexible adjustments on any directions so that the maximum coupling of light into the waveguide can be achieved.

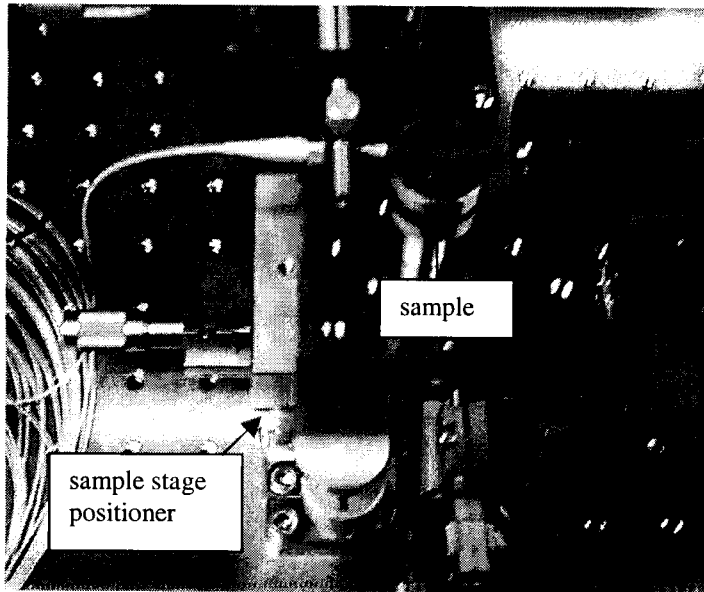


Figure 5-3: Sample Stage

At the output, a Dichroic polarizer from OptoSigma with an extinction ratio of 10,000:1 was utilized to separate the TE and TM modes of the output intensity profile of the waveguide. Also, to avoid saturation in the detector, a reflective neutral density filter from Edmund Scientific was used to control the beam intensity to an acceptable level.

To capture the image, a Thorlabs Omega meter, which consists of a monitor unit and a signal processing unit as shown in Figure 5-4 was used to perform cutting-knife edge scanning of the incoming beam. The Omega meter integrates the intensity along the

horizontal and vertical directions of the beam by using a rotating drum that passes a knife edge over a large area photo-detector. Figure 5-5 shows an Omega meter's monitor. The rotating drum has an open window and as the drum rotates around the photo-detector, exposing the photo-detector to the input light as it turns.

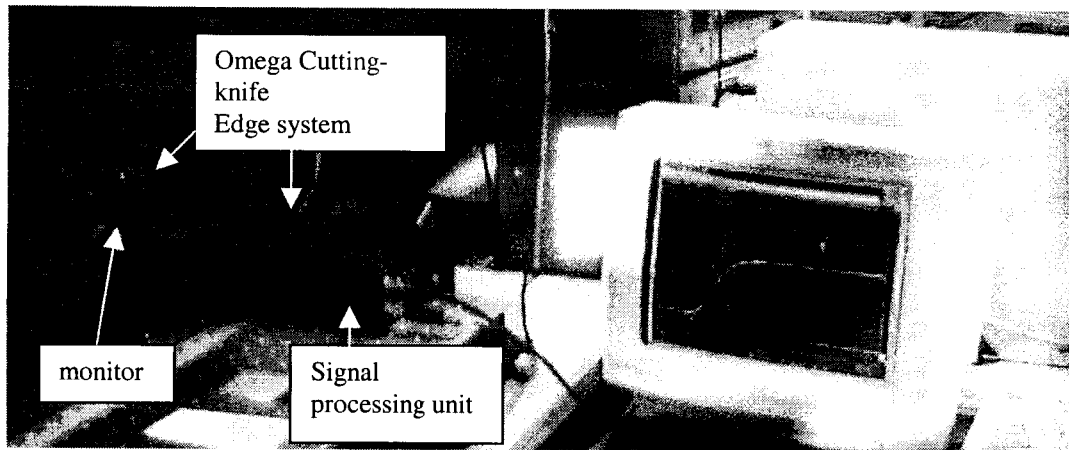


Figure 5-4: Cutting-Knife Edge Scanning System

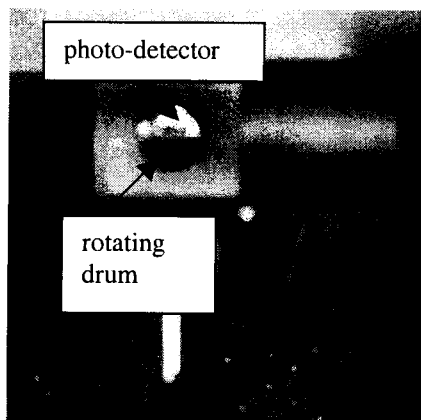


Figure 5-5: Detector with rotating drum

Collecting the intensity on the total exposed area is similar to performing an integral on the intensity along a particular direction. A derivative was performed on these integrated

profiles which represented the equivalent mode intensity profile along either the x and y direction by the signal processing unit of the Omega meter. Since the maximum resolution of the detector is 20 μ m [34], a Thorlabs aspheric lens with focal length equals 8mm was used to magnify and focus the beam image into an acceptably sized spot size on the photo-detector. The Omega meter provides two analog outputs: the actual raw integrated intensity profile from the photo-detector and the derived mode intensity profile. A National Instrument DAQ 5120 digital oscilloscope was used to sample and store the data from the Omega meter. Figure 5-6 shows the sampled outputs on the oscilloscope screen.

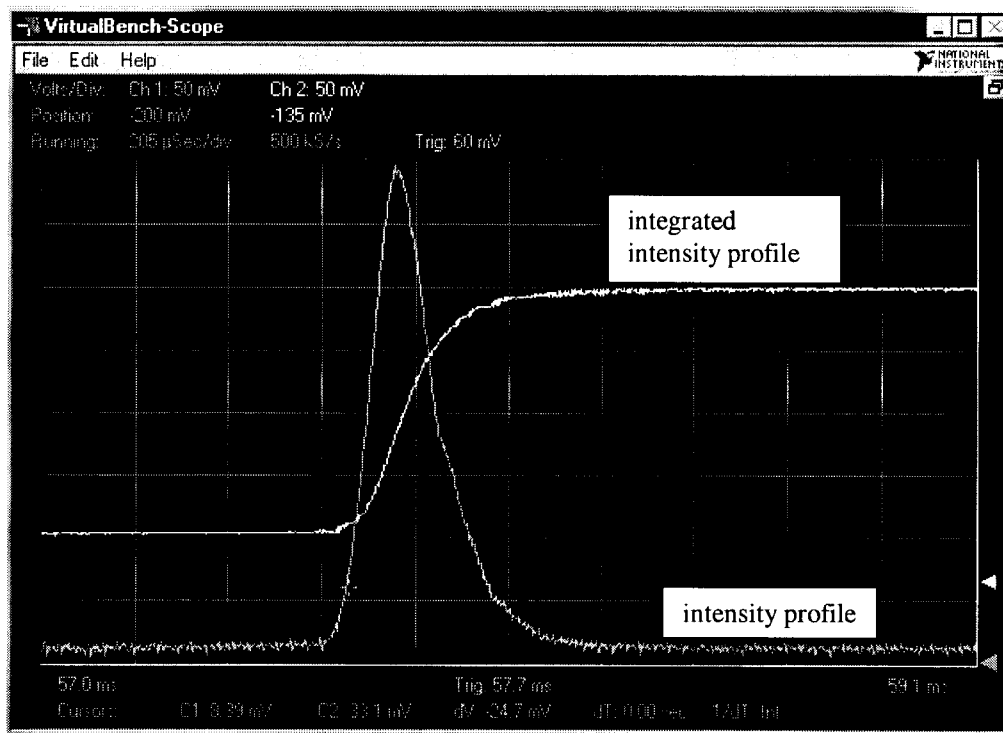


Figure 5-6: Intensity profile along the depth of an optical waveguide

As discussed in chapter 2, the aberrations can affect the accuracy of our profiles and

special care was taken to avoid these errors. One of the aberrations is the comatic aberrations. Since comatic aberrations were mainly due to misalignment, a red laser with a marker pole was used to align the whole system. The reason for choosing a red laser was to simplify the alignment process without using any special detector card. The pole was used to ensure the same height across the beam propagation path.

Another type of aberration is spherical aberration due to the curvature of the lens. One of the techniques for overcoming this aberration is to use multiple lenses or to use aspheric lenses [35], which is our chosen method. There were several considerations required to choose the aspheric lens for our system. First, the amplification had to be appropriate for the photo-detector. The propagation path terminated at the photo-detector with a square area of 4mm^2 . For the optical waveguides of interest, a magnification range from 30 to 40 was required to cover an image area of 2mm in length for maximum accuracy. In addition, most of the aspheric lens has a small clear aperture, which can introduce clipping or unwanted spatial filtering to the image. Therefore, after considering the magnification and lens size, a C240TM-C from Thorlabs, an anti reflection coated aspheric lens with 8mm in both focal length and clear aperture, was used in our experiment.

5.3 Beam Magnification Calculation

Since the intensity profile captured by the Omega system is the image-plane intensity profile, the first step of the TNFIPM is to determine the magnification of the lens which

can provide a good first guess of the size of the intensity profile at the end facet of the waveguide.

The accuracy of the final results depends on the quality of the experimental data and the focusing of the lens. With the mode intensity profile taken when the lens is not correctly focused, the index profile calculated by the TNFIPM would be much flatter and wider than it should be. In order to avoid this problem, the intensity profiles with the sharpest profiles were selected. The sharpest image is the image with the smallest cross section. As discussed in section 2.5, at least two sets of focused intensity profile, captured at different locations along the optic axis, are required in order to apply the Gaussian Beam equation (2.19) and obtain our first guess of the size of the intensity profile at the end facet of the waveguide:

$$\frac{X + \Delta X - f}{Z - f} = \frac{d_0^2}{d_0'^2} \quad (2.19)$$

where Z is the distance from the principal plane of the aspheric lens to the image plane, d_0 is the input beam waist, d_0' is the beam waist in the image plane, X equals to the distance from the waveguide to the principal plane of the lens for the first set of measurements and ΔX equals to the difference between the two waveguide locations, which can be measured precisely with a micropositioner.

However, in order to avoid errors, the intensity profile at the end facet of the waveguide was measured at several locations in the image-plane as listed in table 5.1. Using the polarizer, the intensity profile for either the TE or TM mode can be selected and measured in our system. The measurements of the waist sizes were obtained using the

Omega meter, which has an accuracy of about 5%. From the list, we can choose any two sets of data and apply equation 2.19 to calculate out first guess of the size of the intensity profile at the end facet of the waveguide.

measurement number	image distance to lens, Z, (mm)	delta X (mm)	measured waist size			
			TE mode		TM mode	
			horizontal (um)	vertical (um)	horizontal (um)	vertical (um)
1	500	0	943.25	527	955.5	514.5
2	475	0.007	894.25	490	906.5	490
3	430	0.02	808.5	453	833	428.8
4	400	0.034	771.75	429	759.5	416.5
5	370	0.042	673.75	380	698.25	367.5
6	340	0.062	635.5	338	635.5	348.5
7	310	0.082	574	317.8	574	307.5
8	280	0.102	512.5	287	512.5	287

Table 5-1: Tabulated measurements of the mode intensity profile

In order to reduce the error, all possible combinations of two sets of measurements in table 5-1 were applied with equation 2.19 to calculate the waist size of the intensity profile at the end facet of the waveguide. The average of waist sizes along the x, or horizontal, direction were 16um for the TE mode and 16.5um for the TM mode. The average waist sizes along the y, or vertical, direction for both the TE and TM mode was of 9.5um..

The TE and TM mode profiles captured along the x direction and y directions are shown in figures 5-7 and 5-8, respectively. Since the captured intensity profiles for the both TE and TM modes were almost identical, either one would yield the same index profile. In the rest of the experiment, the TM mode profile measured at location 6 in table 5-1 was

selected for our derivation of the final index profile.

In order to compare with a standard TNFIPM, the lensmarker's formula was applied and yielded a magnification of 33.6 for the measurement at location 6. This means that using the lensmarker's formula results in waist sizes of 18.9 μm along the x direction and 10.5 μm along the y direction, which are 17% and 10% wider than using the Gaussian Beam equation.

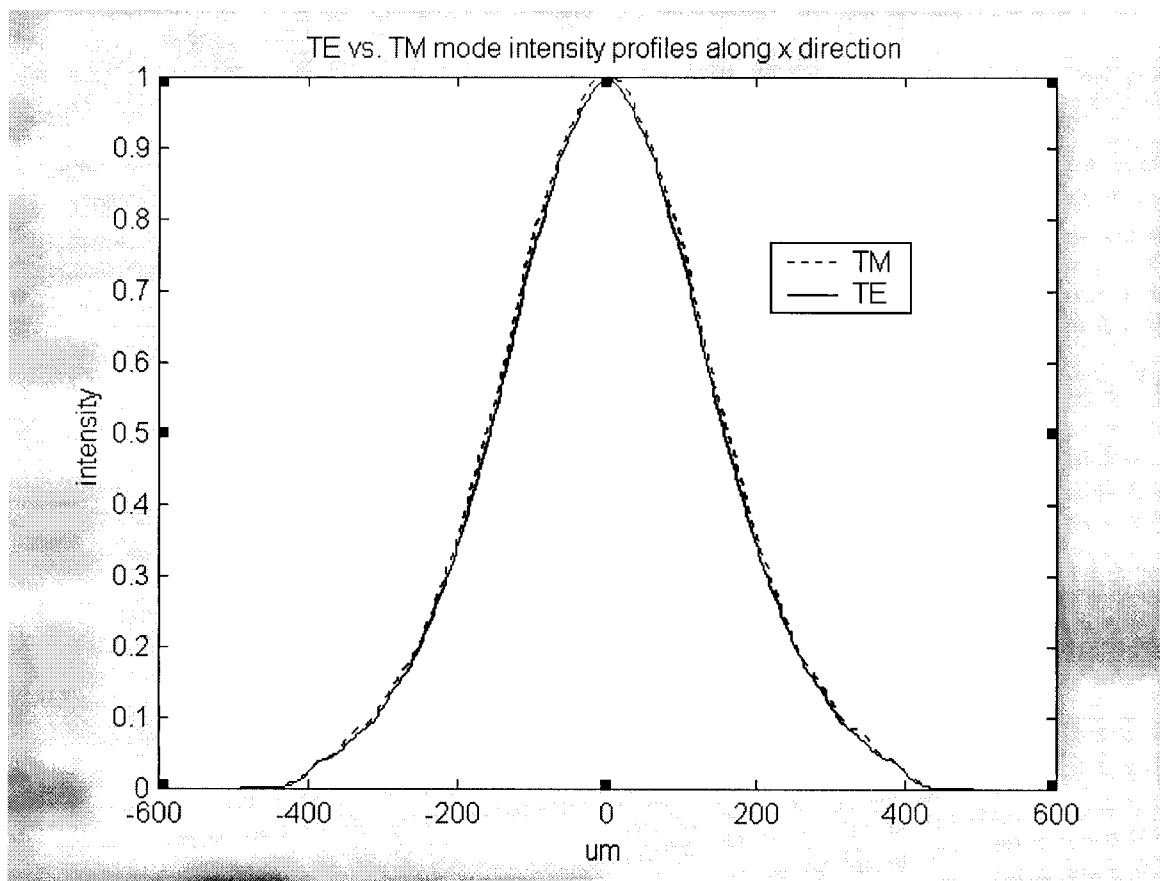


Figure 5-7: Comparison of TE and TM mode profiles along x direction

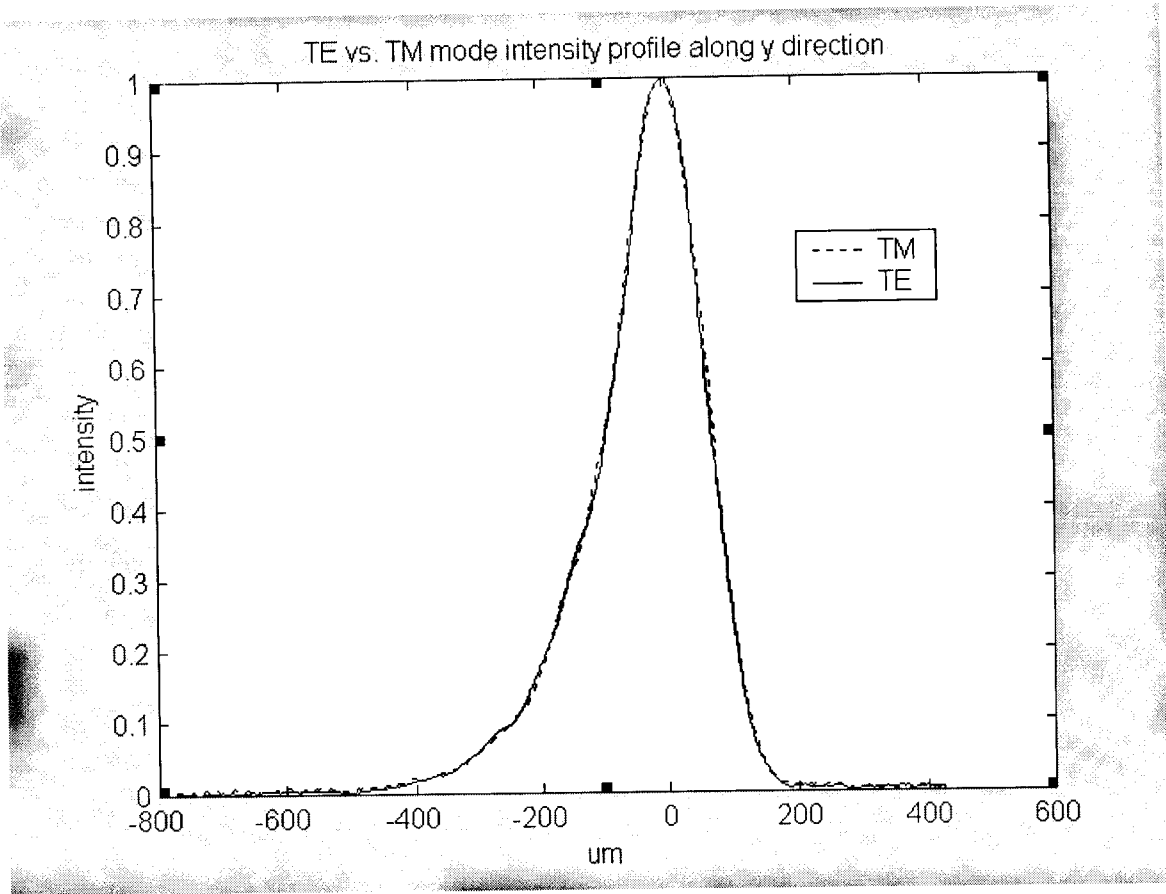


Figure 5-8: Comparison of TE and TM mode profiles along y direction

5.4 Diffraction Reduced Algorithm

As we have discussed previously, the intensity profile in the image-plane contains diffraction, which can cause inaccuracy in our final index profile. Therefore, after having a good estimate of the waist size of the intensity profile, the next step is to employ the diffraction-reduction algorithm to reduce the diffraction effects on the intensity profile. In this section, we describe the results of applying the diffraction-reduction algorithm.

One critical component of the diffraction-reduction algorithm is the lens model used to

model the diffraction effects. The construction and the calibration of an optical lens model are presented in appendix C. After obtaining the magnification of the image in section 5.3, the diffraction-reduction algorithm can now be applied to the measured intensity profile to minimize the error in deriving the intensity profile at the end facet of the waveguide due to the diffraction effects.

As discussed in section 3.4, the core of the algorithm consists of an iterative process and applying an exponentially decaying function. By replacing the exponentially decaying function in the profile at different locations along the falling edge of the profile, one can simulate where the mode field drops rapidly. Figure 5-9 shows a list of the exponentially decaying functions used in the diffraction reduced algorithm. Since a change of curvature can introduce additional noise in the inverse wave equation, a Savitzky-Golay filter was employed to reduce the sharp corner where the exponentially decaying function is joined with the original profile as shown in figure 5-10.

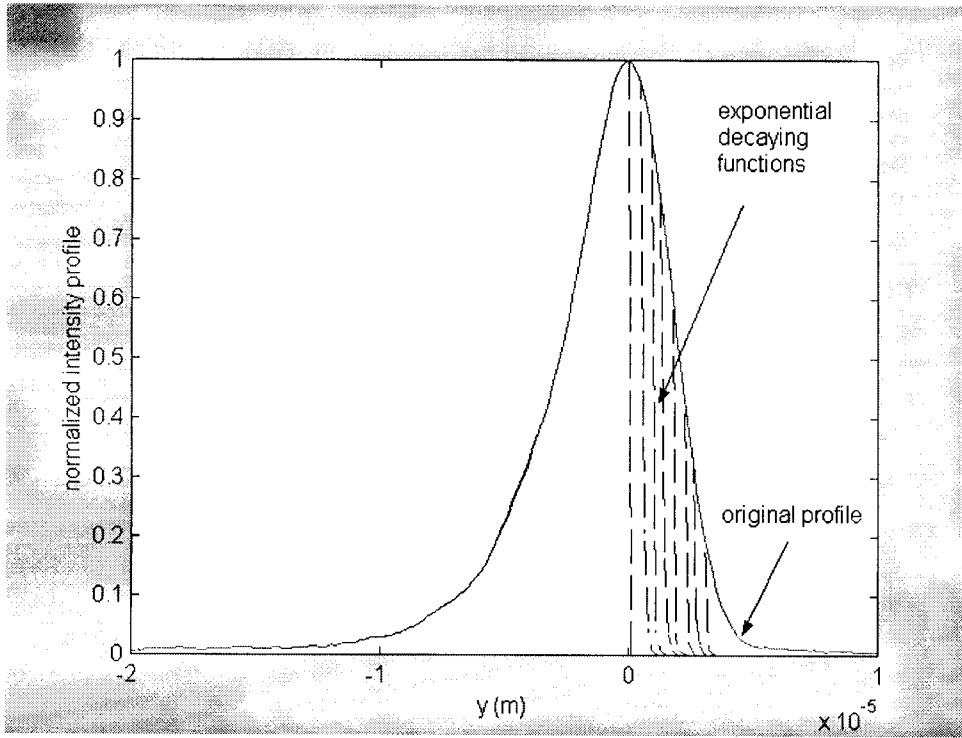


Figure 5-9: List of profiles with the sharply decaying portion replaced with exponentially decaying functions

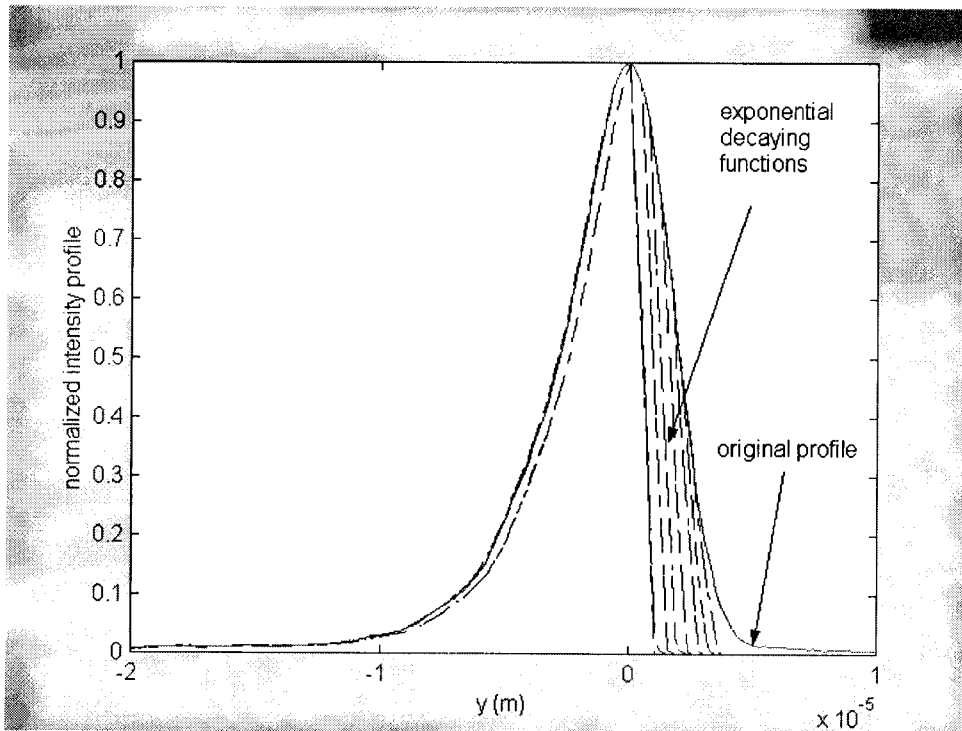


Figure 5-10: List of filtered profiles in figure 5-9

In order to compare with the intensity profile obtained experimentally, each intensity profile is fed into the CodeVTM lens model to obtain the intensity profile at the image-plane. Then the difference between the simulated intensity profile and the experimental intensity profile can be used to produce a new profile. This process is repeated until there is no more improvement. Then the same process is repeated with a profile with a new exponentially decaying function. The profile with the minimum error is chosen to be the diffraction reduced intensity profile. Figures 5-11 a) and b) show the final intensity profile along the x and y directions, respectively. The intensity profiles from the diffraction-reduction algorithm are smaller than the intensity profiles derived using the lensmaker's formula and the Gaussian Beam equation. In figure 5-11 b), the difference along the sharply falling edge along the y direction is more noticeable. Without using the diffraction reduced algorithm, the profile along the y direction appears smoother. On the other hand, with our algorithm, the sharply falling edge of the profile is preserved.

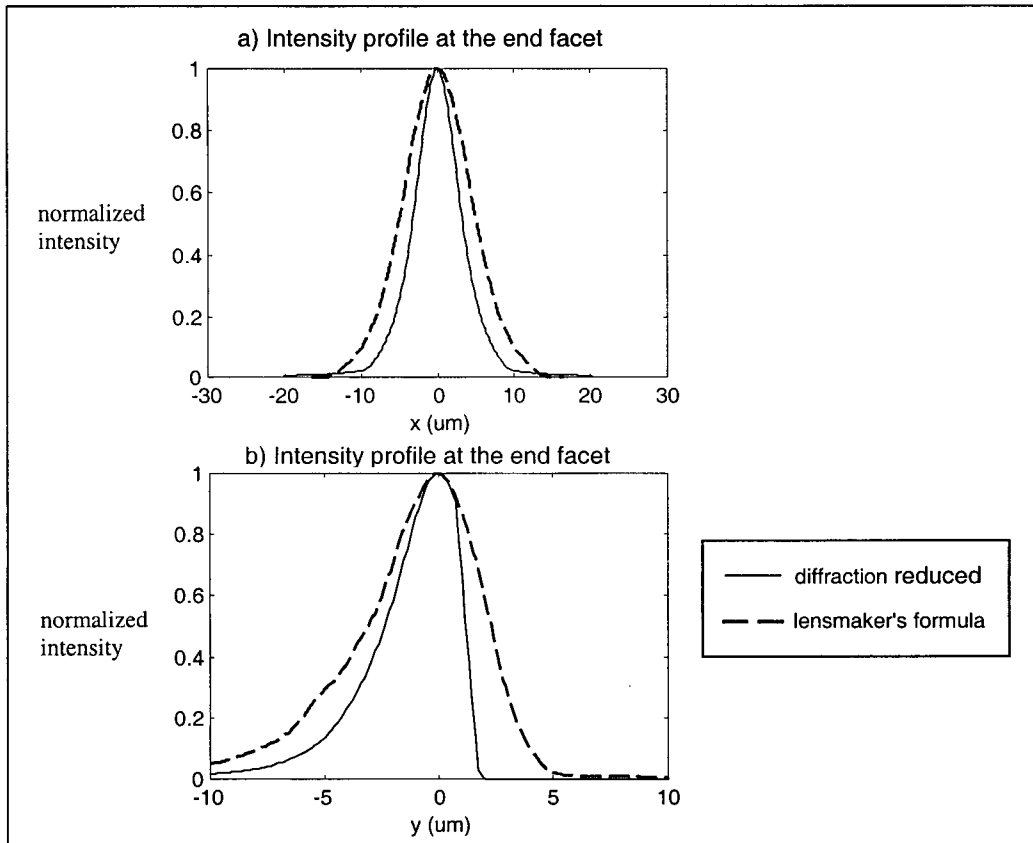


Figure 5-11: Comparison of intensity profiles at the end facet of the waveguide

In order to analyze the improvement in the intensity profile obtained using our algorithm, both the intensity profiles from the diffraction-reduction algorithm and the intensity profiles calculated from the lensmaker's formula are simulated to obtain their image-plane intensity profiles. These image profiles are compared with the intensity profiles obtained experimentally as shown in figure 5-12. In figures 5-12 a) and b), the solid lines represent the intensity profile of our diffraction-reduction algorithm at the image-plane while the dotted line is the intensity profile from the lensmaker's formula.

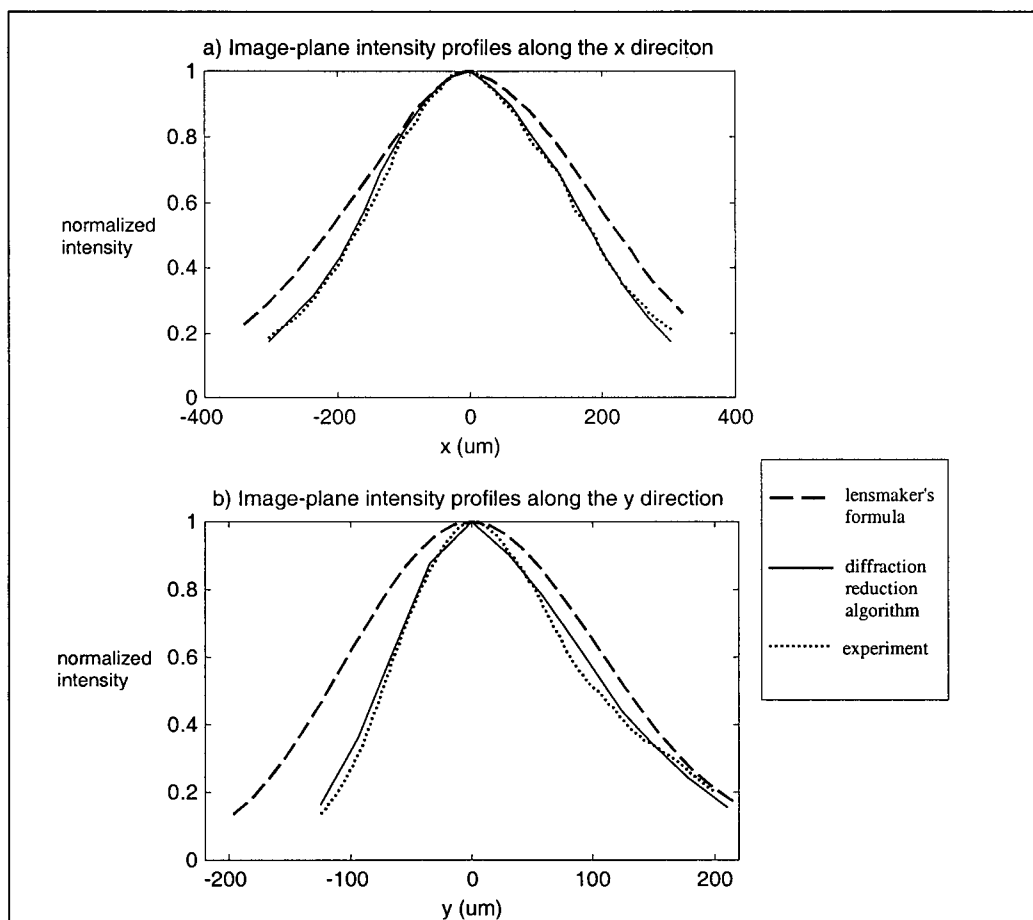


Figure 5-12: Comparison of intensity profiles at the image-plane

By using the lensmaker's formula, the resulting image profile is not only wider but also smoother than the actual intensity profile from the experiment. Figure 5-12 b) shows that while the sharply falling edge of the intensity profile along the y direction was still preserved using our diffraction reduced algorithm, this feature is less apparent in the intensity profile using the lensmaker's formula. The accuracy of the final intensity profile from the diffraction-reduction algorithm is limited to the output resolution of CodeV™. If the simulated intensity profile had a higher resolution, the diffraction-reduction algorithm would be able to make a better adjustment for the predicted profile during the

iterative process. Although the image of the diffraction reduced intensity profile does not exactly match the one obtained experimentally due to the low output resolution of CodeVTM, the error is significantly smaller than that obtained using the lensmarker's formula. Therefore, the diffraction-reduction algorithm can provide a more accurate estimate of the intensity profile at the end facet of the waveguide than the standard TNFIPM does.

5.5 Refractive Index Profile Measurement

In this section, the refractive index profile derived using the diffraction reduced intensity profiles will be presented. There are three main steps involved in deriving the refractive index profile: applying the inverse wave equation, employing the redundancy test algorithm, and processing through the morphing algorithm. They are presented in the following sections.

5.5.1 Results of Applying the Inverse Wave Equation

The purpose of having an accurate representation of the mode profile is to minimize the noise being amplified when the inverse wave equation is applied to derive the refractive index profile. However, due to the high spatial noise in the intensity profile of a titanium indiffused waveguide, there is always noise introduced in the derived index profile when the inverse wave equation is applied. Therefore, even after applying the inverse wave equation, a Savitzky-Golay filter is required to remove noise in the derived index profile.

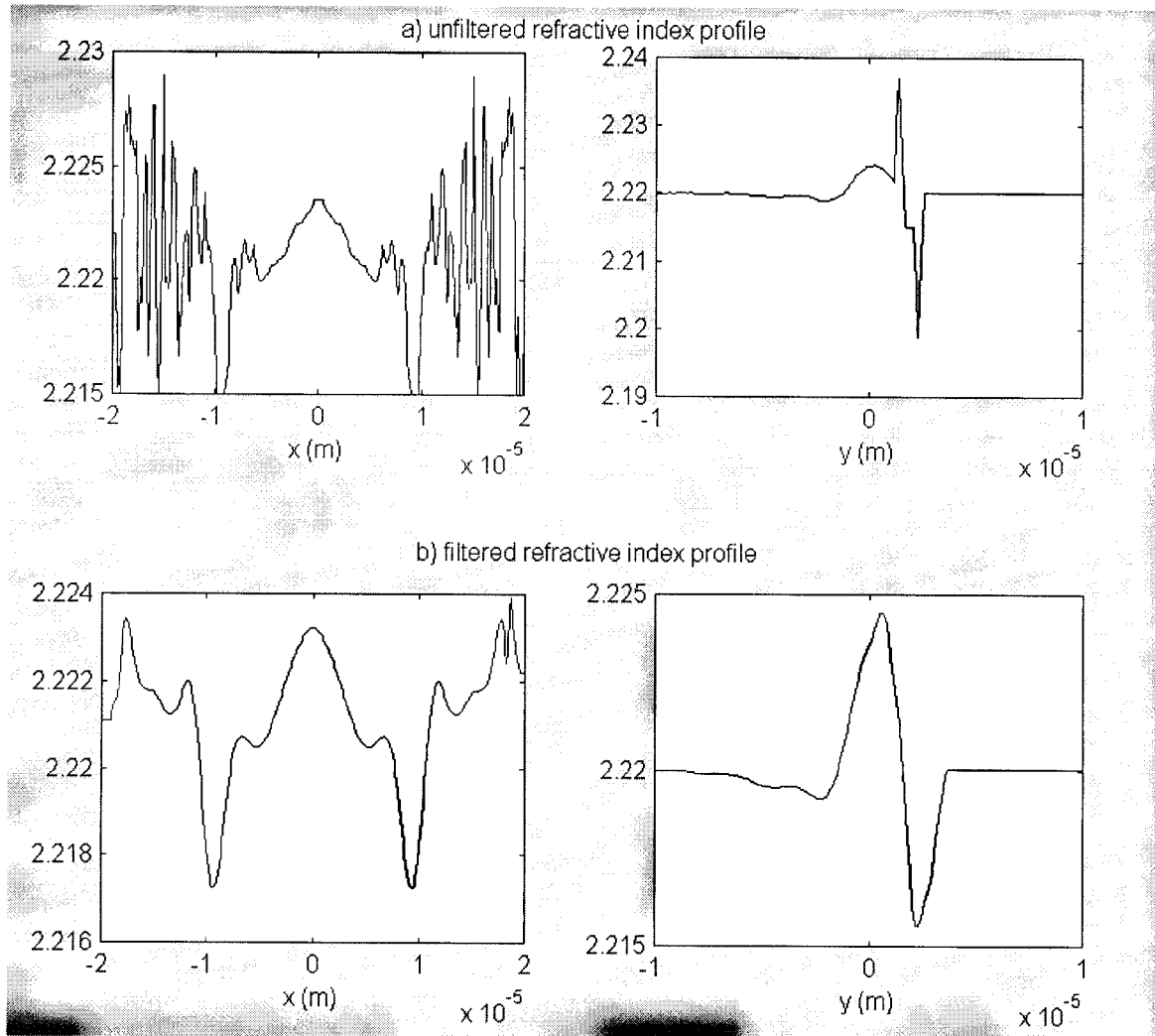


Figure 5-13: Derived index profiles using diffraction reduced intensity profile

Figure 5-13 a) shows the unfiltered refractive index profiles, which are severely distorted by noise, especially in the region where the intensity is the weakest. Since the offset of the refractive index profile is adjusted by matching the derived index profile deep in the substrate with the refractive index of the substrate material as discussed in section 2.2, this error can significantly distort our result. Therefore, it is important to apply the filter to remove as much unwanted noise as possible in the derived index profile. By applying a Savitzky-Golay filter to figure 5-14 a), the noise level is decreased as shown in figure 5-

14 b). Compared with figure 5-14 a), the filtered derived index profile not only has less noise in the core region of the waveguide but also has less noise in the region where the intensity is the weakest. In addition, any residual noise can be removed by reconstructing the weakly guiding section of the index profile with the *a priori* knowledge of the waveguide. Since the waveguide under study was fabricated in LiNbO_3 and was coated with silicone dioxide, the index profiles were adjusted in the weakly guiding part to better describe the waveguide under study and the resulting constructed index profile are shown in figure 5-16.

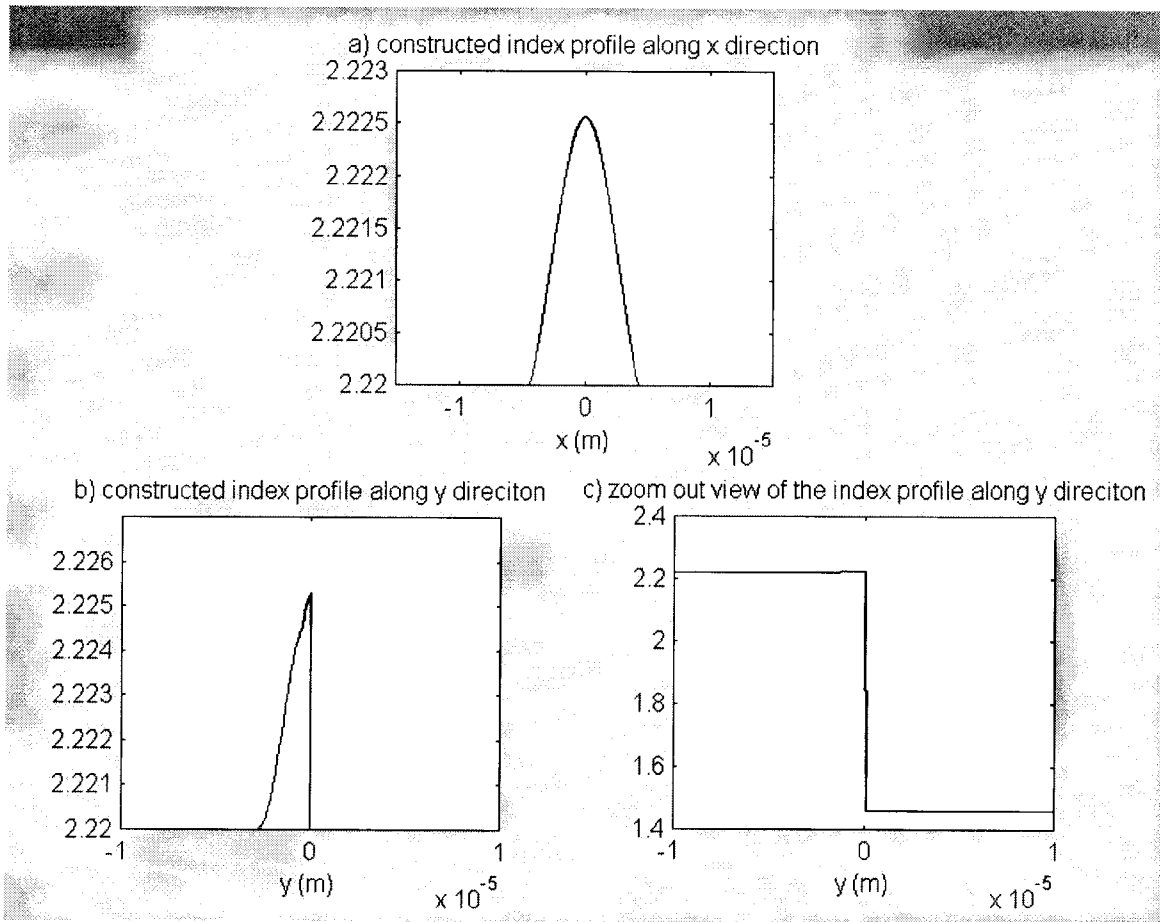


Figure 5-14: Constructed index profile along the x and y directions

In order to compare with a standard TNFIPM, the inverse wave equation was applied to the experimental intensity profiles (i.e., without the diffraction-reduction algorithm). The resulting index profiles are shown in figure 5-15 a). As can be seen the profile is wider and flatter than the one derived using the diffraction reduced algorithm due to the diffraction effects. In the standard TNFIPM, a filtering process is required to remove the unwanted noise in the derive index profiles. Therefore, a Savitzky-Golay filter is applied to figure 5-15 a). The solid lines in figure 5-15 b) show the index profiles after filtering is applied. However, as one can see, the index profiles after filtering is applied are noisier than the ones in figure 5-13 b). In addition, as the last step of the standard TNFIPM, the derived index profiles are fitted with Gaussian functions and are reconstructed with the *a priori* knowledge of the waveguide. The resulting index profiles after applying the standard TNFIPM are shown as the dotted lines in figure 5-15 b). Comparing with figure 5-14, the derive index profiles using the TNFIPM are significantly wider along the x direction and more flattened along the y direction.

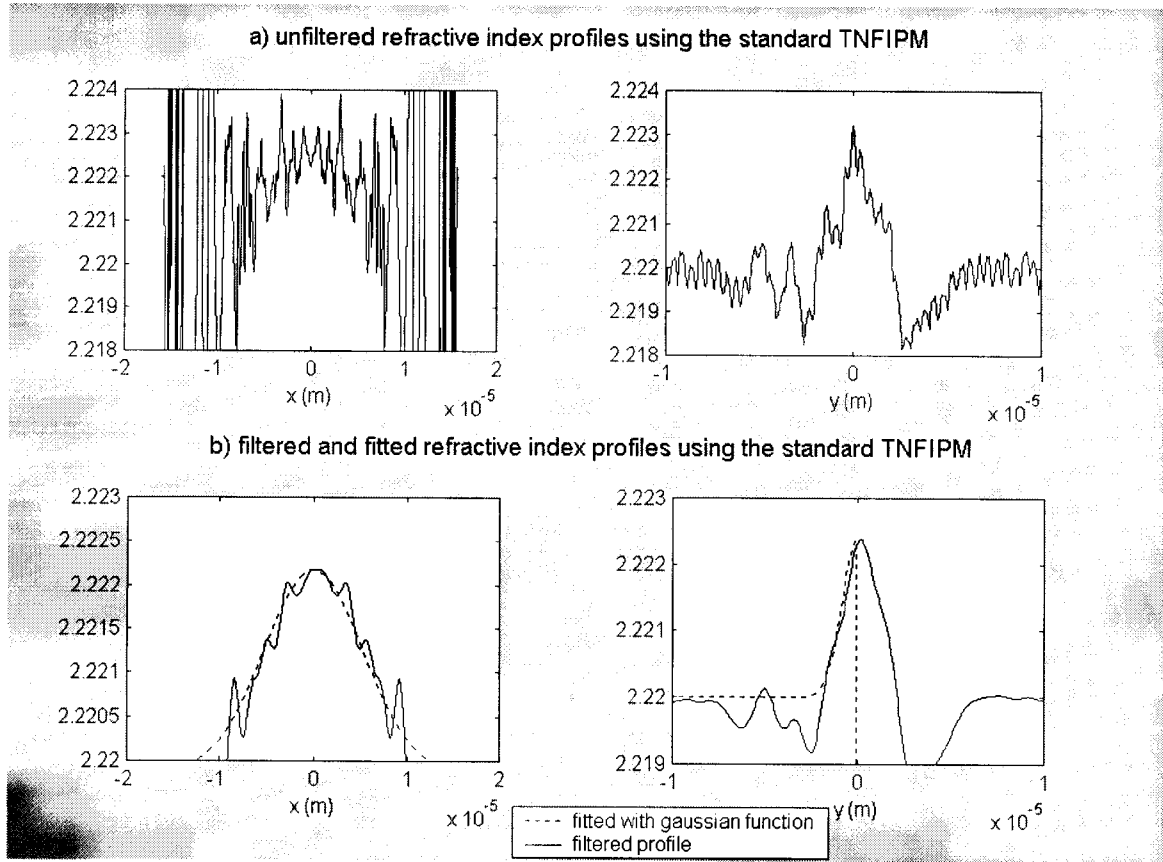


Figure 5-15: Derived index profiles using a standard TNFIPM

In order to compare the accuracy of the derived index profiles after applying the inverse wave equation, the intensity profiles at the end facet of the waveguide with the derived index distributions were obtained using BeamPROPTM. Figures 5-16 a) and b) show the intensity profiles along the x direction and y directions for the derived index profiles from our proposed method and from the standard TNFIPM. While there is only a slight difference in the intensity profiles along the y direction, the intensity profile along the x direction using the derived index profile matches better to the intensity profile calculated from the diffraction-reduction algorithm than the intensity profile obtained from a standard TNFIPM. Therefore, the diffraction-reduction algorithm has helped in obtaining a better estimate of the index profile when applying the inverse wave equation.

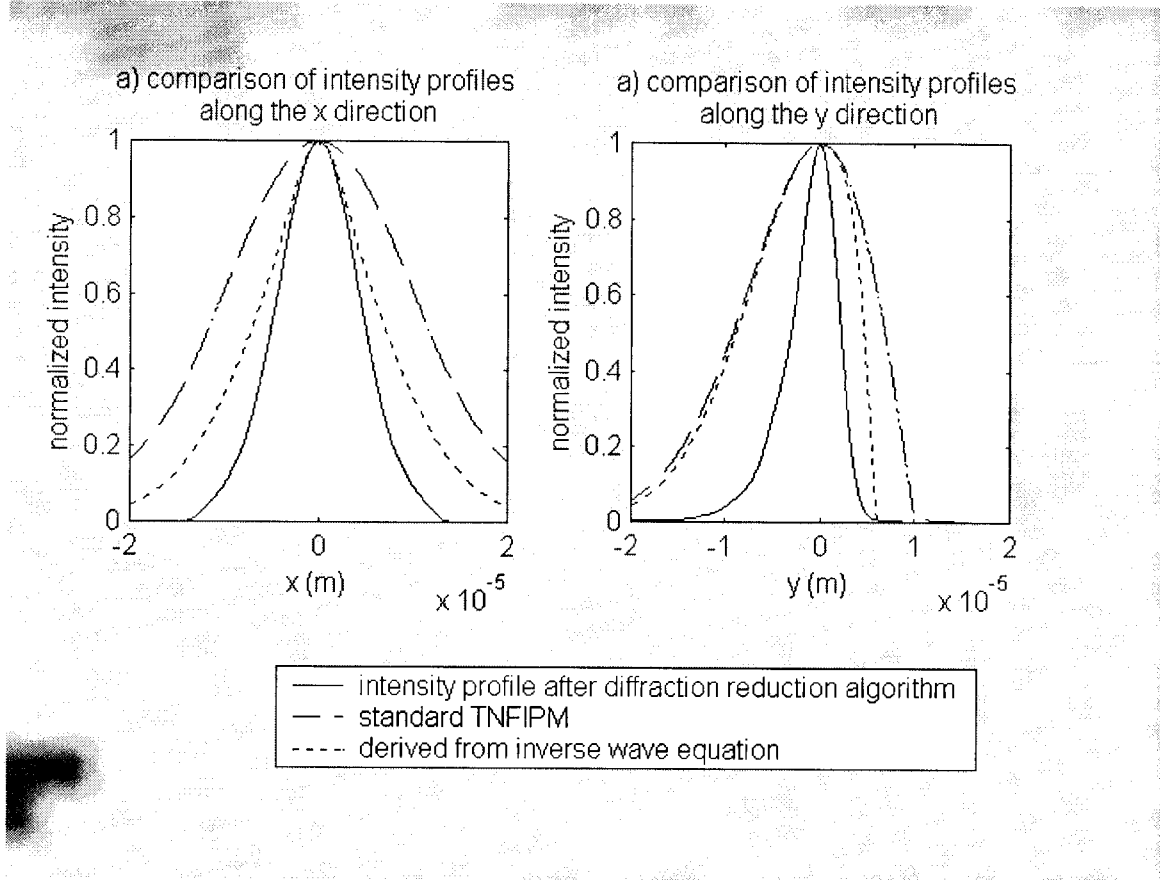


Figure 5-16: Intensity profiles at the end facet of the waveguide with the derived index profiles

5.5.2 Redundancy Test Algorithm

Although the Savitzky-Golay filter provides a good balance between maintaining the shape of the profile and removing the unwanted noise, the noise can sometimes be too high and inevitably the profile shape is flattened due to excess filtering. Therefore, the next step towards having the correct index profile is to apply a redundancy test, which varies the size and the amplitude of the index profiles until a more accurate index profile is found.

Before applying the redundancy test, one should select the search range for a better estimate of the size and amplitude of the index profile. We have chosen the range to be from 80% to 120% initially for both the size and amplitude of the derived index profile for the first attempt in applying the redundancy test. One observation after applying the redundancy test with this initial search range indicates that the error decreases the most when the amplitude of the y index profile is increased. This means that the filtering in the previous section has flattened the index profile along the y direction. Therefore, before repeating the redundancy test to find the profile with the minimum error, the search range for the amplitude of the y profile is modified to be from 100% to 160% in the second attempt of the redundancy test and from 150 to 200% in the third attempt. In addition, the resolution of the search range was adjusted to improve the search time and accuracy.

Figures 5-17 a) and b) show the index profile of the waveguide along the x and y directions, respectively, found in the second attempt of the redundancy test. Their simulated intensity profiles are shown in figures 5-17 c) and d). Figures 5-18 c) and d) are the simulated intensity profiles of the waveguide from the third pass, which has a better match with the intensity profile from the experiment when compared with figure 5-17 c) and d). Figures 5-18 a) and b) are the index profiles of the waveguide with the minimum error after the redundancy test is applied. Although the morphing algorithm is still required in order to obtain the final index profile, its simulated mode profiles are already much more accurate than the ones found using the standard TNFIPM, which are much wider than they should be.

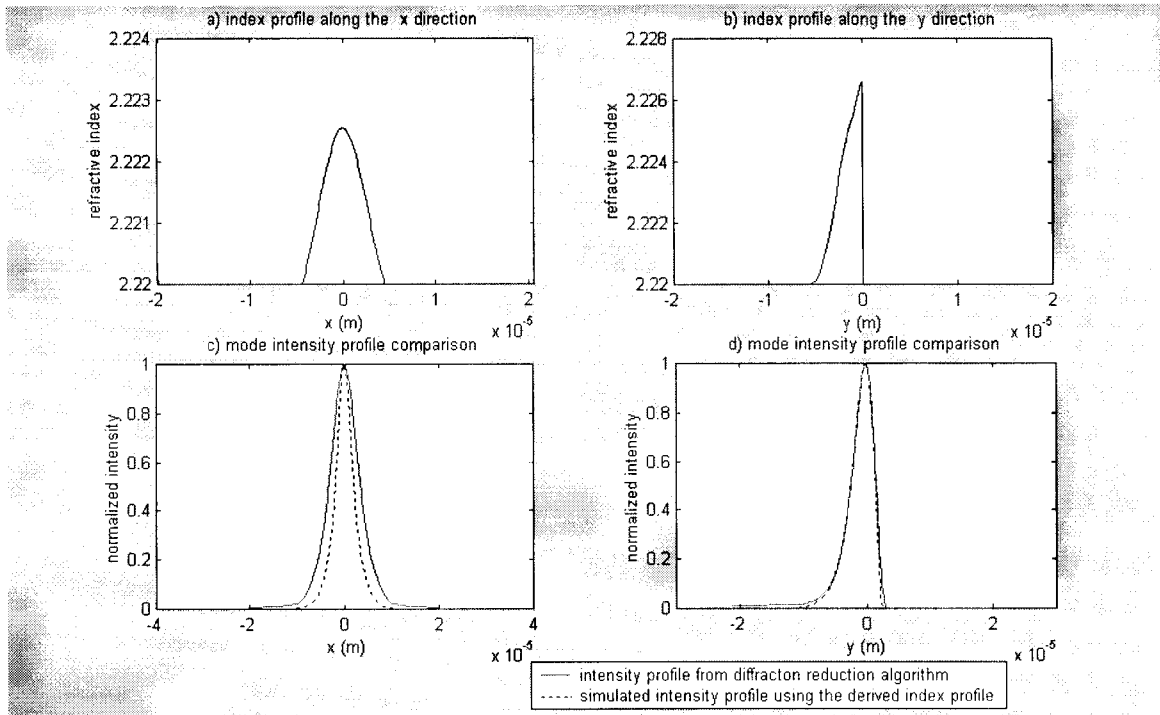


Figure 5-17: The index profiles and their simulated intensity profiles in applying the redundancy test for the second time

Figure 5-18: The index profiles and their simulated intensity profiles in applying the redundancy test for third time

5.5.3 Morphing Algorithm

The last step in our proposed TNFIPM is the morphing algorithm, which modifies the shape of the index profiles so that a better profile can be used to describe the index distribution of the waveguide. In the previous section, after applying the redundancy test, a more accurate index profile was obtained. This index profile is used as the basic profile for our morphing algorithm. The search range used in the redundancy test is also applied to find the best possible index profile for each function generated during the morphing process.

As suggested in section 2.7 and 3.4.2, two types of functions were chosen for performing the proposed morphing algorithm: the Parabola and the Gaussian functions. The algorithm starts with the parabola and morphs it into a Gaussian function. Figures 5-19 and 5-20 show some of the functions generated during the morphing process. There are in total 25 functions generated during the morphing process. For each index profile along the x and y directions, the profile is separated into the middle and outer sections. The curvature of the profile in each section for both the x and y directions are modified to produce a function.

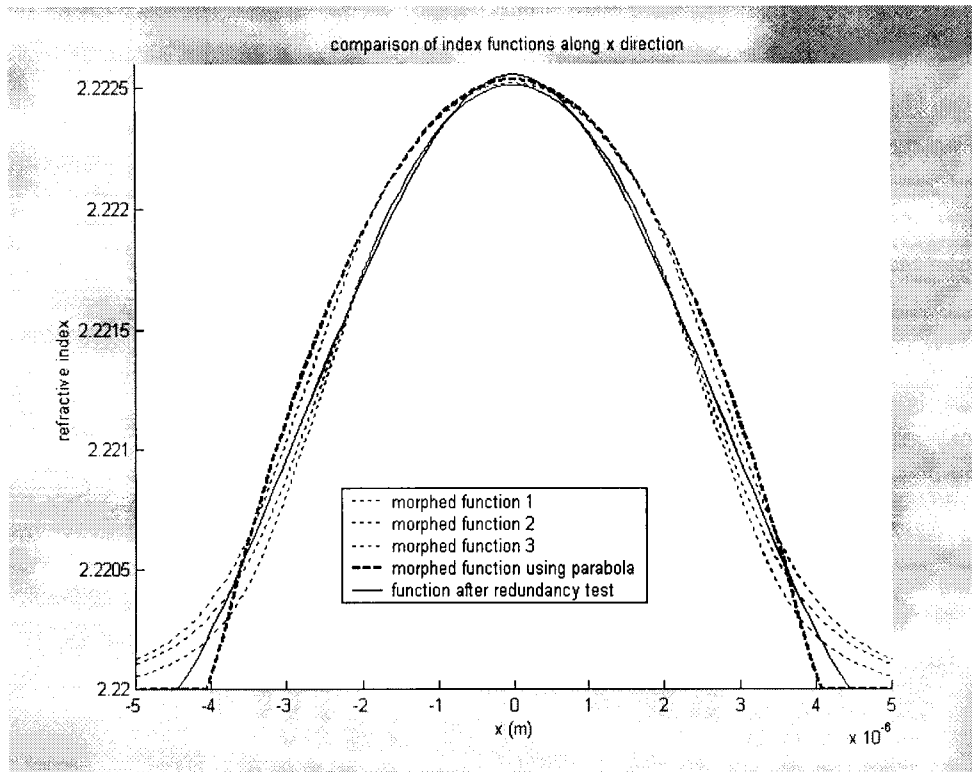


Figure 5-19: Functions generated during the morphing process for x direction

Figure 5-20: Functions generated during the morphing process for y direction

Although a lot more functions can be generated for testing, the testing time increases with the number of functions generated since the redundancy test is required. With each of the functions generated from morphing process, a redundancy test is required to find the index profile that produces the minimum error. For the 25 functions generated in the morphing algorithm, the total number of mode profile simulations required is approximately 8000 and the whole morphing process takes 14 days to complete on a 400MHz computer using BeamPROP™ (this could be reduced with a better mode solver).

In our simulation, for every function, the profile with the minimum error always happens in the range specified by the redundancy test, which means that the search ranges for the best amplitude and the size of the index profile are adequate. In addition, the profile with the minimum error does not always happen at the same point of the amplitude and waist search ranges for each function. Therefore, the shape of the index profile does play an important role in obtaining a correct index profile.

One of the observations made during this experiment was that there was a close relationship between the index profile along the x and y directions. It is possible to produce a good match in the intensity profile along the x direction but the mismatch in the intensity profile along the y direction will be quite severe. Therefore, the comparison of the intensity profile must be done for both the x and y directions for every simulation.

Figure 5-21: Final index profiles found in the morphing process with their corresponding intensity profile

The final index profiles that produced the best match to the intensity profiles from diffraction reduced algorithm are shown in figure 5-21 a) and b), for the x and y directions, respectively. The simulated intensity profiles using the final index profiles are shown in figure 5-21 c) and d) for the x and y directions, respectively. The match between the simulated intensity profile from the final index profile and the intensity profile from the diffraction-reduction algorithm is excellent compared with the previous results from applying the redundancy test. This has also proven that in order to find the most accurate index distribution, one must not only consider the amplitude and size of the index distribution but also the curvature or shape of the index profile.

To summarize the results found in this chapter, figure 5-22 shows a list of the index profiles generated from the experiment and figure 5-23 shows the comparison of the intensity profiles simulated using the index profile obtained from a standard TNFIPM and the proposed TNFIPM. A standard TNFIPM produces a much wider index profile along the x direction and a much lower index profile along the y direction due to the noise, the diffraction, and the filtering as expected. The intensity profile obtained from a standard TNFIPM produces a much wider intensity profile for both the x and y directions. With the redundancy test the derived index profile is much closer to the final result since the sizes of the profiles have been adjusted to improve the accuracy. Although the intensity profiles from the redundancy test match quite nicely with the intensity profiles after the diffraction-reduction algorithm, there are still some differences in the index profiles compared to the final ones. This is mainly due to the difference in the curvature of the index profiles, which are resolved in the simple morphing algorithm. The final simple morphing algorithm further increases the accuracy of the results. Figure 5-23 shows that the intensity profile of the final index profile almost matches with the intensity profile obtained from the diffraction-reduction algorithm. Therefore, the proposed TNFIPM is a much improved and more accurate method for acquiring the refractive index distribution of a waveguide than the standard TNFIPM method.

Figure 5-22: Index profile comparison

Figure 5-23: Intensity profile comparison

5.6 Conclusion

In this Chapter, the results of the proposed TNFIPM has been presented using a titanium in-diffused waveguide. The proposed TNFIPM incorporates several algorithms, such as diffraction reduction, redundancy test and morphing, whose improvements have been shown in each section. Using the diffraction-reduction algorithm, we had a much better estimate of the intensity profile at the end facet of the waveguide, which helped in deriving a more accurate index profile. We have also shown that the index profiles obtained through the redundancy test and the morphing algorithm provide a more accurate mode intensity profile that better matches the intensity profile from the diffraction-reduction algorithm. Therefore, the proposed TNFIPM does provide significant improvements as compared to the standard TNFIPM.

Chapter 6: Conclusion and Suggestions for Future

Work

Although the concept of TNFIPM is quite simple, its implementation presents a lot of challenges such as diffraction and noise. Diffraction effects can cause the mode profiles to appear smoother and wider than they should be, while the inverse wave equation amplifies any noise in the mode profile making the derived index profile inaccurate and unusable.

In this thesis I have presented an improved version of the TNFIPM, which addresses these problems. The diffraction-reduction algorithm reduced the diffraction effects on the intensity profile while the redundancy test and morphing algorithm removed errors caused by noise in the index profile. By applying the diffraction-reduction algorithm we were able to obtain an intensity profile at the end facet of the waveguide that would yield the same image-plane intensity profile as the one from the experiment whereas the standard TNFIPM yields a profile that is much wider. With a much more accurate intensity profile, the inverse wave equation is applied to obtain the index profile, which can be noisy due to the noise of the index profile. While most standard TNFIPM would fit a commonly known function to the obtained index profile to describe the final index profile, our proposed TNFIPM introduces the redundancy test and the morphing algorithm, which changes the size, amplitude, and shape of the possible index profiles

until a better result is obtained. This means that with our proposed TNFIPM, the index profile produces a more accurate intensity profile than with a standard TNFIPM.

Although our method offers a more accurate result, it takes much longer to execute as compared to a standard TNFIPM, which would only take a few minutes. In our proposed TNFIPM, the redundancy test currently takes about 1 day to run on a 400MHz machine and the morphing test may take up to two weeks. The main problem is that while the Beam Propagation Method used in our experiment is very accurate it is not efficient enough for our purpose. Therefore, for the future work, more efficient mode solving software (which is available), is required, which will significantly speed up the time in simulation. It will also allow the morphing algorithm to search more function types to fit to the index profile and need not be limited to two functions as in the current system.

Another improvement that can be made is to implement a two-dimensional measurement system instead of using a cutting-knife edge detector. The cutting-knife edge technique provides the average of the intensity profile of the waveguide along both the x and y directions. The derived index profile is then the average index profile of the waveguide. If one needs the refractive index profile at a particular position in the waveguide, a narrow slice of the waveguide output-intensity profile along the x and y direction should be used to derive the index profile of a waveguide. Although by using a small slit with the cutting-knife edge system can provide similar results, the diffraction from the small slit can introduce greater complexity in modeling the optical system model in the diffraction-reduction algorithm. A better solution is to use a high resolution two-

dimensional video camera to sample the intensity profile. The output of the video camera is an array of data, representing the intensity of the waveguide output image. With high resolution CCD, any slice of the intensity profile can be extracted from the data and used for deriving the index profile. This means that instead of having the average index profile, a two-dimensional index profile of the waveguide can be obtained.

Appendix A: Savitzky-Golay Filter

The Savitzky-Golay filter algorithm is based on finding a least-square fit polynomial of degree d on a set of data with a window size of $2n+1$ [28][29]. For each point p in our samples, the window covers a set of data of size $2n+1$ with its center at p . The coefficients are chosen so that they provide the best least-square fit with a polynomial of degree d to this set of data. Then we replace the value p with the fitted value in the polynomial function at point p .

Although finding the least-square fit polynomial can be computationally intense, Savitzky and Golay showed that a set of integers could be derived as weighting coefficients to carry out the smoothing operation. These integers are called "convolution integers", which turn out to be exactly equivalent to fitting the data to a polynomial and significantly reduces the computation [30]. The following discussion is the derivation of these "convolution integers" taken from *"Introduction to Signal Processing"* by S. J. Orfanidis[28].

Considering a set of data where xm is the original data, d is the degree of the polynomial, and $2n+1$ is the window size. We can write xm' , the least-squares polynomial fitted values that will be fit to the data, as

$$xm' = C_0 + C_1m + C_2m^2 + \dots + C_dm^d \quad (A.1)$$

where m ranges from $-n$ to n . Then $C_i s$ are determined optimally such that the corresponding polynomial curve best fits the given data. This can be accomplished by a least-squares fit, which chooses the $C_i s$ to minimize the total mean-square error:

$$f = \sum_{m=-n}^{m=n} e_m^2 = \min \quad (\text{A.2})$$

where

$$e_m = xm - xm'. \quad (\text{A.3})$$

This is called the performance index.

Writing $s_0(m) = 1, s_1(m) = m, s_2(m) = m^2, \dots, s_n(m) = m^n$, and $-n \leq m \leq n$, then, vectorially, one obtains:

$$x' = c_0 s_0 + c_1 s_1 + c_2 s_2 + \dots + c_n s_n = SC \quad (\text{A.4})$$

where $S = [s_0, s_1, s_2, \dots, s_n]$ and $C = \begin{bmatrix} c_0 \\ c_1 \\ c_2 \\ \vdots \\ c_n \end{bmatrix}$. Then writing $e = x - x' = x - SC$, the

performance index can be expressed as the dot product:

$$f = e^T e = (x - SC)^T (x - SC) = x^T x - 2C^T S^T x + C^T S^T SC \quad (\text{A.5})$$

Setting the gradient $\partial f / \partial C = 0$ and solving for C , one obtains

$$\frac{\partial f}{\partial C} = -2S^T e = -2S^T (x - SC) = -2(S^T x - S^T SC) = 0 \quad (\text{A.6})$$

The minimizing condition gives the so-called orthogonality equation:

$$S^T e = 0 \quad (\text{A.7})$$

which can be written as the normal equation:

$$S^T SC = S^T x \quad (\text{A.8})$$

with optimal solution:

$$C = (S^T S)^{-1} S^T x \equiv G^T x \quad (\text{A.9})$$

where $G = S(S^T S)^{-1}$.

Then we can obtain the smoothed value as

$$x' = SC = SG^T x = S(S^T S)^{-1} S^T x \equiv Bx \quad (\text{A.10})$$

$$\text{and } B = SG^T = GS^T = S(S^T S)^{-1} S^T \quad (\text{A.11})$$

b_0 , the center column of B is the most important one because it is the one that smooths the value x_0 , which is symmetrically placed with respect to the other data in x . The components in this column are the weighted coefficients that give the minimum least-square error.

For a fixed window size and a predetermined polynomial degree, B matrix or its center column, b_0 , can be calculated using equation A.11. However, Savitzky-Golay published a table of coefficients in their paper which can be used for a range of window size and polynomial degree[30].

Appendix B: Beam Propagation Method(BPM)

Beam Propagation Method (BPM) is commonly used to simulate beam travel through a longitudinally invariant waveguide with a particular transverse refractive index profile. BPM is the most widely used propagation technique for modeling integrated optics and fiber optic devices due to its simplicity and efficiency while still yielding very accurate results. The following BPM discussion is based on the documentation accompanying BeamPROPTM, a commercial package used in our experiments [8]. BPM can be explained most easily using the scalar field and assumes paraxiality

With the scalar field assumption, the wave equation can be written in the form of Helmholtz equation for monochromatic waves:

$$\frac{\partial^2 \phi}{\partial x^2} + \frac{\partial^2 \phi}{\partial y^2} + \frac{\partial^2 \phi}{\partial z^2} + k(x, y, z)^2 \phi = 0 \quad (\text{B.1})$$

with the scalar electric field $E(x, y, z, t) = \phi(x, y, z)e^{-i\omega t}$ and the wavenumber $k(x, y, z) = k_0 n(x, y, z)$. The waveguide is defined entirely by the refractive index distribution $n(x, y, z)$. The phase of ϕ changes rapidly due to propagation along the z direction. By introducing the average wavenumber \bar{k} with a slowly varying field $u(x, y, z)e^{i\bar{k}z} = \phi(x, y, z)$ in (B.1), it becomes

$$\frac{\partial^2 u}{\partial z^2} + 2i\bar{k} \frac{\partial u}{\partial z} + \frac{\partial^2 u}{\partial x^2} + \frac{\partial^2 u}{\partial y^2} + (k^2 - \bar{k}^2)u = 0 \quad (\text{B.2})$$

Since the variation of u with the propagation direction, z , is sufficiently slow, the first term above can be neglected with respect to the second. This approximation is referred as the paraxial approximation. With this assumption, the above equation reduces to:

$$\frac{\partial u}{\partial z} = \frac{i}{2k} \left(\frac{\partial^2 u}{\partial x^2} + \frac{\partial^2 u}{\partial y^2} + (k^2 - \bar{k}^2)u \right) \quad (\text{B.3})$$

This is the basic BPM equation in three dimensions (3D). Given an input field, $u(x,y,z=0)$, the above equation determines the evolution of the field in the space $z>0$.

The efficiency of equation (B.3) is based on two factors. First, although by introducing a slowly varying field approximation the phase variation cannot be modeled accurately, the computation step for the field along the z propagation direction is increased to be larger than the wavelength. Second, the elimination of the second derivative term in z reduces the problem to a first order initial value problem that can be solved by integration along the z direction. These simplifications imply a computation time reduction by a factor of at least of the order of N , the number of longitudinal grid points, compared to full numerical solution of the Helmholtz equation.

What makes BPM an ideal choice for our application, besides it's efficiency, is its input requirement. The simulated field at the end facet of a waveguide only depends on two main factors: the input field, $u(x,y,z=0)$, and the refractive index profile of the waveguide, $n(x,y,z)$. Since the light source is a laser coupled with a single mode fiber, the input field, $u(x,y,z=0)$, can be approximated with a Gaussian function. The $n(x,y,z)$ is the index profile under study. Therefore, it is very convenient to obtain an index profile's mode profile using BPM.

Appendix C: Calibration of Lens Model

An accurate software model was required for image convergence in our diffraction free algorithm. CodeVTM was selected for our simulation program because it includes a diffraction based beam propagation simulator. In this section, we discuss the procedures for setting up an accurate lens model and the accuracy of our lens model.

In order to be able to verify our lens model, a calibration experiment was setup using a Corning SMF-28 single mode fiber with 1310nm laser as the known light source. SMF-28 fiber has a mode field diameter of $9.3 \pm 0.5 \mu\text{m}$ with a near Gaussian intensity distribution. After passing light through the aspheric lens, as in our TNFIPM system, the mode profile of the fiber was captured and sampled using the omega meter and a digital sampling scope

Figure C-1: CodeVTM paraxial setup of a lens system

The first step for setting up the optical system model is to construct a paraxial lens model that represents the lens system used in our experiment. Most of the parameters can be obtained or measured such as the fabrication parameters of the lens and the distance from the image to the lens. The only two unknown parameters are the source size and the distance from the source to the lens, which can be calculated using the same Gaussian beam magnification equations as in the section 2.5. Figure C-1 shows the paraxial setup window for our experimental system.

CodeVTM's Paraxial Ray Tracing Tool can only provide us an approximate estimate of the image. In order to improve the accuracy in our simulation a diffraction-based Beam

Propagation Tool is required after the paraxial Ray Tracing Tool is employed. Figure C-2 shows the intensity profile at the image plane using CodeVTM's diffraction-based Beam Propagation tool.

Figure C-2: Intensity profile at the image-plane simulated with the diffraction-based Beam Propagation Tool

The diffraction-based Beam Propagation Tool is able to provide us a more precise lens model since it accounts for the diffraction effects. By adjusting the light source's distance to the lens, the magnification of the image size can be adjusted until a match is obtained between the simulated and experimental images. Figure C-3 provides a comparison between the experimental mode profile and the simulated mode. The two profiles match almost perfectly, which means the lens model is quite accurate.

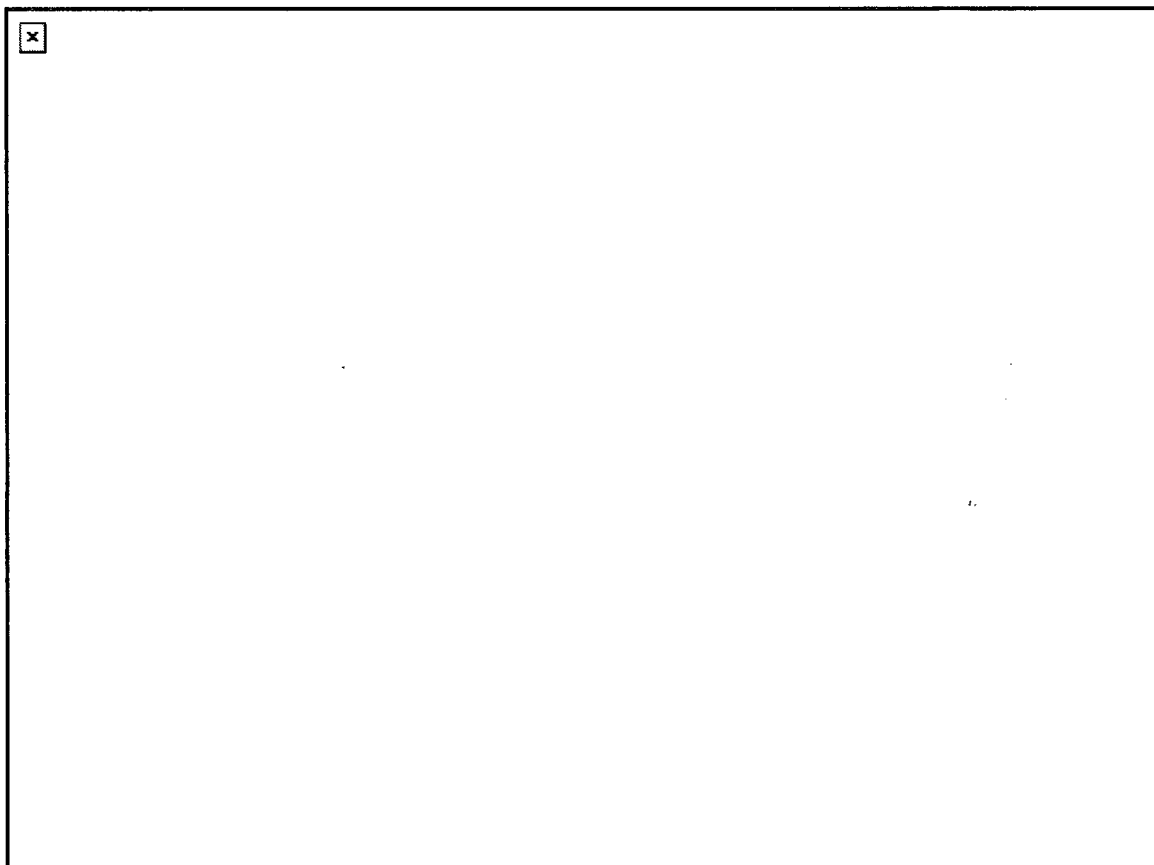


Figure C-3: Image profile comparison

References

- [1] F. Caccavale, P. Chakraborty, A. Quaranta, G. Gianello, I. Mansour, R. Corsini, and G. Mussi, "Secondary Ion Mass Spectrometry and near field studies of Ti:LiNbO₃ Optical Waveguide," *J. Appl. Phys.*, vol.78, p.5345, 1995
- [2] K. S. Chiang, "Construction of refractive index profiles of planar dielectric waveguides from distribution of effective indexes", *J.Lightwave Technol.* vol LT-3, pp. 385-391, 1985
- [3] J. M. White and P. F. Heidrich, "Optical Waveguide refractive index profiles determined from measurements of mode indices: A simple Analysis," *Appl. Opt.*, vol. 15, pp. 151-155, 1976
- [4] F. Caccavale, F. Gonella, G. Caneva, and I. Mansour, "Iterative Simplex-Finite Difference Method for the Characterization of Optical Waveguides", *J. Lightwave Technol.* p. 1825-1830, 1996
- [5] R. Bernini, R. Pierri, , "An Iterative Method for Optical Reconstruction of Graded Index Profiles in Planar Dielectric Waveguides," *J. Lightwave Technol.* vol. 16, pp. 729-736, 2000
- [6] F. Caccavale, F. Segato, I. Mansour, and M. Giancesin, "A finite differences methods for reconstruction of refractive index profile from near field measurements," *J. Lightwave Technol.* vol. 16, pp. 1348-1353, 1998

- [7] M. L. Bibra and A. Roberts, "Refractive Index Reconstruction of Graded-Index Buried Channel Waveguides from Their Mode Intensities", *J. Lightwave Technol.*, vol.15, pp.1695-1699, 1997
- [8] D. Brooks and S. Ruschin, "Improved near-field method for refractive index measurements of optical waveguides," *J. Lightwave Technol.* vol 8, pp, 254-256, 1996
- [9] K. Morishita, "Refractive-index Determination of Single-Mode Optical Fibers by a Propagation-mode Near-field Scanning Technique,". *J. Lightwave Technol.*, vol. LT-1, pp. 445-449, Mar. 1983.
- [10] I. Mansour and F. Caccavale, "An Improved Procedure to Calculate the Refractive Index Profile from the Measured Near-Field Intensity", *J. Lightwave Technol.* p. 423-428, 1996
- [11] L. McCaughan and E. E. Bergmann, "Index Distribution of Optical Waveguides from their mode profile, "*J. Lightwave Technol.*, vol. Lt-1, pp. 241-244, Jan. 1983
- [12] K. Morishita, "Index Profiling of Three-dimensional Optical Waveguides by the propagation-mode near-field method," *J. Lightwave Technol.*, vol Lt-4, pp. 1120-1124, 1986
- [13] J. Helms, J. Schmidtchen, B. Schuppert, and K. Petermann, "Error Analysis for Refractive-index Profile Determination from Near-field Measurements," *J. Lightwave Tech.*, vol. 8, pp. 625-633, Apr. 1990
- [14] L. Dhar, H. J. Lee, E. J. Laskowski, S. K. Buratto, c. Narayanan, H. M. Presby, C. C. Bahr, P. J. Anthony, and M. J. Cardillo, "Refractive Index Profiling of Planar Optical Waveguides using Near-field Scanning Optical microscopy," in *Proc. SPIE*, 1995, vol. 2535, pp. 120-124.

- [15] D. Brooks and S. Ruschin, "Improved Near-Field Method for refractive Index Measurement of Optical Waveguides," *OEEE Photon. Technol. Lett.*, vol. 8, pp. 254-256, Feb. 1996
- [16] F.W. Sears, "Optics", *Addison Wesley*, pp221-281, 1949
- [17] M. Born and E. Wolf, "Principle of Optics", 6th ed. New York:Pergamon, 1980
- [18] E. A. J. Marcatili, "Dielectric rectangular waveguide and directional coupler for integrated optics," *Bell Syst. Tech. J.* 48, 2071-2102(1969).
- [19] D. Marcuse, " Theory of Dielectric Optical Waveguides", *Academic Press*, 60-94, 1974
- [20] A. Vanderlugt, "Optical Signal Processing", *John Wiley&sons, Inc.*, p. 75-100, 1992
- [21] J. W. Goodman, "Introduction to Fourier Optics", *McGraw-Hill*, 1968
- [22] F. Yu and I. C. Khoo, "Principles of Optical Engineering", *John Wiley & Sons*, 1990
- [23] J. C. Dainty, "Laser Speckle and Related Phenomena", *Springer-Verlag*, Pg 286-309, 1984
- [24] V. N. Mahajan, "Optical Imaging and Aberrations", *SPIE*, Pg. 139-172, 1998
- [25] M. Davidson, Interactive Tutorial for light and color.
<http://microscopy.fsu.edu/primer/lightandcolor/index.html>, *The University of Florida*.
- [26] D. O'Shea, "Elements of Modern Optical Design", *John Wiley & Sons. Inc.*, Pg. 236-247, 1985
- [27] H. Kogelnik and T. Li, "Laser Beams and Resonators, " *Appl. Opt.* 5, 1550-1567, 1966
- [28] S. J. Orfanidis, "Introduction to Signal Processing," *Prentice-Hall*, sgn. proc. series, 1996

- [29] W. H. Press et al., "Numerical Recipes in C: The Art of Scientific Computing ,"
Cambridge Univ. Press, Chpt 14, 1993
- [30] A. Savitzky, and M. Golay, "Smoothing and Differentiation of Data by Simplified
Least Squares Procedures," *Anal. Chem.*.. vol. 36, pp.1627, 1964
- [31] P. Barak, "Smoothing and Differentiation by an Adaptive-Degree Polynomial
Filter," *Anal. Chem.* 1995
- [32] S. Ramos, J. Whinnery, T. Van Duzer,"Fields and Waves in Communication
Electronics", *John Wiley & Sons. Inc.*, Pg. 111-161, 1985
- [33] BeamProp Manual, <http://www.rsoftinc.com> , *Rsoft, Inc.*,
- [34] Thorlabs Omega Meter manual, <http://www.thorlabs.com> , *Thorlabs Inc.* 1999,
- [35] Newport application notes, "focusing and collimating", <http://www.newport.com>,
Newport Inc.